Spatial computations in entorhinal cortex after degradation of perineuronal nets

Master thesis in Molecular Bioscience

Main field of study in physiology and neurobiology

Anne Marte Sjursen Kvello

60 credits

Program for Physiology and Neurobiology

Department of Biosciences

The Faculty of Mathematics and Natural Sciences

UNIVERSITY OF OSLO

2014

Acknowledgements

The work presented in this thesis was conducted at the Program for Physiology and Neurobiology at the Department of Biosciences, University of Oslo, between January 2013 and February 2014, under the supervision of associate professor Dr. Marianne Fyhn and associate professor Dr. Torkel Hafting.

First and foremost, I would like to thank my supervisors Marianne and Torkel for motivation and guidance through practical work and writing, and for giving me the opportunity to learn so many advanced methods. I would also like to thank Dr. Gunnar Dick for useful advice about immunohistochemistry and feedback on writing.

A big thanks to the office crew, for inspiring conversations, shared frustrations, and the extracurricular chatter. I would especially like to thank Kristian for always helping out – with everything. Thank you Ida for pep talks and help with histology and to Charlotte for useful tips and encouragement along the way.

Thanks to my family and friends for all their support.

Most of all: Thank you Arngeir.

Oslo, February 2014

Anne Marte Sjursen Kvello

Abstract

The medial entorhinal cortex (MEC) is essential for spatial navigation and memory, and must therefore maintain a high level of plasticity throughout life in order to respond to a changing world. The key component in the brain's navigational system is proposed to be a subpopulation of neurons named grid cells. The activity of these cells reveals a strikingly regular pattern of repetitive activity nodes tiling the environment traversed by the animal. The regularity and seemingly hard-wired nature of the grid cell network suggest that they are under strong inhibitory control by local populations of interneurons. A prominent subset of interneurons in the MEC is parvalbumin-positive (PV^+) cells. The PV^+ cells are linked to several plasticity mechanisms and are involved in the maintenance of brain oscillations, controlling the synchronous firing of local neuronal ensembles.

In the adult cortex, a large proportion of PV^+ cells are tightly enwrapped by a condensed form of extracellular matrix termed perineuronal nets (PNNs). The compact structure of PNNs restricts plasticity in adult animals and can be disrupted by the enzyme chondroitinase ABC (chABC). The role of PV^+ cells and PNNs for spatial representations in the MEC has never been investigated.

In this study, I investigated the potential role of PNNs in cortical processing and plasticity in MEC of adult rats. This was done by combining intracortical microinjections of chABC with electrophysiological large-scale recordings from populations of neurons in MEC of awake and behaving rats.

The PNNs were found in all cellular layers of the MEC, where they enwrapped subtypes of neurons, including PV^+ cells. The PNNs were completely digested three days after chABC treatment and showed a regeneration of 30% after 21 days. The chABC treatment lead to a reduced grid cell firing rate and bursting compared to controls, whereas firing rates in head direction cells and interneurons were not significantly altered. When animals are introduced to a novel environment, it has previously been shown that the oscillations of the local field potentials in the theta frequency band decrease, and this has been proposed as a potential novelty signal. In contrast, the chABC treated animal showed an increase in theta frequency in the novel environment.

Altogether, these results suggest that PNNs may play a role for the grid cell network and for spatial computations in the MEC, both in terms of single cell activity and for the synchronized firing of neuronal ensembles.

Table of contents

1. Introduction

1.1 Central nervous system plasticity

During childhood and adolescence our brain is more prone to learning of certain skills than later in life. This is caused by a pronounced neuroplasticity seen in the developing brain, which makes it highly susceptible to new experience. Neuroplasticity includes mechanisms at the level of neural circuitry, where neuronal connections are lost and others are formed, and at the synaptic level, which encompasses the weakening and strengthening of already established synaptic connections.

At well-defined periods during development, the brain is particularly sensitive to external stimuli and may undergo large scale synaptic changes. This window of heightened plasticity is termed the critical period (CP), in which new synaptic connections form and others disappear (reviewed by Hensch, 2005). If a brain area does not receive the appropriate stimulus during its critical period, it may be difficult or even impossible to develop these functions later in life (reviewed by Levelt and Hübener, 2012). In some areas of the brain such plasticity is crucial for the correct refinement of neuronal networks.

For many cortical areas, the closure of critical periods introduces the restricted plasticity observed in adulthood (Pizzorusso et al., 2002). Reduced plasticity may contribute to maintain stable connections that persist despite changes in stimuli (e.g. short-term sensory deprivation). However, certain brain circuits remain a high level of plasticity throughout life. This is particularly important for cognitive functions such as learning and memory, because they require constant refinement of neuronal networks in order to encode new information.

1.2 Plasticity in learning and memory

The most widely studied cellular mechanisms underlying learning and memory are synaptic plasticity processes known as long-term potentiation (LTP) and long-term depression (LTD) (reviewed by Malenka and Bear, 2004). In both processes, neuronal activity affects the molecular composition at the synapse, changing the efficacy of signal transduction between neurons. Induction of LTP causes enhanced signal transduction, while induction of LTD causes

reduced signal transduction (Martin et al., 2000). These mechanisms cause long-lasting changes in the synaptic efficacy in animals upon learning, and are therefore considered important mechanisms for memory formation (Martin et al., 2000; Whitlock et al., 2006).

In addition to the physiological changes at the synapse, structural changes of dendritic spines (protrusions of neuronal dendrites for synaptic input), can be observed as a result of neuronal activity (reviewed by Bhatt et al., 2009). Dendritic spine dynamics encompasses the formation and loss of synaptic connections. Recent studies using in vivo imaging techniques showed that learning a motor task induced a rapid increase in spine turnover, indicating that structural changes of the neural network may be important during learning and memory encoding (Yang et al., 2009; Xu et al., 2009).

Studies of the molecular and structural changes at synapses may provide some basis for understanding the mechanisms underlying learning and memory. However, the mechanisms for the neural circuitry plasticity in these areas remain elusive.

1.3 The role of the hippocampal formation and parahippocampal areas in spatial memory

Spatial memory is a form of episodic-like memory which encompasses the "what", "when" and "where" components of experienced events. Spatial memory is mainly attributed to the hippocampal formation and the parahippocampal areas (Scoville and Milner 1957; Squire et al., 2004). Several studies have proved the importance of the hippocampal formation in spatial memory in mammals, including humans. Studies using the classic water maze task, has showed that rats with hippocampal or parahippocampal lesions failed to find a hidden platform already visited by the animal (Morris et al., 1982; Steffenach et al., 2005). In a study by Maguire and collegues (1997), London taxi drivers were asked to recall the routes of the city while their brains were scanned using positron emission tomography. The scanning showed activation of the hippocampus and parahippocampal areas in the subjects during this task (Maguire et al., 1997). In order to ensure the encoding, consolidation and recall of episodic memories throughout life, functional changes of neuronal networks continuously occur in this circuitry. Thus, the hippocampus and parahippocampal areas encompass a high degree of plasticity.

The parahippocampal region is the main input and output structure from the hippocampal formation to the neocortex (Witter and Amaral, 2004) and consists of the pre- and parasubiculum, and postrhinal, perirhinal and entorhinal cortices. The entorhinal cortex (EC) is an area of particular interest in relation to spatial memory, because if its role in the processing of spatial memories and navigation (reviewed by Van Strien et al., 2009).

The entorhinal cortex will be the main focus of this thesis.

a)

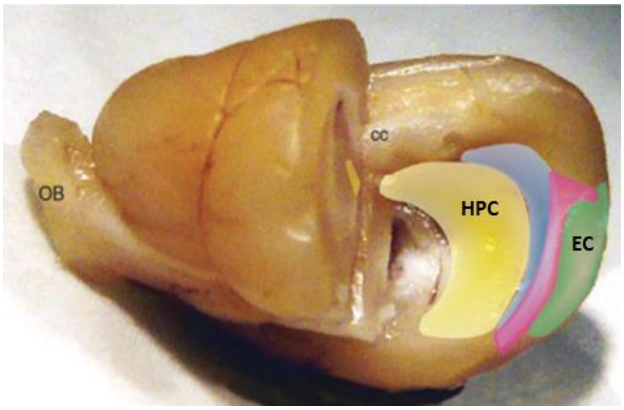

b)

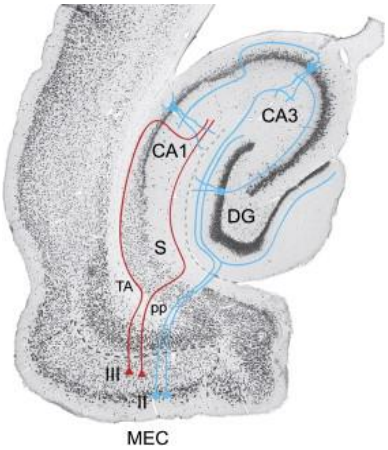

Figure 1.1. The hippocampal formation and parahippocampal areas in rats. a) Sagittal view of a rat brain where the posterior part of the right hemisphere has been removed to show the hippocampal formation and parahippocampal areas (Boccara et al., 2010). b) A horisontal coronal section of the hippocampal formation and parahippocampal areas from a rat brain illustrating the connectivity between the medial entorhinal cortex (MEC) and hippocampal formation (Brun et al., 2008). CA1/3 (cornus ammoni 1/3); CC (corpus callosum); DG (dentate gyrus); EC (entorhinal cortex); HPC (hippocampus); MEC (medial entorhinal cortex); OB (olfactory bulb); pp (perforant path).

1.4 The medial entorhinal cortex and spatial navigation

In mammals, the EC represents the interface between the association cortices and the hippocampus, and is traditionally viewed as a nodal point between these areas (Wouterlood et al., 1995; Dolorfo and Amaral, 1998). The EC is typically divided into a medial and lateral band, with different functional properties (Insausti et al., 1997). The lateral EC (LEC) is an area associated with object recognition, attributing LEC as the "what" component of episodic

memory, whereas the medial EC (MEC) appears to mainly process spatial information, and is attributed to the "where" component of episodic memories.

Similar to other neocortical areas, the MEC displays a laminar organization of six distinct layers, divided into superficial (I-III) and deep (V-VI) layers. Layer I and IV contain few neurons and the latter is commonly known as the lamina dissecans (Dolorfo and Amaral, 1998).

The MEC redirects information from association cortices to the hippocampus through the so-called perforant path (PP), projecting from MEC layers II/III to various hippocampal areas (Witter and Amaral 2004) (figure 1.1). Information from the hippocampus is sent to the neocortex via deep layers (V/VI) of the MEC (reviewed by Canto et al., 2008). Studies have shown that lesions to the MEC result in impaired spatial representations in the hippocampus (Brun et al., 2008) and a disruption of spatial memory function (Steffenach et al., 2005). In humans, neuronal cell loss in EC from epilepsy (Schwarcz and Witter, 2002) or during normal ageing and Alzheimer's disease (Simic et al., 2005; Stranahan and Mattson, 2010; Khan et al., 2013) most likely account for the memory impairments associated with such conditions. Furthermore, inactivation of the hippocampus leads to impaired spatial information processing in the rat EC (Hafting et al., 2008; Bonnevie et al., 2013), and contextual fear conditioning is impaired in rodents with hippocampal or entorhinal lesions (Maren and Fanselow, 1997). Taken together, these studies support the notion that the entorhinal-hippocampal circuitry is essential for coding of spatial representations.

The EC contribute to self-location, navigation and the formation of spatial memories (van Strien et al., 2009). Spatial representations in the hippocampus appear to be updated whenever environmental changes occur, suggesting a high level of plasticity in the hippocampal-entorhinal circuitry (Fyhn et al., 2002).

Key units for the formation of episodic-like memories are spatially modulated cells of the hippocampus and entorhinal cortex. Such cells encode spatial maps of the external environment, and methods for studying their firing activity are well established (O'Keefe, 1976; Fyhn et al., 2004; Boccara et al., 2010). Thus, they may serve as valuable tools for studying adult plasticity mechanisms in spatial memory and navigation.

1.5 Spatially modulated cells in the hippocampus and entorhinal cortex

1.5.1 Hippocampal place cells

Place cells are principal neurons of the hippocampus that are excited and fire action potentials whenever the animal is at a particular location in the environment. Thus, each place cell has its own firing field or place field (O'Keefe, 1976).

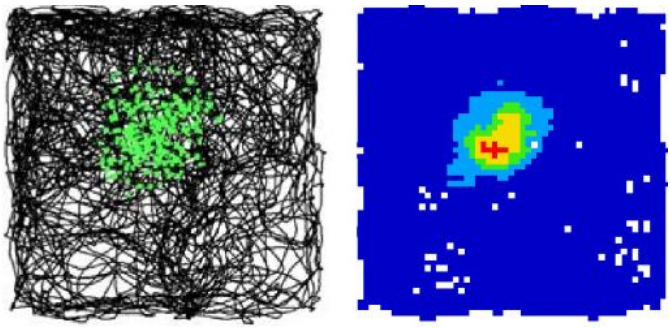

Figure 1.2. A place cell recorded from the rat hippocampus. Left: The trajectory (black line) of a rat running in a square box showing the firing location of a single neuron recorded from the hippocampus, with action potentials from the place cell superimposed in green, representing the cell's place field. Right: The same place field shown as a color coded rate map. Colors correspond to the firing rate of the cell: red equals the highest firing rate, whereas dark blue corresponds to no firing activity (Barry and Bush, 2012).

When the animal encounters a novel environment, place cell remapping may occur in which the place field and/or firing rate of the place cell is changed (reviewed by Colgin et al., 2008). Remapping allows for a mechanism by which very similar, but slightly different, memories can be encoded and stored separately in the brain. This mechanism prevents interference of related memories and is termed pattern separation (Leutgeb et al., 2004). The encoding of new spatial representations provides an example of functional plasticity mechanisms in the hippocampus.

Place cells are suggested to code for episodic-like memories, and are not driven solely by location. The hippocampus receives input about location along with sensory and other contextual information from the surrounding cortices (Fyhn et al., 2002; Hafting et al., 2005). The information about self-location is forwarded to the hippocampus through projections from the EC (Fyhn et al, 2004; Hafting et al., 2005) The hippocampus associates all incoming

spatial and non-spatial information and may generate a cognitive spatial map. However, the mechanism underlying spatial map formation remains elusive.

A great diversity of cell types is expressed in the different layers of the MEC (reviewed by Canto et al., 2008) and cells significant for spatial coding are described in the following section.

1.5.2 Entorhinal grid cells

A proportion of the principal neurons in MEC are spatially modulated neurons termed grid cells (Hafting et al., 2005). Grid cells have multiple firing fields in a given environment which form a characteristic triangular firing pattern spanning the surface of the area visited by the animal (figure 1.3). Grid cells fire at constant periodic positions and are not affected by the direction of movement of the animal (Fyhn et al., 2004; Fyhn et al., 2007).

a) b)

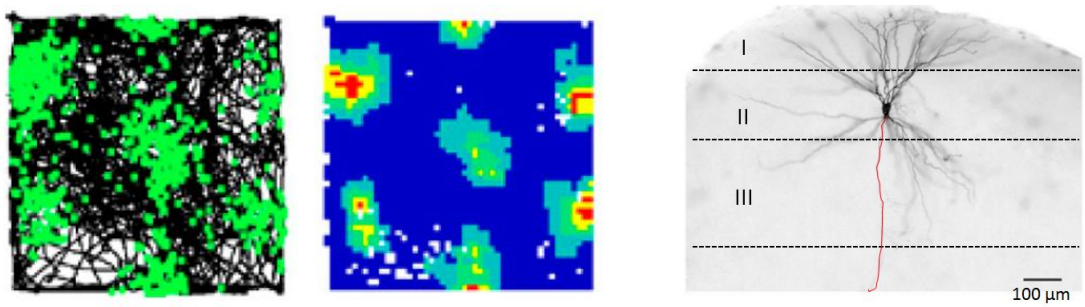

Figure 1.3. a) A grid cell recorded from the medial entorhinal cortex (MEC) of a rat running in 1x1m square box. Left: Rat trajectory is shown in black with action potentials of a single grid cell superimposed in green. Right: Color coded rate map of the same grid cell. Red represents high firing activity whereas dark blue corresponds to no firing activity (Barry et al., 2012). b) Photomicrograph of a stellate cell spanning the superficial layers (I-III) of MEC. Cell soma and dendrites are shown in black; axon is shown in red. Modified from Tahvildari and Alonso (2005).

In contrast to place cells, which may or may not be active in different environments, grid cells have persistent firing across environments, suggesting that the grid map is applied everywhere (Fyhn et al., 2007). Furthermore, the grid pattern is maintained across days and persists in darkness, suggesting that it is driven by self-motion cues (Hafting et al., 2005).

Firing fields of individual neurons in an ensemble of grid cells overlap, leaving the entire surface of the area covered by a local grid ensemble (Hafting et al., 2005). Thus, grid cells may comprise a metric system coding for immediate periodic self-location, and form a map of the external environment, which is independent of context or events (Hafting et al., 2005; Moser et al., 2010).

In layer II of MEC, approximately half of all principal neurons are grid cells (Sargolini et al., 2006), and recent studies indicate that the majority of layer II/III grid cells are stellate and pyramidal cells (Domnisoru et al., 2013; Schmidt-Hieber and Häusser, 2013).

Grid cells are topographically organized, with grid size increasing in the dorso-ventral axis of the MEC (Hafting et al., 2005; Brun et al., 2008). The increase in grid size is proposed to reflect the increase in place field size along the dorsoventral axis of the hippocampus (figure 1.4) (Kjelstrup et al., 2008). The locational input to the hippocampus originating from MEC grid cells is suggested as a place field generator in the hippocampus (Moser et al., 2010).

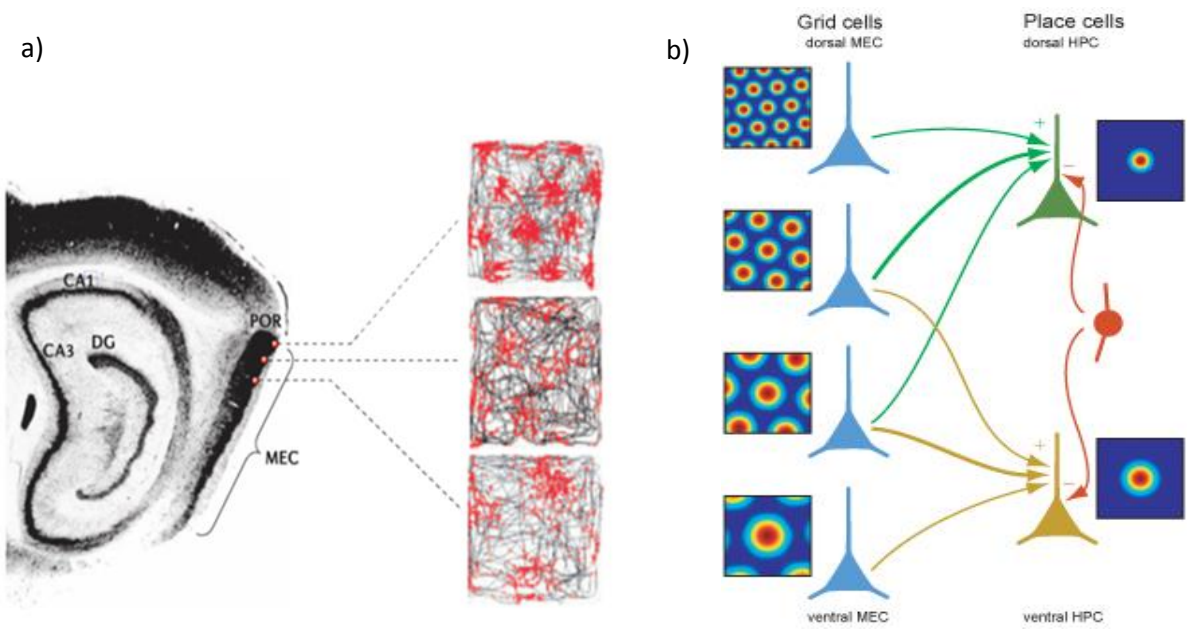

Figure 1.4. Grid size increases in the dorsoventral axis of medial entorhinal cortex (MEC). a) Sagittal section (left) from rat brain showing the dorsoventral grid increase in the MEC and activity patterns from these three grid cells recorded at different dorso-ventral positions in MEC (right) showing trajectory (black) of the rat with action potentials superimposed (red) (McNaughton et al., 2006). b) Schematic drawing of the proposed connectivity

between grid cells in MEC and place cells in the hippocampus and the suppressive control by inhibitory interneurons (Solstad et al. 2006). (CA, Cornu ammonis; DG, dentate Gyrus; HPC, hippocampus; MEC, medial entorhinal cortex; POR, postrhinal cortex).

The formation of the grid pattern has been heavily debated and several models have been proposed (reviewed by Moser et al., 2014). Due to its rigid firing pattern, it is likely that grid cell firing activity is under strong inhibitory control. A recent study by Couey and collegues (2013) demonstrated that stellate cells of MEC layer II are interconnected via fast-spiking inhibitory interneurons, and that excitatory connections between stellate cells are virtually absent. This suggests that an inhibitory microcircuitry of stellate cells in MEC layer II is sufficient for grid pattern formation (Couey et al., 2013). Disrupting interneuron activity in MEC might therefore impact the grid structure and the overall activity of grid cells.

1.5.3 The introduction of a novel environment requires plasticity mechanisms

Well-established methods to investigate the properties of spatially modulated cells include remapping and introduction to a novel environment. When an animal is placed in a novel arena, the grids shift relative to the familiar environment (Barry et al., 2012). Thus, introduction of a novel environment causes the encoding of new location-specific information, which is likely to involve plasticity mechanisms.

As described in chapter 1.5.1, remapping refers to pattern separation of similar input information, in which various populations of place cells encode different environments. While hippocampal place cells show an unpredictable reorganization of the cell ensemble between a familiar and a novel environment, the entorhinal grid cell ensemble retain the same spatial and temporal firing organization, but show a coherent shift in the grid vertices (grid realignment) relative to the representation in the familiar environment, (Fyhn et al., 2007).

The introduction of a novel environment induces plasticity in the hippocampal-entorhinal circuitry, but the mechanisms of such plasticity in the grid cell network remain elusive. Thus, a novelty paradigm can be used to study plasticity in the grid cell network.

1.5.4 Other spatially modulated neurons in MEC

Grid cells in the MEC co-exist with head direction (HD) cells which fire selectively when the animal's head is oriented in a specific direction, and cells with conjunctive grid and HD cell properties (conjunctive cells) (Sargolini et al., 2006). Additionally, the MEC contains border cells, which fire selectively in the proximity of geometrical borders (Solstad et al., 2008). A recent study showed that similar to grid cells, layer III HD cells are topographically organized in the dorso-ventral axis of MEC (Giocomo et al., 2014).

Principal neurons in MEC also intermingle with populations of inhibitory interneurons (Melzer et al., 2012) which form synapses on principal cells, serving as "breaks" on their firing activity (Couey et al., 2013). In addition, inhibitory interneurons are important for the maintenance of network activity, or brain oscillations (reviewed by Buszáki, 2002). Furthermore, inhibitory interneurons are linked to CNS plasticity (Hensch et al., 1998; Fagiolini and Hensch, 2000), however their role for grid cell plasticity in MEC is not known.

1.6 Parvalbumin-positive interneurons in MEC

A large variety of interneurons are found in MEC layers II and III, most of which are gamma-aminobutyric acid positive (GABAergic) (reviewed by Canto et al., 2010). These interneurons have local projections, or long-ranging projections to the hippocampus. One of the main types of GABAergic interneurons in the MEC are fast-spiking basket cells expressing the calcium-binding protein parvalbumin (PV^+ cells) (Sik et al., 1995; Wouterlood et al., 1995). The PV^+ cells form inhibitory synapses on principal cells in the MEC, and control their spiking activity. Thus, PV^+ cells are important for the synchronization of principal neuron firing activity (Wouterlood et al., 1995; Buzsáki, 2002). These neurons fire bursts of action potentials with high frequency and a high expression of PV^+ cells in EC layers II-III has previously been observed (Wouterlood et al., 1995; Menno Witter; Canto et al., 2008).

Recent studies showed that principal neurons in MEC are mainly interconnected through inhibitory interneurons of which a large proportion is fast-spiking cells (Dhillon and Jones, 2000; Couey et al., 2013). Another study showed that stellate cells of MEC layer II are embedded in an inhibitory microcircuit provided by PV^+ cell input, and that the inhibitory circuit shows a decreasing gradient along the dorsoventral axis of the MEC (Beed et al., 2013).

The PV^+ cells are believed to be key players in regulation of plasticity (Bartos and Elgueta, 2012), and it is plausible that fast-spiking PV^+ cells exert a precise control on grid cell activity, and are responsible for their rigid periodic firing pattern. The interactions between principal MEC neurons and PV+ cells and their contribution to grid formation, remains elusive.

1.6.1 Plasticity mechanisms involving PV^+ cells

In the mammalian visual cortex the PV^+ cells mature at the onset of the critical period (del Rio et al., 1994; Pizzorusso et al., 2002). Donato and colleges (2013) found that the level of parvalbumin expressed by fast-spiking basket cells modulates learning and structural plasticity in adult mouse hippocampus. By pharmacogenetic activation and inhibition, they induced high-PV and low-PV network configurations, respectively. They demonstrated that low PV expression enhanced synaptic plasticity, memory consolidation and retrieval, whereas high PV expression produced the opposite result. Moreover, when the mice performed spatial learning tasks, a low-PV-network configuration was induced in the hippocampus (Donato et al., 2013).

Little is known about PV^+ cells and adult plasticity in the EC. Studies of the role of inhibitory activity of PV^+ cells in critical period plasticity models point to the interplay between PV^+ cells and a special form of extracellular matrix, the perineuronal net, as a key players for the reduced plasticity in the adult brain.

1.7 Perineuronal nets

The PV^+ cells in the adult cortex are to a large extent enwrapped by a specialized form of extracellular matrix (ECM) termed perineuronal nets (PNNs) (figure 1.5) (reviewed by Kwok et al., 2011). The PNNs are found in a number of cortical areas, in the hippocampus and the in EC (Härtig et al., 1992; Morris and Henderson, 2000; Yamada and Jinno, 2013). Co-localization of PNNs and PV^+ cells was found to overlap by 60-70% in the mouse cortex (Cabungcal et al., 2013), and in a previous study, Callahan and co-workers observed a 37% overlap in rat hippocampus (Callahan et al., 2013). However, reports on PV/PNN overlap in the rat brain are scarce and the quantification of PV^+ and PNN overlap in the EC has not been reported.

a) b)

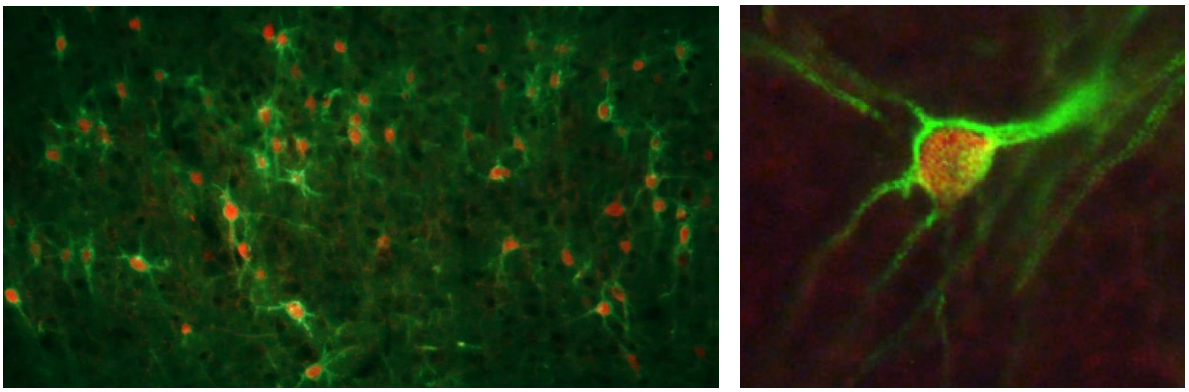

Figure 1.5. Perineuronal nets stained with *Wisteria floribunda* (WFA) and streptavidin fluor conjugate enwrap parvalbumin-positive cells (PV^+) in the rat cortex. a) The PNNs (green) co-localize with PV^+ cells (red) in rat cortex. b) The soma and dendrites of a PV^+ cell are densely packed by PNNs.

The PNNs are a highly condensed form of ECM which largely consist of negatively charged chondroitin sulfate proteoglycans (CSPGs), hyaluronan, link proteins and tenascin-R, while fibrous proteins such as collagen are absent (Deepa et al 2006; Kwok et al., 2011; Zimmerman and Zimmerman, 2008). In certain subpopulations of neurons, hyaluronan synthase (HAS) attached to the surface of neuronal somata, produces long chains of hyaluronan and secretes them into the extracellular space. Members of the lectican family, which belong to a subgroup of CSPGs, are linked to the hyaluronan chains via link proteins (Deepa et al 2006; Kwok et al., 2011). The lecticans (aggrecan, versican, brevican and neurocan, respectively) are composed of a core protein and chondroitin sulfate glycosaminoglycan (CS GAG) chains (Kwok et al., 2011). The assembly of these molecular components on neuronal surfaces form the tightly organized, lattice-like PNN structure (figure 1.6).

a)

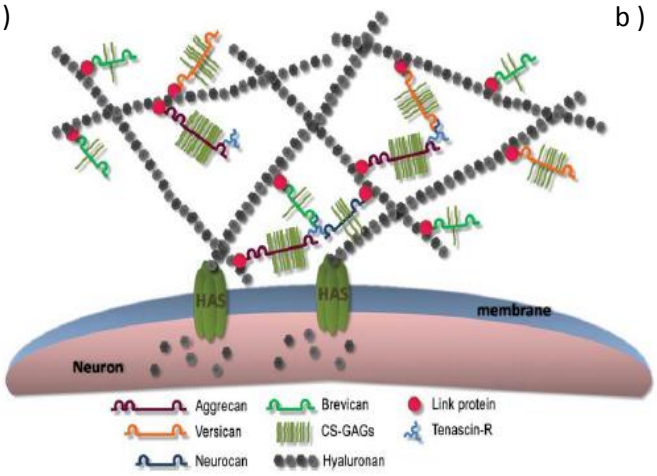

b)

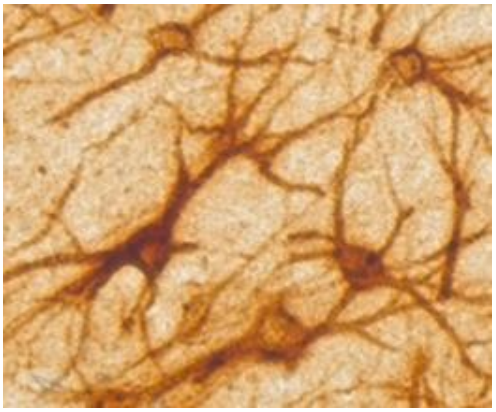

Figure 1.6. a) Schematic representation of the molecular composition of perineuronal nets (PNNs) on the surface of a neuron (Kwok et al., 2011). b) The PNNs enwrap neuronal somata and dendrites in the rat cortex, stained with *Wisteria floribunda* agglutinin and diaminobenzidine (DAB). CS-GAGs (chondroitin sulphate glycosamingoglycans); HAS,(hyaluronan synthase).

The tight organization of PNNs is largely caused by the cross-linking of GAG side chains of different core proteins. The dense PNN aggregates surround neuronal soma, proximal dendrites (including dendritic spines), and axon initial segments, and opens up only at points of synaptic contact (reviewed by Frischknecht et al., 2009 and McRae and Porter, 2012). This condensation coincides with the maturation of PV^+ inhibitory neurons, which happens towards the end of the critical period (Frischknecht and Gundelfinger, 2012; Pizzorusso et al., 2002). The fast-spiking activity of PV^+ cells requires a high metabolic turnover of ions, and the negatively charged GAGs of PNNs are thought to support the ion homeostasis of the extracellular milieu surrounding the PV^+ cells (Morris and Henderson, 2000)

The PNNs are involved in many processes, such as neuronal development, axonal growth, neuroprotection and ion homeostasis, and are proposed as a key factor in storage of long term memory (Dityatev, 2010; Shah and Lodge, 2013; Soleman et al., 2013; Mauney et al., 2013; Gaultrey and Fawcett, 2007; Tsien, 2013). Most interestingly, PNNs seem to play an essential role in CNS plasticity.

1.7.1 The PNNs and plasticity

The PNNs stabilize synaptic connections at the closure of critical periods for learning, and constrain cortical plasticity in adult animals (Pizzorusso et al., 2002). In addition, the formation of PNNs seems to be activity-dependent, as this process is delayed in animals receiving reduced sensory input (Pizzorusso et al., 2006; Dityatev et al., 2007).

In both the adolescent and adult CNS the ECM is continuously modified by a group of enzymes termed matrix metalloproteinases (MMPs). The MMPs conduct proteolytic cleavage of PNNs (van Hove et al., 2012), and are linked to CNS plasticity mechanisms, such as LTP and remodeling of synapses and dendritic spine dynamics (reviewed by Huntley, 2012; van Hove et al., 2012). Furthermore, learning and memory tasks such as fear conditioning, which induces LTP, are accompanied by increased levels of MMPs (Huntley et al., 2012).

The PNNs can be artificially digested in vivo by the enzyme chondroitinase ABC (chABC), isolated from the bacterium *Proteus vulgaris* (Brückner et al 1998a; Massey et al., 2006; Kwok et al., 2011). Specifically, chABC acts by cleaving the chondroitin sulfate disaccharides from the GAG side chains of the core protein (Kwok et al., 2011). In contrast to the natural MMPs, enzymatic digestion by chABC results in a loss of the tight organization of ECM molecules, and leads to disruption of the overall PNN structure (figure 1.7).

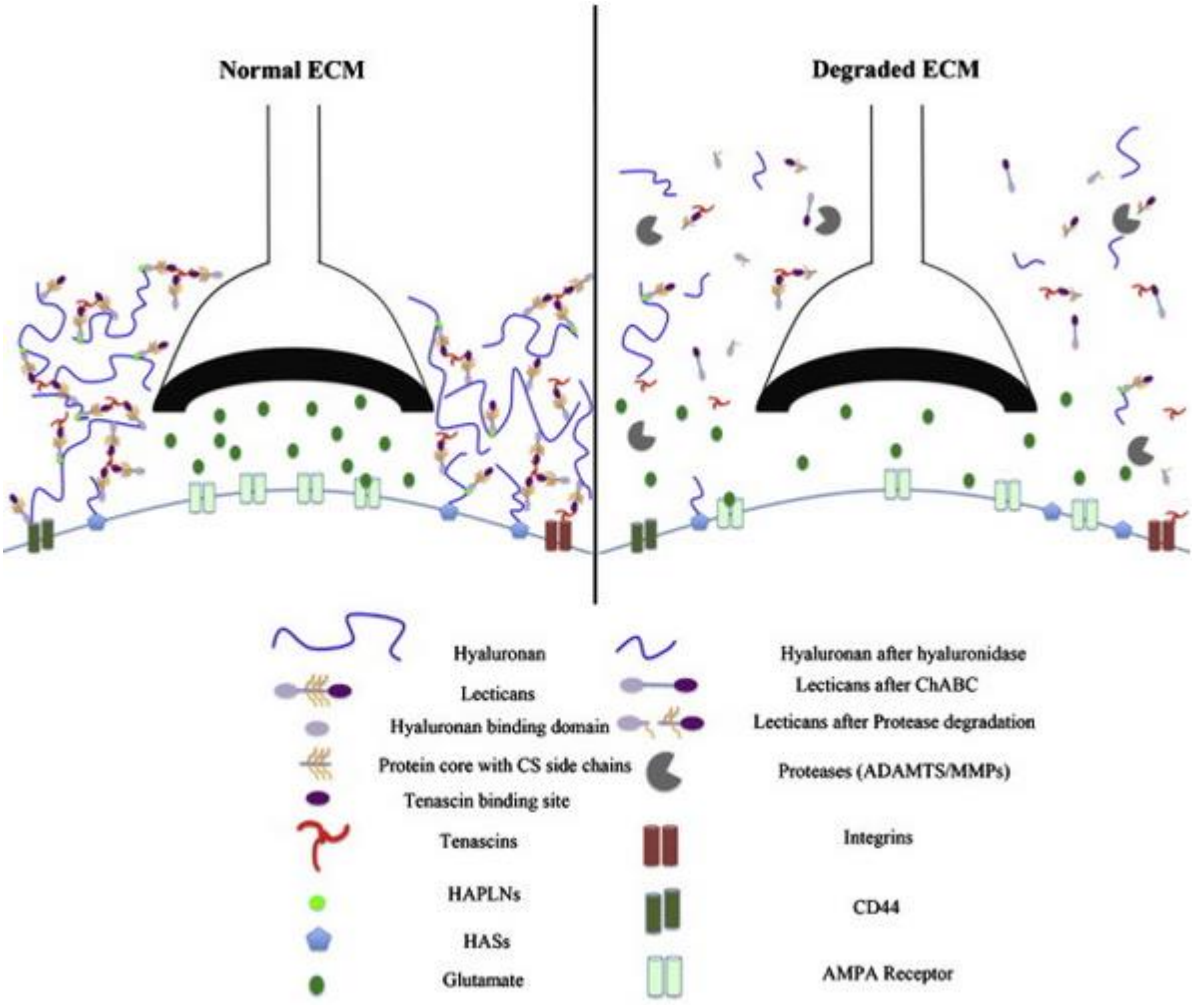

Figure 1.7. Schematic figure showing the potential mechanism by which the perineuronal net (PNN) restricts synaptic plasticity (left), and enzymatic digestion of PNN by chondrotitinase ABC (chABC) (right) (McRae and Porter 2012).

Functionally, chABC digestion increases plasticity in the adult visual cortex to a level similar to that of critical period plasticity (Pizzorusso et al., 2002). Moreover, spine density is increased in rat visual cortex after chABC treatment (Pizzorusso et al., 2006).

1.7.2 A possible role for PNNs in learning and memory

In recent years, the role of PNNs in learning and memory plasticity has gained more attention. Studies have shown that chABC administration increases plasticity in relation to fear-conditioning and memory involving the amygdala (Gogolla et al., 2009) and disruption of the hyaluronan component of PNNs in the hippocampus leads to impaired fear memory

(Kochlamazashvili et al., 2010). Additionally, PNN disruption by chABC and hyaluronidase in the hippocampus and medial prefrontal cortex, an area linked to storage of long-term memories, results in impaired fear memory in adult rats (Hylin et al., 2013). Moreover, chABC treatment in perirhinal cortex of adult mice produces enhanced object recognition and LTD (Romberg et al., 2013).

Due to the tight enwrapping of neurons in the CNS, PNNs may be essential for mature synaptic function. Furthermore, the PNNs subsequently inhibit juvenile plasticity in adult animals by restricting new synapse formation. These properties suggest a highly stable molecular composition of the PNNs, which might have the ability to maintain long-lasting neuronal connections. Such properties are necessary for storage of information, and based on these arguments, Tsien (2013) proposes PNNs as a molecular substrate for long-term memory storage. It is further suggested that the gaps in PNNs around synaptic contacts are created by the MMPs, and that memories might be stored in these "holes" (Tsien, 2013).

A large body of evidence points to a role of PNNs for CNS plasticity in several brain circuits, including the hippocampal formation and parahippocampal areas. However research on PNNs and plasticity in regards to principal neuronal activity in EC has not been studied. The enwrapping by PNNs of MEC neurons might serve as an explanation for the rigidity and hard-wiring of the grid cell network. Furthermore, PV^+ cells co-localize with PNNs and it is possible that disruption of PNNs in the MEC will impair fast-spiking activity of PV^+ cells, ultimately causing downstream effects on principal neuron activity. In the current project, the potential role of PNNs for spatial learning and navigation will be investigated in the MEC.

1.8 Oscillations of the local field potential

The PV^+ cells are involved in the maintenance and regulation of brain wave oscillations (Freund 2003). Such oscillations are the result of synchronized activity of local populations of neurons, collectively creating the local field potential (LFP). Depending on the frequency, the activity can be synchronized across the two hemispheres (Kandel et al., 2000). In particular, oscillations in the gamma and theta frequency bands have been implicated as important for

memory formation, and are linked to synaptic plasticity mechanisms (Buzsáki, 1989; Buszaki 2002; Freund, 2003).

In the EC, a profound theta activity is typically observed in the 5-10 hertz band (Buzsáki, 2002). Theta activity is associated with REM sleep and active behavior, such as locomotor activity, and seems to be absent when the animal does not move (Buzsáki, 2002). Furthermore, theta activity is associated with the "learning mode" of the brain, and theta frequency stimulations can induce LTP/LTD in the entorhinal cortex in vitro (Yun et al., 2002; Yang et al., 2004). The faster gamma frequency oscillations (25-100 Hz) are generated locally by PV^+ cells and may be important for information coupling between the hippocampal-entorhinal areas and the neocortex (Freund 2003; Colgin et al., 2009).

In a study by Jeewajee and coworkers, they showed that theta frequency is reduced when an animal moves from a familiar to a novel environment, suggesting that these oscillations are linked to plasticity mechanisms induced by novel spatial experience (Jeewajee et al., 2008).

Melzer and collegues showed that some GABA-ergic inhibitory interneurons, including PV+ cells, have long-range projections between MEC and the hippocampus and exert modulation on local interneurons in both areas. They further demonstrated that some of the projections from the hippocampus targeted MEC stellate cells (Melzer et al., 2012). This suggests that the long-range GABA-ergic projections synchronize activity, such as theta oscillations, across the hippocampus and the MEC, and might play an indirect role in the modulation of principal cell activity. Thus, theta rhythm is implicated as a mechanism involved in both grid pattern formation in the EC, and as a mechanism for synaptic plasticity (Buzsáki, 2002; reviewed by Buzsáki and Moser, 2013).

The notion that PV+ cells are enwrapped by PNNs and that PV+ cells are involved in oscillatory rhythm generation, points to the possibility that chABC treatment might interfere with such activity, and further affect firing activity of MEC principal neurons. This has not been investigated, and could provide important knowledge to the general plasticity mechanisms underlying learning and memory.

1.9 Aim of study

In the current project I investigate if degradation of PNNs affects entorhinal network oscillations and spatial processing. I hypothesize that PNNs might play a role in stabilization of neuronal connections in the entorhinal cortex. The hypothesis will be tested by conducting the following:

1. Investigate whether removal of PNNs by the enzyme chondroitinase ABC in MEC will affect the activity patterns of grid cells (e.g. firing rates, spatial map formation and stability).

2. Investigate the properties of other cell types within the MEC, such as head-direction cells and interneurons.

3. Investigate the potential effect of PNN removal on brain oscillations in the theta frequency band.

In the experimental approach, microinjections of chABC will be combined with electrophysiological recordings in the MEC of awake and behaving rats.

2. Materials and methods

2.1 Approval and research animals

All practical work in the current project was conducted between January 2013 and January 2014 at the Department of Biosciences (IBV) at the University of Oslo, Norway. Experiments were approved by the Norwegian Animal Research Committee (FDU – Forsøksdyrutvalget). The housing and treatment of research animals followed requirements set by the European Union and the FDU. All contributors in the project have passed a Course with Experimental Research and Animals approved by the Norwegian Food Safety Authority (Mattilsynet) to conduct research with experimental animals.

Seventeen male Long Evans hooded rats (*Rattus norvegicus*) acquired from Charles River, Germany, and bred at IBV, were used in the project. The rats were 3-6 months of age and weighed 350-600 grams. Surgery training and establishment of coordinates for EC injections and implantation was performed as a pilot study. When coordinates were established, rats were injected with the enzyme chondroitinase ABC (chABC) for degradation of perineuronal nets (PNNs), and implanted with microdrives for electrophysiological recordings. Electrophysiology controls were implanted with microdrives only, and histology controls were injected with enzyme only. Electrophysiological experiments were conducted on control animals within 40 days after surgery, whereas animals injected with chABC and microdrives were used for experiments within 21 days after surgery. This time period was chosen to ensure low levels of PNN as PNN regeneration exceeds 40% after 21 days in the rat cortex (Lensjø, 2013).

The animals were kept on a 12 hour light/dark schedule. The light phase was between 8 p.m. and 8 a.m, with light intensity below 100 lux, and the dark phase lasted from 8 a.m. to 8 p.m. Because rats are nocturnal animals, all training and recordings were performed during the dark phase. The temperature of the housing cabinets was kept at 21°C and the air humidity was approximately 55%. Ventilation of the cabinets had a changing rate of 5-20 times per hour. The animals were housed three or four together in polycarbonate cages (35x55x19 cm)

with food and water ad libitum prior to surgery. The bedding of the cages consisted of woodchip (Scanbur A/S), and plastic toys were provided for environmental enrichment.
In order to prevent post-surgical injury to the animals and damage to the microdrive implants, the implanted animals were kept individually in plexiglass cages (35x55x30 cm) after surgery. For motivation of performance in the behavioral tests, animals were restricted to 6-10 pellets per day. Animals kept their body weight during the experiments in spite of this light food deprivation.

2.2 Surgery preparations

2.2.1 Tetrode and microdrive assembly

A 17 µm-diameter platinum-iridium wire (California Fine Wire Company, CA, U.S.A), was used to make recording electrodes in a tetrode configuration (four electrodes twisted together). A single piece of wire was looped using a piece of tape and then looped again over a metal rack. The looped wire was placed above a magnetic stirrer plate, with a stirrer bar hanging from the loops, to twist it together, creating a tetrode. To ensure a tight assembly of the wires, the tetrodes were heated using a heating gun for approximately 20 seconds, such that the insulation of the individual wires were tethered together. The insulation covering the free endings to be connected to the microdrive was removed by passing them quickly through a lighter flame.

Construction of microdrives was conducted by the assembly of four tetrodes into one Microdrive (figure 2.1, Axona Ltd, Herts, UK). In order to ensure optimal electric contact between the electrode wire and the wire on the microdrive, silver conductive paint (HK Wentworth, Leicestershire, UK) was applied. Furthermore, several layers of nail polish were applied for protection of the tetrodes. Finally, the tetrodes were cut to the proper length (6-7 mm) using fine scissors, and electroplated in platinum solution to reduce the impedance (from approximately 1500 kΩ to 150-250 kΩ).

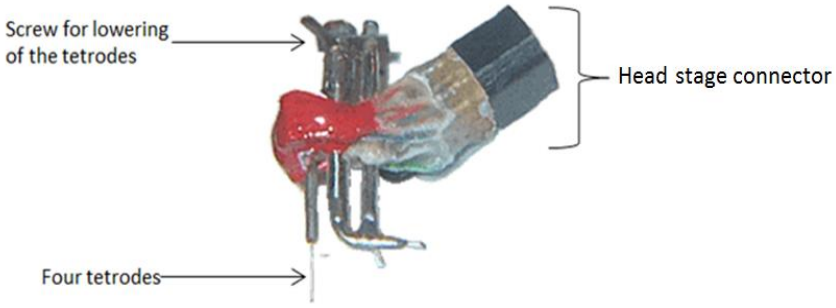

Figur 2.1. Microdrive, photo adapted from Axona Ltd., Herts, UK.

2.2.2 Chondroitinase ABC

Protease free chondroitinase ABC (chABC) (Amsbio, Abingdon, UK), in 10U vials was diluted in 1X phosphate buffer solution (PBS) to 61 U/mL aliquots (3.1 µl) and stored at -20°C. Immediately prior to use, the aliquots were thawed and further diluted with Fast Green FCF(Sigma-Aldrich Chemie, Munich, Germany) to a working concentration of 48U/mL, in accordance with Pizzorusso and coworker (2002). Fast Green allows both the filling of the pipette and the pipette track to be visualized.

2.2.3 Micropipettes

Borosilicate capillary glass pipettes with an outer diameter of 1.2 mm were pulled using a P-30 pipette puller (Sutter Instrument Company, CA). Injections in the MEC were performed at 1.8-3.2 mm below (dorsoventrally) the dura mater. In order to reduce the risk of tissue damage to the cortex, the pipette tapers were made approximately 3.2 millimeters long. The pipette openings were initially <5 µm in diameter, which is too narrow for the fluid to pass through. To obtain pipette openings of 15-30 µm in diameter and an angled break of taper, the pipettes were carefully pushed through a thin tissue paper (“kimwipe” as described by Oesterle, (2011; optimized by Lensjø, 2013). The pipettes were backfilled with mineral oil and mounted in a NanoJect II micro injector (Drummond Scientific Company, PA, USA).

2.3 Surgical procedures

All equipment used for surgery was kept clean and aseptic during the whole procedure. Cotton q-tips were autoclaved and surgery tools heat sterilized in 150˚C for 90 minutes prior to surgery. All surgery equipment was kept in 70% ethanol during the procedure.

2.3.1 Anesthesia and analgesia

The animals were anaesthetized using Isoflurane gas mixed with air at a flow of 2L/min (Baxter, Oslo, Norway). The starting concentration was 5%, but was quickly reduced and kept between 1-2.5% for the remaining of the procedure. Due to occasional instability of the gas anesthetics apparatus, three of the animals were instead anaesthetized by a mix of Ketamine (60 mg/kg) and medetomidine (0.6 mg/kg) injected intraperitonally (i.p.). Once anaesthetized, the rat was placed in a stereotactic frame (World Precision Instruments Ltd, Hertfordshire, UK). The ear bars were placed in the external auditory meatus and the nose-clamp put in position to immobilize the head and ensure a flat-scull position. Local analgesic, Marcain adrenaline (bupivacaine; adrenaline, 1mg/kg), was injected subcutaneously (s.c.) at four positions in the scalp. Temgesic (buprenorphine, 0.04 mg/kg) was used as analgesia during surgery and injected s.c. Heart rate, blood O_2-saturation and core temperature were constantly monitored using a MouseStat system (Kent Scientific, USA). Breathing rate was closely inspected at frequent time intervals. For post-surgical pain relief and infection prevention, animals received s.c. injections of Rimadyl (carprofen 5mg/kg), and the antibiotics penicillin G (13.2 mg/kg) and Convenia (cefovecin 28 sodium, 8 mg/kg), respectively. Animals received this treatment for three consecutive days after the surgery. The edges of the wound was kept clean and provided with antibiotic emollient Fucidin.

2.3.2 Stereotactic surgery and craniectomy

When properly placed in the stereotactic frame, the animal's head was shaved from behind the eyes to the neck, and the area was cleaned with ethanol, chlorhexidine and iodine solution. A scalpel was used to make a longitudinal incision spanning from between the eyes to the back of the skull. The underlying skin was moved aside using artery clamps. The skull was exposed and the lambda and bregma located (figure 2.2). Coordinates for the

craniectomy was measured using lambda and the sutures spanning medio-laterally (ML) relative to lambda as reference points. A hand-held Perfecta-300 dental drill (WandH Nordic, Sweden) with a polishing drillbit (Dental Burs, USA) was used to make the craniectomy, and drilling was continued until the transverse sinus was visualized. An area of the cortex of approximately 1.5x1.0 mm was exposed in front of the sinus edge. During the entire procedure, the scull and exposed cortex were kept moist by applying sterile 0.9% sodium chloride (NaCl) solution. Jewelers' screws were used for grounding and stabilization of the implant. Four screw holes were made anterior of bregma (two for grounding) and three posterior of lambda.

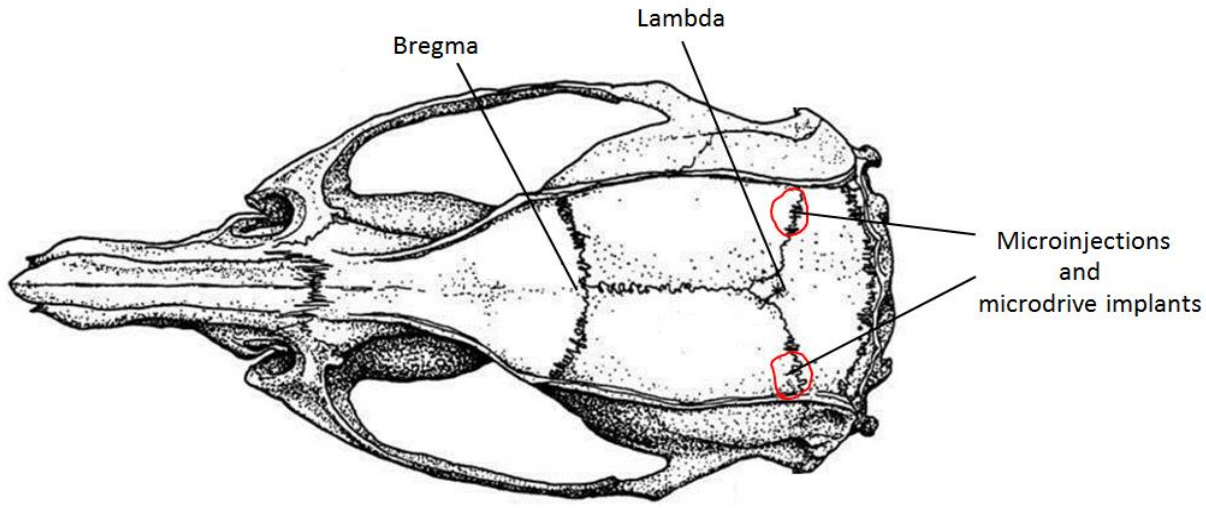

Figure 2.2. Dorsal view of the rat skull showing the bregma, lambda and sites for microinjections and microdrive implantation (marked by red circles). Modified from Paxinos and Watson (1998).

2.3.3 Microinjections of chondroitinase ABC

A glass pipette was loaded with the chABC/Fast Green mix. The enzyme was injected in the MEC of both hemispheres at two ML coordinates and two DV coordinates (see table 2.1), approximately 0.4-0.5 mm anterior of the sinus edge, and in a 10-15 degree angle posterior-anterior in the sagittal plane. Each site received 30-40 single injections of 9.2 nl chABC/Fast Green, and the pipette was kept in position in the injected area for at least ten minutes after the last injection in order to let the enzyme diffuse into the tissue before removing the pipette.

Table 2.1. Stereotatic coordinates for chABC injections. AP, anterioposterior relative to the transverse sinus; ML, mediolateral relative to the midline; DV, dorsoventral relative to the dura mater. Each injection site received a dose of 40x9.2 nL chABC/FastGreen (total: 370 nL per site). Total volume injected per hemisphere was approximately 1.5 µL.

	ML	AP	Angle	DV	Dose
Left/right hemisphere	4.7±0.3 mm	0.4±0.1 mm anterior of sinus	10-15° anterior of sinus, sagittal	2.4±0.2 mm	370 nL
				3.0±0.2 mm	370 nL
	4.4±0.2 mm	0.4±0.1 mm anterior of sinus	10-15° anterior of sinus, sagittal	2.4±0.2 mm	370 nL
				3.0±0.2 mm	370 nL

2.3.4 Microdrive implantation

Microdrives were implanted bilaterally in the same area of the craniectomy as the chABC injectons. However, to ensure that the tetrodes were lowered ideally in between enzyme injection positions, the coordinates were used for the microdrives were adjusted accordingly.

The following coordinates were used for bilateral microdrive implantation:

AP, 0.4±0.1 mm anterior of the transverse sinus; ML, 4.5±0.3 mm; DV, 1.6±0.1 mm.

The dura mater was carefully removed and the microdrives mounted to special holders on the stereotactic frame. The correct coordinates were measured using the same landmarks as described for the chABC injections. The microdrives were lowered carefully into the cortex in a 5-10° angle posterior-anterior in the sagittal plane. Coordinates varied to some extent (0.1-0.3 mm), as the animals were of different sizes and blood vessels in the cortex had to be avoided when lowering the tetrodes.

When placed at approximately 1500-1600 µm, the outer cannula enveloping the inner cannula and tetrodes were lowered and placed on top of the dura. For protection of the cannulas and tetrodes, the exposed area of the cortex was filled with Spongostan (Ethicon, Norderstedt, Germany) and saline solution. To anchor the microdrive implant and cover the exposed skull, dental acrylic cement was applied and left to dry for stabilization. If needed, any sharp edges of the dental cement around the implant were removed. The two microdrive

implants and the dental cement had a total weight of approximately 7 grams. This corresponds to 1.5-2.0 % of the body mass of an adult rat of 500 grams, which represent a minimal load on the animal.

All animals used for electrophysiology had bilateral implants, ensuring recordings from both hemispheres simultaneously.

For control animals, with microdrive implants only, the procedure was the same as described above, however no injections of chABC were performed. For animals used as histology controls, the craniectomy and microinjections were conducted as described above, but no dental cement was applied. The craniectomies were filled with KwikSil silicone (World Precision Instruments Ltd, Hertfordshire, UK), and the wound sutured by 6-10 stitches. Animals without implants were housed in normal cages post-surgically and had ad libitum access to food and water. Animals with Microdrive implants were housed individually to prevent damage to the implant by other animals.

2.4 Electrophysiology

Prior to electrophysiological recordings, the animals were handled once a day for several weeks, and trained to run in the recording arena. The recording arena was a 1x1 m square metal box with black walls (height 0.5 m) and black laminate floor. To ensure good behavior and coverage of the entire box, the rats were encouraged to run continuously by giving them small chocolate treats scattered on the floor during trials. The animals were lightly food deprived in order to motivate them to search for the treats. All recordings were conducted in awake and behaving animals. In order to let them recover from surgery, recordings were not initiated until minimum three days after surgery.

2.4.1 Recording set up

Animals with microdrive implants were connected to a daqUSB recording system (Axona, Herts, UK) via a multichannel head stage. The lightweight multi-wire cable from the head stage was interconnected to a counter-weight system, allowing the animal to move around freely during recording sessions. A tracker system (Axona Ltd., UK) connected to a camera in

the ceiling above the recording arena was used for tracking of two-spot light diodes attached to the animal's head stage (at 50 samples/s). Thus, running path and head direction during sessions was recorded.

Recording was initiated shortly after placing the animal in the box. To ensure coverage of the entire surface, standard duration time of a recording session was 10 minutes. This made it possible to detect spatially modulated cells. There was only dim lighting of the recording room.

Bilateral implants yielded recording from 32 channels, of which 30 channels were used for single unit recordings. When the signal amplitudes of the spikes exceeded 4-5 times the noise level, data collection started. Signals were amplified 10 000 to 20 000 times, band-pass filtered between 0.8 and 6.7 Hz, and stored to disk at 48 kHz (50 samples/waveform, 8 bits/sample), with a 32-bit time stamp (clock rate at 96 Hz). Spike waveforms were time-stamped and digitized at 32 kHz for 1 ms, and saved to hard-drive for offline analysis.

If no spiking activity was present at a given tetrode depth, the tetrodes were advanced 50 µm in the dorso-ventral plane. Whenever neuron activity was detected, recording trials of twenty minutes were initiated to investigate the response property of the cells. When neuron activity was stable across two consecutive trials, and the cell response properties indicated that the cells were in the entorhinal cortex, novelty and/or remapping experiments were initiated.

Two channels (one from each hemisphere) were used for local field potential (LFP) recordings. Signals were amplified 1500 to 5000 times, lowpass-filtered at 500 Hz and stored to disk at 4.8 kHz (16 bits/sample). Parahippocampal LFP activity is characterized by prominent oscillations in the theta band (6-10 Hz). When the tetrodes were advanced into the EC from the above postrhinal cortex, theta band activity was seen as large regular waves.

2.4.2 Novelty task

Novelty tasks were performed by first conducting one recording trial of 20 minutes in the familiar arena (room A). This was the box in which all prior training and recordings had been performed. The box in the familiar arena had black walls and black laminate floor. A white cue card (A4) was attached to one of the walls. Following the first trial in the familiar arena, the

animal was placed in a novel environment, i.e. a similar box in a separate room (room B). A recording trial of at least 40 minutes was performed in the novel arena, before placing the animal back in the familiar arena for another twenty minutes.

The recording set up scheme is shown in figure 2.4.1.

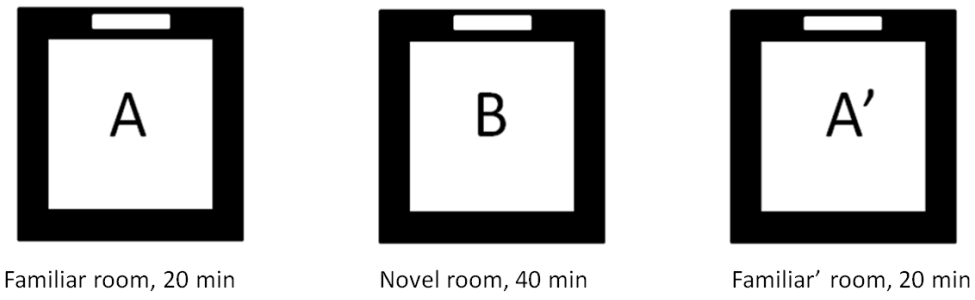

Figure 2.3. Schematic figure of the experimental set up for novelty experiments. Familiar environment: A black metal box in which all training of the animals prior to recordings as well as all first time recordings were performed until grid cells were detected. Novel environment: A similar box with black laminate floor and black walls in a separate room (room B).Both boxes were 1x1 m with 0.5 m high walls on all sides with a white cue card (A4) on one side.

In order to follow the neural activity as the novel room got more familiar, the experiment was repeated for two consecutive days, in which trial duration was reduced to 20 minutes in room B. Both single unit recordings and LFP recordings were conducted in order to examine possible developments in activity of single cells and LFPs. If neuron activity was not stable enough to follow the same neurons through the experiment, the recordings were continued nevertheless, and LFP data were analyzed.

2.5 Histology and immunohistochemistry

Upon sacrifice, animals were anaesthetized with Isoflurane gas (5%), before receiving an i.p. overdose of Pentobarbital sodium (52.5 mg/kg; 25 mg/kg). Transcardial perfusion was performed when the animal was deeply anaesthetized using 0.9 % saline solution followed by 4% performaldehyde solution (PFA) in PBS. The brain was removed and post-fixed in 4% PFA for at least 24 hours.

After incubation in 30% sucrose/PBS solution for minimum 48 hours, the brain was flash-frozen and mounted in a cryostat (CM1950, Leica Biosystems) holding -19°C. Sections of 40-60 µm (depending on the staining protocol) were cut in the sagittal plane and put into wells containing PBS, or directly onto SuperfrostPlus glass slides (Thermo Fisher Scientific, Oslo, Norway).

2.5.1 Nissl staining using Cresyl violet

Sections from animals used for electrophysiology were stained for Nissl bodies in order to locate traces of the implanted tetrodes. This was done to verify the recording position of the tetrodes and to examine tissue damage caused by the implants and glass pipettes. Sections on Superfrost slides were treated with chloroform/ethanol overnight, then hydrated in distilled water and immersed in Cresyl Violet (Sigma-Aldrich) solution, before dehydration in ethanol and finally xylene. Cover slips were mounted with Entellan (Merck Millipore, Darmstadt, Germany) and the slides left to dry under fume hood overnight.

Tissue shrinkage was accounted for when investigating the depth of the tetrode tracks. Fixation and freezing of brain tissue normally causes a shrinkage of <20% (M.P. Witter, personal communication). A more detailed description of the Nissl staining protocol is found in the Appendix.

2.5.2 Staining of PNNs using *Wisteria floribunda* agglutinin and diaminobenzidine

In order to investigate the distribution and morphology of PNNs in MEC, sections were with a biotin-conjugated agglutinin from *Wisteria floribunda* (WFA) for labeling of PNNs.

Sections containing the injected area were collected in wells containing PBS, with a maximum of six sections per well. Free floating sections were blocked in TS-PBS and incubated on an automatic shaker at 4̊C overnight in 1/200 dilution with primary biotin-conjugated agglutinin antibody, from the plant *Wisteria floribunda* (WFA) (Sigma-Aldrich Chemie, Munich, Germany). The following day, sections were treated with H_2O_2 to quench endogenous peroxidase activity, and incubated with biotinylated horse raddish peroxidase, followed by an avidin-biotin complex staining solution (Thermo FisherScientific, Oslo, Norway). A 3,3'-

diaminobenzidine (DAB)(Sigma Aldrich Chemie, Munich, Germany)/Tris-HCl solution was added to the sections for visualization of the staining, and the DAB-reaction was stopped by adding TNS. Sections were washed with TNS, followed by mounting onto Superfrost plus glass slides using a fine brush and TNS. Sections were dried at 37° C and dehydrated in 70%, 80%, 90% and absolute ethanol respectively. Sections were finally immersed in xylene and mounted as described for the Nissl stained sections. Sections from animals used for electrophysiology were double stained for Nissl bodies by doing a hydration protocol (absolute ethanol, 90%, 80%, 70% ethanol respectively, and water, followed by the Nissl protocol). A more detailed protocol for the DAB staining is found in the appendix.

2.5.3 Fluorescent double staining of PNNs and PV^+ cells

Sagittal free floating sections ranging from 25-60 µm were used for fluorescent staining of PNNs and double staining parvalbumin-positive (PV+) cells. Sections were washed, blocked and incubated as described for the DAB stained sections. If double staining for PV+ cells, sections were incubated with WFA and a primary rabbit-anti-parvalbumin (Swant, Marly, Switzerland) in TS-PBS at 4° overnight. The following day, sections were washed and incubated with secondary antibodies goat-anti-rabbit Texas Red-X (Invitrogen Life Tech, California, USA) and Streptavidin Alexa 488 fluor conjugate (Invitrogen Life Tech, California, USA), respectively. Incubations were kept in the dark at room temperature. Cover slips and FluorSave Reagent (Merck Millipore, Darmstadt, Germany) were used to secure the sections. Detailed protocol is found in the Appendix.

2.6 Data analysis

2.6.1 Immunohistochemical analysis

Sections stained with WFA/DAB and Nissl were assessed for PNN regeneration and/or tetrode tracks. The sections were photographed using an Axiocam HRZ camera connected to an Axioplan 2 microscope (both provided by Carl Zeiss, Oberkochen, Germany). Photos were taken as single snaps at different magnifications (5x, 10x and 20x respectively), or as whole-section photos stitched together using AxioVision (Carl Zeiss, Oberkochen, Germany) and the

MosaiX Acquisition/Stitching modules. For light and epifluorescent microscopy, images were taken using 5x, 10x or 20x objectives. For fluorescent microscopy, RFP longpass filter (BP 546/ LP 590) and GFP bandpass filter (BP 450/BP 515-565) were used. A 40x Leica objective (Numerical Aperture 0.8) and GFP 920 nm excitation was used for the two-photon laser microscopy.

Sections stained with fluorescence were photographed using the same software, and performed in the dark to avoid photo bleaching of the sections. Some of the fluorescence stained sections were used for two-photon laser microscopy. Adobe Photoshop2 (Adobe, California, USA) was used for image merging, cropping and minor contrast adjustments.

In order to quantify the PNN regeneration in chABC treated animals, the relative intensity of WFA staining was measured using a grey scale converting method. Images were loaded into ImageJ (National Institute of Health, Maryland, USA) and inverted relative to an 8-bit color scale of 255 grey shades of individual intensity values. Three locations of 1.0 x 0.4 mm in the injected area of MEC were compared to the control area. In order to compare the staining intensity between different animals with different levels of background staining, a reference area of the same size in the frontal cortex was selected. This area is situated far from the injection sites and it shows a high intensity of WFA staining. The ratio between the staining intensity measured in EC divided by the intensity in frontal cortex was used to compare the expression of PNNs between animals. In order to quantify the regeneration of PNNs, the mean ratios of the grey scale measurements were normalized relative to the 3-day control (which was set as 0% regeneration of PNNs), and converted to percentages.

2.6.2 Spike sorting

The graphical cluster-cutting software Tint (Axona Ltd, Herts, UK) was used for spike sorting. Based on waveform amplitudes of single spikes on the four-channel tetrode, a two-dimensional scatter-plot is created. Spikes from individual neurons tend to have different waveform or amplitude on the different channels, thus forming distinguishable spike clusters, separated from clusters of other cells on the same tetrode, and separated from the noise (Harris et al., 2000). Clusters are manually enclosed within a boundary and assigned a unique color (figure 2.4). Noise was removed, and effort was made to ensure that all spikes belonging

to one cell were included. Furthermore, to verify proper separation of the clusters, temporal autocorrelation in Tint was used. This reveals the lag period between spikes within a cluster. If the lag period was less than 2 ms, the cluster was assumed to contain spikes from more than one cell (Harris et al., 2000), and were excluded from the analyses.

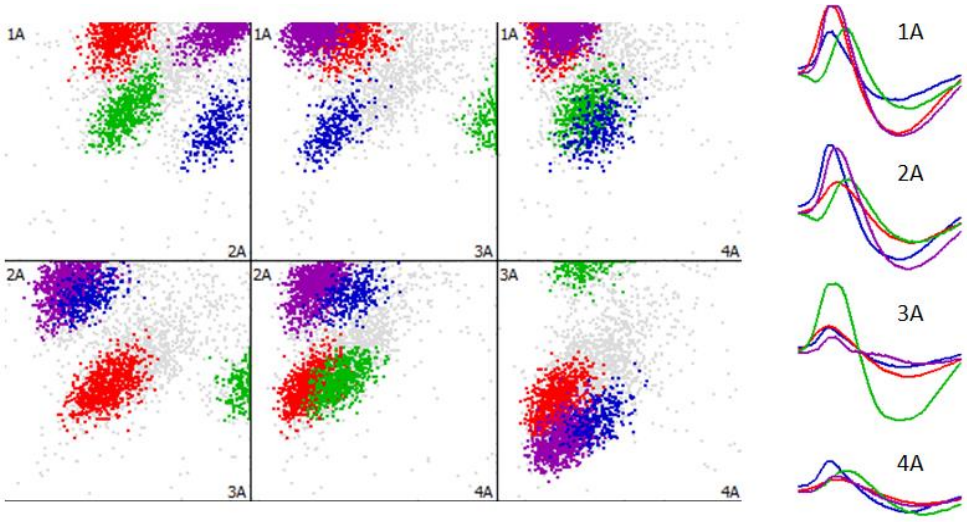

Figure 2.4. Manual spike sorting. The different distances from the electrodes to neurons in the tissue will result in different waveform and amplitude on each of the four electrodes in a tetrode. The amplitude of single spikes from each tetrode (1A-4A) is measured and plotted as scatter plots. Spikes from different cells tend to form separate clusters. Clusters are cut manually by enclosing them within a boundary, and labelling them with a unique color. Mean waveform for each spike cluster is shown to the right in corresponding colors.

2.6.3 Classification of cells

Recorded cells were classified as either inhibitory interneurons or excitatory cells, using the AxWaveform 2.1 application in MatLab (R. Skjerpeng, NTNU,Trondheim, Norway). This program calculates different parameters based on cell waveform. The parameters that give the clearest separation of cells are peak-to-trough time and peak-to-base:base-to-trough ratio (Csicsvari et al., 1999; Iurilli et al., 2013). Peak-to-baseline and peak-to-trough amplitudes (in mV) were used to calculate base-to-trough values (figure 2.5). Thereafter, the ratio peak-to-base:base-to-trough was calculated and plotted against peak-to-trough time (ms). The criteria set for selection of inhibitory interneurons were a peak-to-trough time <0.3 ms and peak-to-base:base-to-trough ratio <5 (Iurilli et al., 2013). Cells which passed these criteria were manually inspected by looking at cluster cut quality and rate maps.

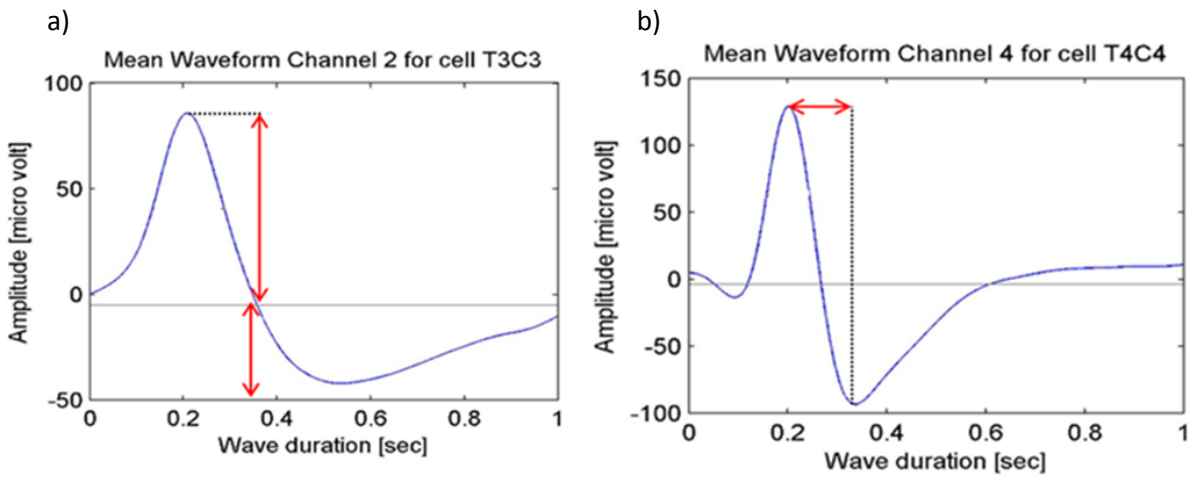

Figure 2.5. Cell waveform images from the AxWaveform analysis. a) Typical waveform of an excitatory neuron. Red arrows indicate peak-to-trough and trough-to-base amplitudes. b) Typical waveform of an inhibitory interneuron. Red arrows indicate peak-to-trough time.

By superimposing spikes from separated unit into the trajectory of the rat, we can visually inspect the spatial firing pattern of the cells (figure 2.6). Thus, neuronal activity which is strongly correlated with space can be detected (i.e. grid cells). An interneuron will typically have spike activity covering the entire surface of the recording arena. Moreover, the recording of the two head stage light diodes provides information about head direction of the animal whenever a cell is firing, thus head direction cells and conjunctive cells can be detected. If a cell fulfilled the waveform analysis criteria, but did not display typical interneuron properties in terms of spatial distribution of spikes, they were not classified as interneurons.

2.6.4 Spatial correlation

For assessment of the stability of the grid cells' firing patterns, spatial correlation between individual sessions was calculated (using custom written MatLab, Molden and Skjerpeng, NTNU, Trondheim, Norway). This program correlates the firing rates in corresponding bins for the pair of smoothed rate maps for each cell. Pixels visited more than 150 ms in either trial were included in the sample.

To investigate the establishment of grid fields in a novel environment, spatial correlation for two minute blocks of the session were compared to the last twenty minutes of the session. This gives a measure of how rapidly the grid fields establish in the novel arena.

2.6.5 Analysis of local field potentials (LFPs)

The LFP data were analyzed using the custom written MatLab program AxTheta (T. Hafting, University of Oslo, Oslo, Norway). The program calculates the power of the oscillations at different frequencies from 1-30 Hz (the abundance of a given frequency within one recording session).

2.6.6 Statistical analyses

Statistical analyses were performed in Microsoft Excel 2010 (Microsoft, Washington, USA) and SigmaPlot 12.0 (Systat Software, San Jose, California, USA). For group comparisons, normality tests were conducted. If normality was detected, a two-sided student's T-test was applied. If normality failed, a non-parametric Mann-Whitney rank sum test was used. Values are reported as single values or as median and/or mean with standard errors of mean (SEM).

3. Results

For electrophysiology analyses, firing rate comparisons are presented as box plots. The box plots show the variations within a population, standard deviation and median values. Error bars indicate standard deviation and outliers are marked as black dots. Seventy-five % of the data are included in the upper quartile, and the lower quartile includes the lower 25% of the population. The animal count is denoted N and cell count denoted n, if not stated otherwise.

3.1 Methodological assessments

In order to establish correct coordinates for the microinjections, surgical training on three rats was performed prior to chronic implantation of electrodes and electrophysiology experiments. Thereafter, microinjections with chABC were performed in eleven rats, of which six were used as histology controls and five rats had electrodes implanted. In addition, three rats were implanted with electrodes only.

The histology from four chABC treated animals implanted with microdrives showed no sign of PNN degradation in MEC upon sacrifice 21 days after microinjections. The WFA stained sections from these animals were further assessed using grey scale measurements. It was concluded that the microinjections had no visible effect on the desired area. Electrophysiological data from these animals were therefore treated as control data. Most likely, improper aliquotation or storage of the enzyme rendered it ineffective. A new batch was therefore acquired. One animal with bilateral chABC injections and microdrive implants showed a profound digestion of PNNs in the MEC. In this animal, the electrodes were also confirmed to be located in the MEC and the regeneration of PNNs in MEC at day 21 was approximately 30%. In two animals implanted with electrodes the electrophysiological recordings from MEC yielded few single units, however the LFP recording of brain oscillations (EEG) were included in the analyses.

Post mortem inspection of the histology was performed to determine the electrode trace and recording location in all animals used for electrophysiology. Brains from animals injected with chABC were stained for PNNs and counterstained for Nissl bodies in order to confirm the PNN digestion at recording sites, whereas brains from control animals were stained for Nissl bodies

to detect the tetrode tracks. Staining sections for Nissl bodies showed minimal damage to the tissue from the microinjections and electrode implantation (see Appendix, section 6.4).

3.2 Histology

3.2.1 Perineuronal nets in MEC

The distribution and expression pattern of PNNs is highly variable across different brain areas. In order to confirm the expression of PNNs and investigate their distribution in MEC, control sections were stained with WFA/DAB. The different cell layers in MEC have different functional properties, which may be reflected in the PNN expression.

a)

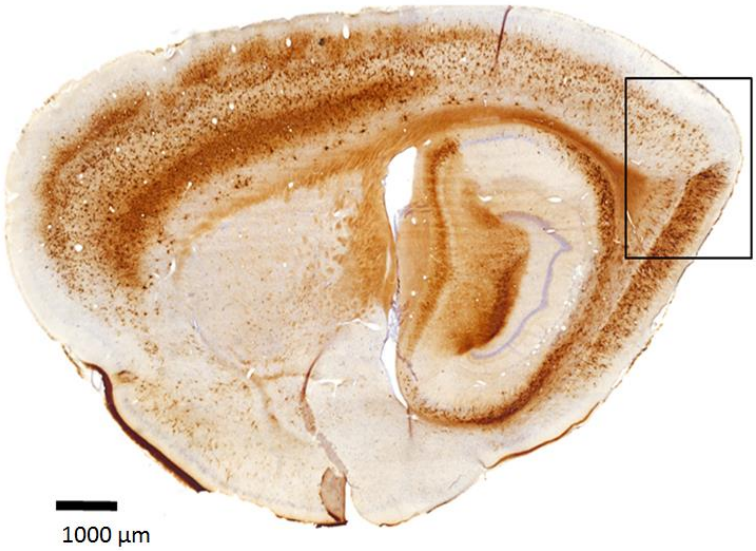

b)

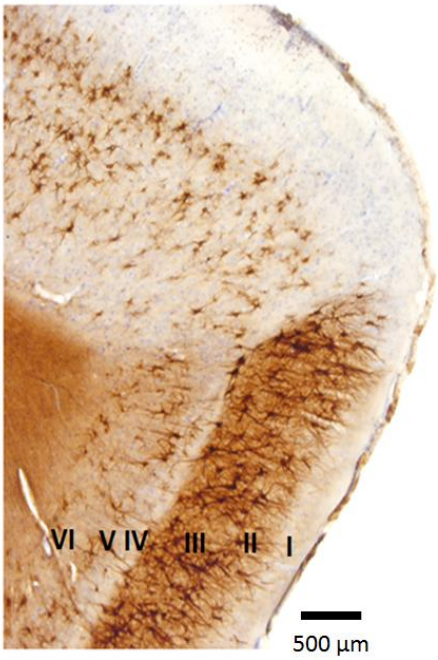

c)

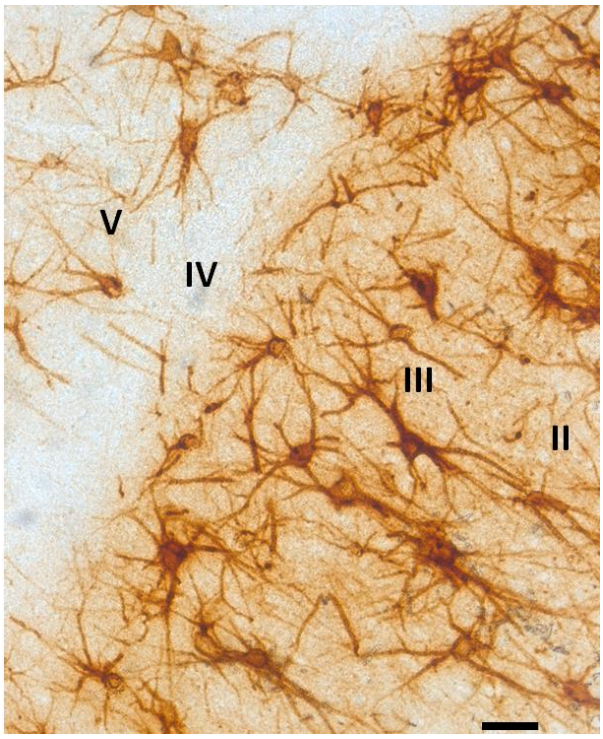

Figure 3.1. Staining of perineuronal nets (PNNs) in the rat medial entorhinal cortex (MEC) using *Wisteria floribunda* agglutinin (WFA) and diaminobenzidine (DAB). a) Sagittal section stained for PNNs with WFA/DAB and cell bodies using Cresyl violet. b) Magnified view of PNN staining of different layers of the dorsal MEC. Layer I is the molecular cell-free layer; superficial layers II/III show dense, pronounced labeling; the lamina dissecans (layer IV) shows minimal labeling; deep layers V/VI show some labeling. c) A different section magnified to show details of PNNs stained with WFA/DAB. Cells in different layers of MEC are tightly enwrapped by PNNs. Note the distinct labelling around cell somata in layers II/III and less dense staining in layer V. Scale bar = 50 µm.

The WFA/DAB staining showed dense expression of PNNs in the entire MEC (figure3.1), with more prominent staining in superficial cell layers (II/III) compared to deep layers (V/VI). The PNNs surround the soma and proximal dendrites of specific neurons (figure 3.1c). Counterstaining with Cresyl violet which labels cell somata, revealed that not all neurons in the MEC are enwrapped by PNNs.

For further assessment of PNN structure around neurons in MEC, control sections were stained with WFA and fluorescent Streptavidin Alexa Fluor and photographed using fluorescent microscopy and two-photon laser scanning microscopy. The fluorescent staining confirmed the expression pattern seen in MEC with WFA/DAB staining, and further showed that dendrites and somata of MEC neurons are enwrapped by PNNs with hole-like openings, which may be sites of synaptic contacts (figure 3.2).

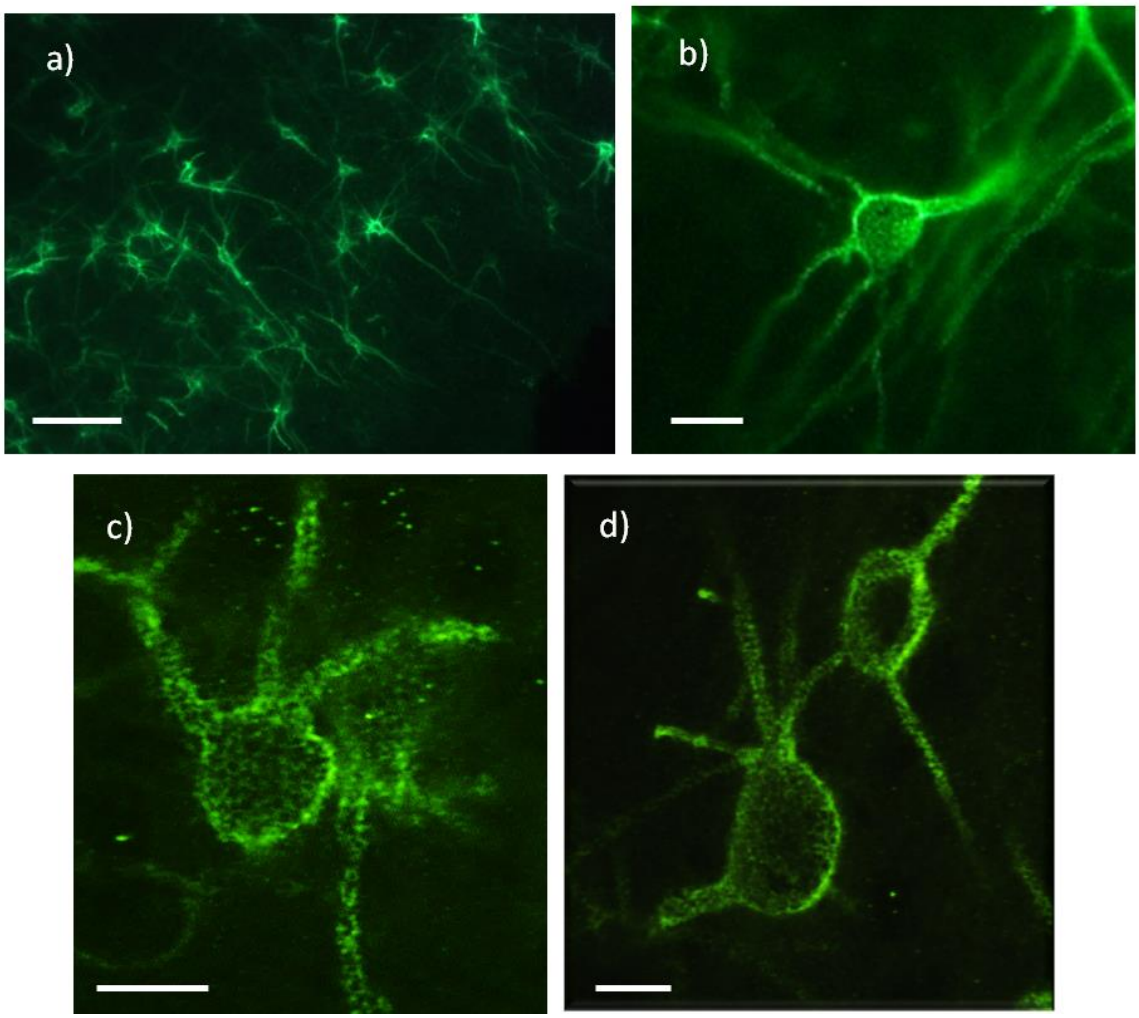

Figure 3.2. Perineuronal nets (PNNs) in the medial entorhinal cortex (MEC) visualized by *Wisteria floribunda* agglutinin (WFA) and streptavidin. a) PNNs enwrapping neurons in MEC superficial layers (II/III), scale bar = 100 µm. b) Single neuron in MEC layer II showing PNN enwrapping cell soma and proximal dendrites. Scale bar = 20 µm .c)-d) Two-photon laser scanned microscopy showing structure of PNNs enwrapping proximal dendrites and somata of neurons in MEC. Sites of synaptic contact may be seen as small black holes spanning the mesh-like structure of the PNNs. Scale bars = 10 µm.

3.2.2 Perineuronal nets co-localize with PV^+ cells in MEC

In the visual cortex, PNNs have been shown to selectively enwrap PV+ cells. In order to investigate whether such co-localization of PNNs and PV+ cells also applies for the MEC, fluorescent double staining was conducted using WFA/streptavidin for visualization of PNNs, and anti-parvalbumin/Texas Red for staining of PV+ cells.

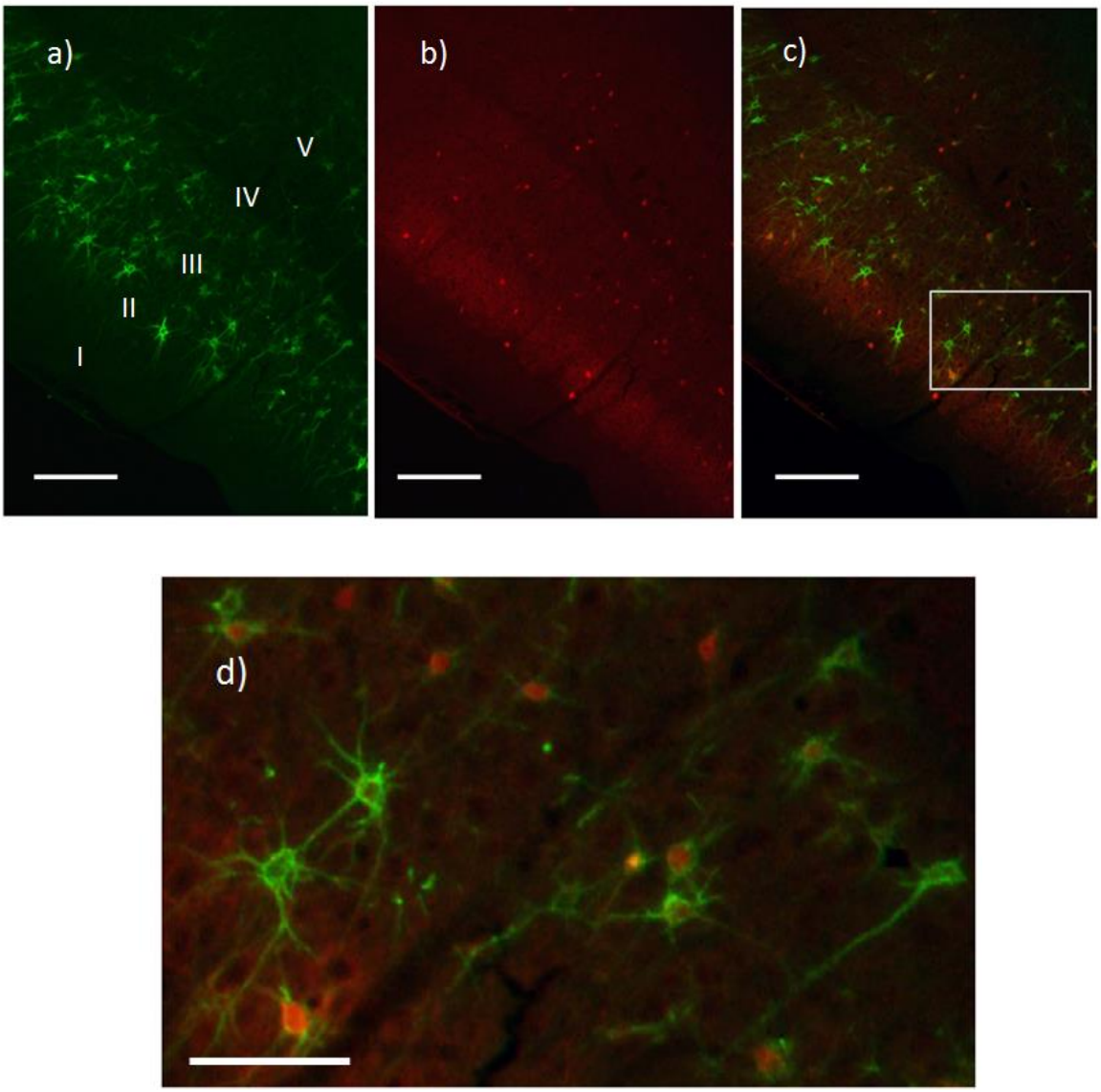

Figure 3.3. Epifluorescent microscopy images showing double staining for perineuronal nets (PNNs) and parvalbumin (PV) positive cells in the medial entorhinal cortex (MEC) using *Wisteria floribunda* (WFA)/streptavidin and parvalbumin/Texas Red. a) WFA/streptavidin staining for PNNs (green). b) Same section stained with PV/Texas Red. c) Merged, scale bars 500 µm. d) Magnification for visualization of PNNs enwrapping PV+ cells in MEC layers II/III, scale bar = 200 µm.

Cells expressing PV was present in all cell layers of MEC and the PV^+ cells co-localize with PNNs in MEC ((figure 3.3). There were also PV^+ cells without PNNs and PNNs enwrapping parvalbumin-negative cells (figure 3.4). There was a tendency across several sections, and animals, that the proportion of overlap between PV and PNN labeling appeared to be lower than what has been reported in the rodent cortex (60-70% overlap). However, quantification of the PNN/PV overlap was beyond the scope of this study and was not pursued further.

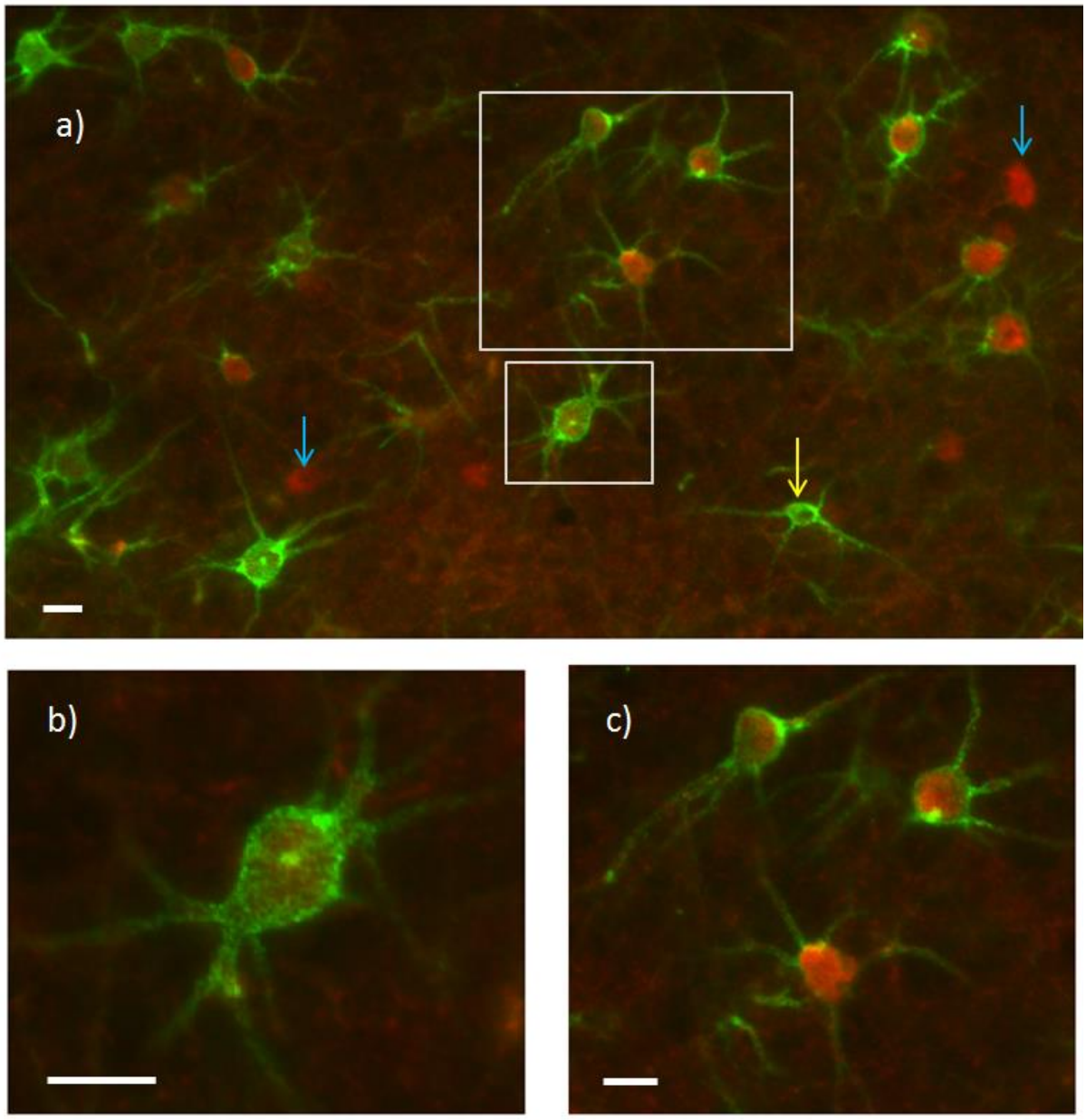

Figure 3.4. Double staining for perineuronal nets (PNNs) and parvalbumin (PV) positive cells in medial entorhinal cortex (MEC). a) Section from layer I/III MEC stained with WFA/streptavidin for labeling of PNNs (green) parvalbumin for labeling PV^+ cells (red). Blue arrows indicate PV^+ cells with no PNN around soma and dendrites and yellow arrow indicates PNN enwrapping a parvalbumin-negative cell. b)-c) Magnifications of PNN enwrapped PV+ cells showing the dense packing of PNN around cell somata and proximal dendrites. Small hole-like openings can be seen covering the surface of PNNs. Scale bars = 20 µm.

3.2.3 Regeneration of PNNs after chondroitinase ABC treatment

In the visual cortex, PNNs regenerate relatively quickly after chABC treatment (Lensjø, master thesis 2013). In order to confirm that the enzyme chABC had indeed degraded PNNs in MEC,

and to ensure that the PNN labeling was low throughout the period of electrophysiological recordings, sections were stained with WFA and the labeling quantified at different time-points after injection. The injections of chABC resulted in enzymatic digestion of PNNs in all layers of MEC (figure 3.5). The PNNs were completely digested by chABC after three days. At day 21, the PNNs showed 30 % regeneration. The calculation of PNN regeneration was assessed by using grey scale measurements in ImageJ in accordance with Lensjø (2013,). For details, see figure 6.3 in the Appendix.

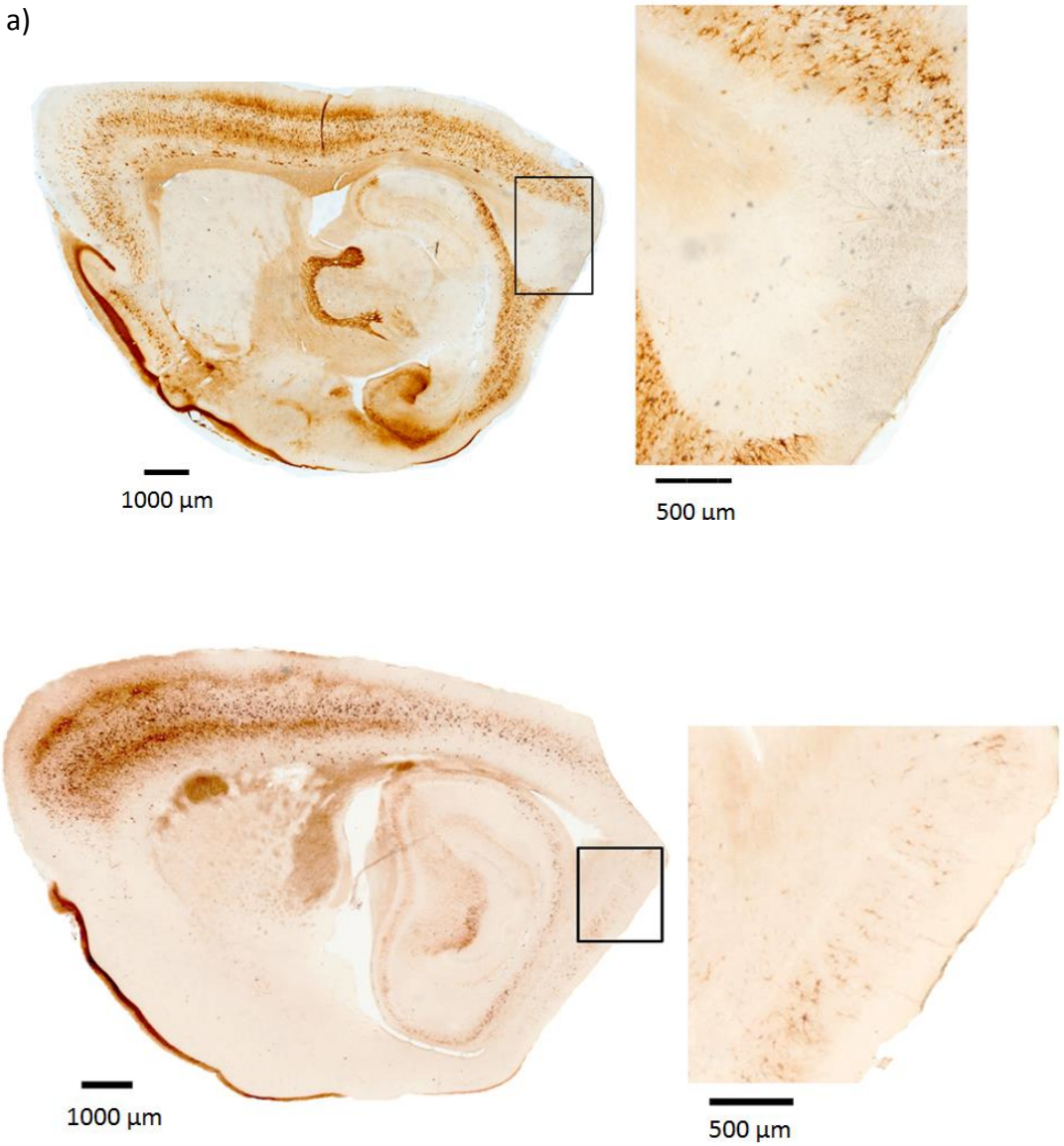

Figure 3.5. Sagittal sections stained with *Wisteria floribunda* agglutinin (WFA) for labeling of perineuronal nets (PNNs) after chondroitinase ABC (chABC) injections in medial entorhinal cortex (MEC). a) The PNNs are completely digested 3 days after chABC treatment. b) Twenty-one days after chABC treatment, he PNNs show a regeneration of approximately 30%.

3.3 Electrophysiological recordings

3.3.1 Cluster cutting and classification of neurons

Different classes of neurons were recorded from MEC in five control animals and in one chABC treated animal. A total number of 343 single units were recorded from the MEC of five control animals (n=204) and one chABC treated animal (n=139).

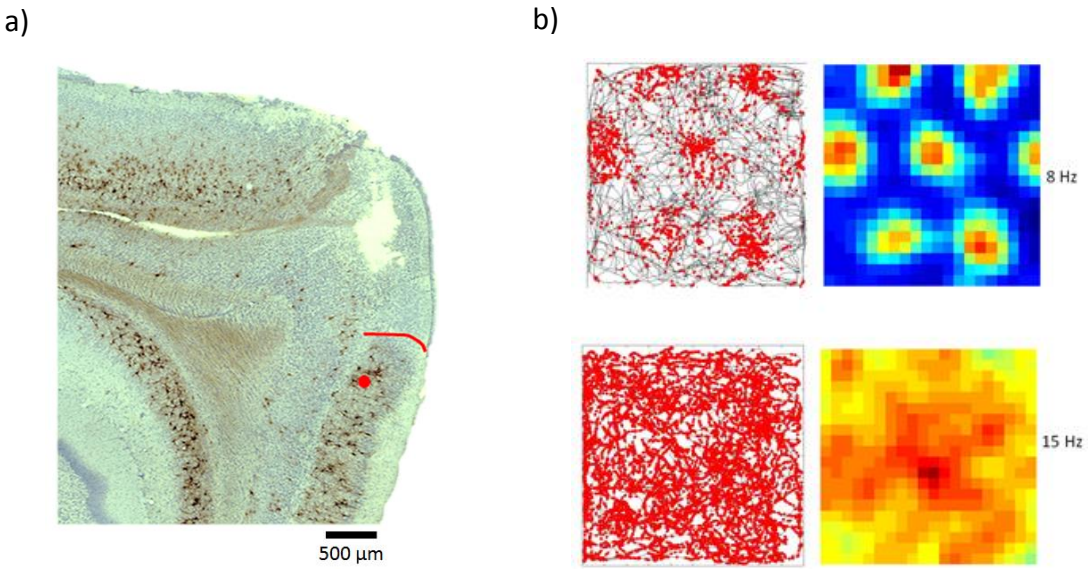

Figure 3.6. Electrophysiological recordings of neuronal spiking activity in medial entorhinal cortex (MEC). a) Sagittal section stained with Cresyl violet for cell bodies and Wistera floribunda (WFA) for labeling of perineuronal nets (PNNs) in MEC. Ret dot indicates one of the recording positions of the tetrodes and red line indicates the dorsal border of MEC. Scale bar = 500 µm. b) Spatial distribution of neuronal spikes from cells recorded from EC in a rat running in a square box. Top panel: Spatial distribution of spiking activity typically seen for grid cells. Note the regular spacing between the firing fields. Trajectory of the rat is shown in black with spiking activity of single neurons superimposed in red (left). Color coded rate map is shown to the right. Bottom panel: Spatial distribution of spiking activity typically observed for interneurons. Note that the cell has spiking activity covering the entire surface of the box.

Neurons were classified as either excitatory cells or inhibitory interneurons based on different waveform parameters. Briefly, neurons were separated based on peak to trough time and the ratio in amplitude between wave peak to baseline and baseline to trough (see figure 2.6, section 2.6.3). Furthermore, the spatial distribution of spiking activity and rate maps of individual cells were manually inspected for confirmation of their properties (figure 3.6b).

A total number of 49 cells were characterized as inhibitory interneurons, 41 from controls and eight from the chABC animal.

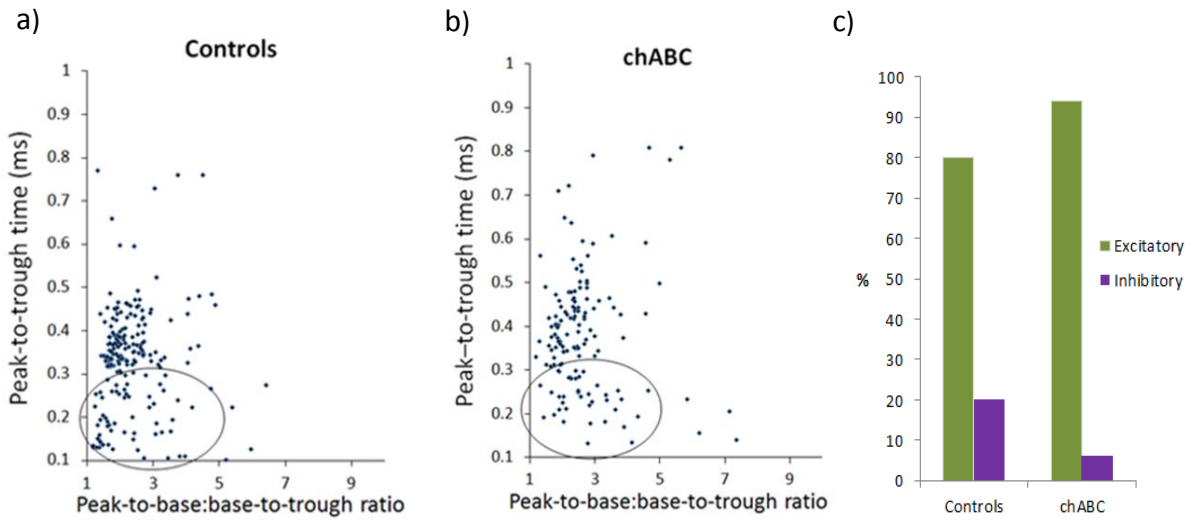

Figure 3.7. Classification of neurons as excitatory or inhibitory cells. a)-b) Scatter plots showing the clustering of neurons from a) five control animals (n = 204) and b) one chondroitinase ABC treated animal (n = 139) based on waveform peak-to-trough time and peak-to-base:base-to-trough ratio. Cells with peak-to-trough time <0.3 ms were manually inspected by looking at firing pattern and cut quality. c) Percentages of excitatory and inhibitory neurons recorded from control animals (excitatory cells = 163, 80%, interneurons= 41, 20%) and the chABC animal (excitatory cells=131, 6%, interneurons = 8, 94%).

A number of 34 cells (corresponding to 11.2 % of total cell numer) were further classified as grid cells (chABC n=14, controls n=20) and 48 were identified as HD cells (chABC n=22, controls n=26). Two border cells and three conjunctive cells were also characterized in the population of excitatory neurons. The remaining excitatory neurons did not show spatial or directional modulation and were therefore excluded from further analyses.

3.3.2 Neurons recorded from MEC

First, we wanted to investigate the spatial modulation of neurons in animals treated with chABC. Grid cells, conjunctive cells and head direction cells were recorded from MEC in a chABC treated animal and controls (figure 3.8).

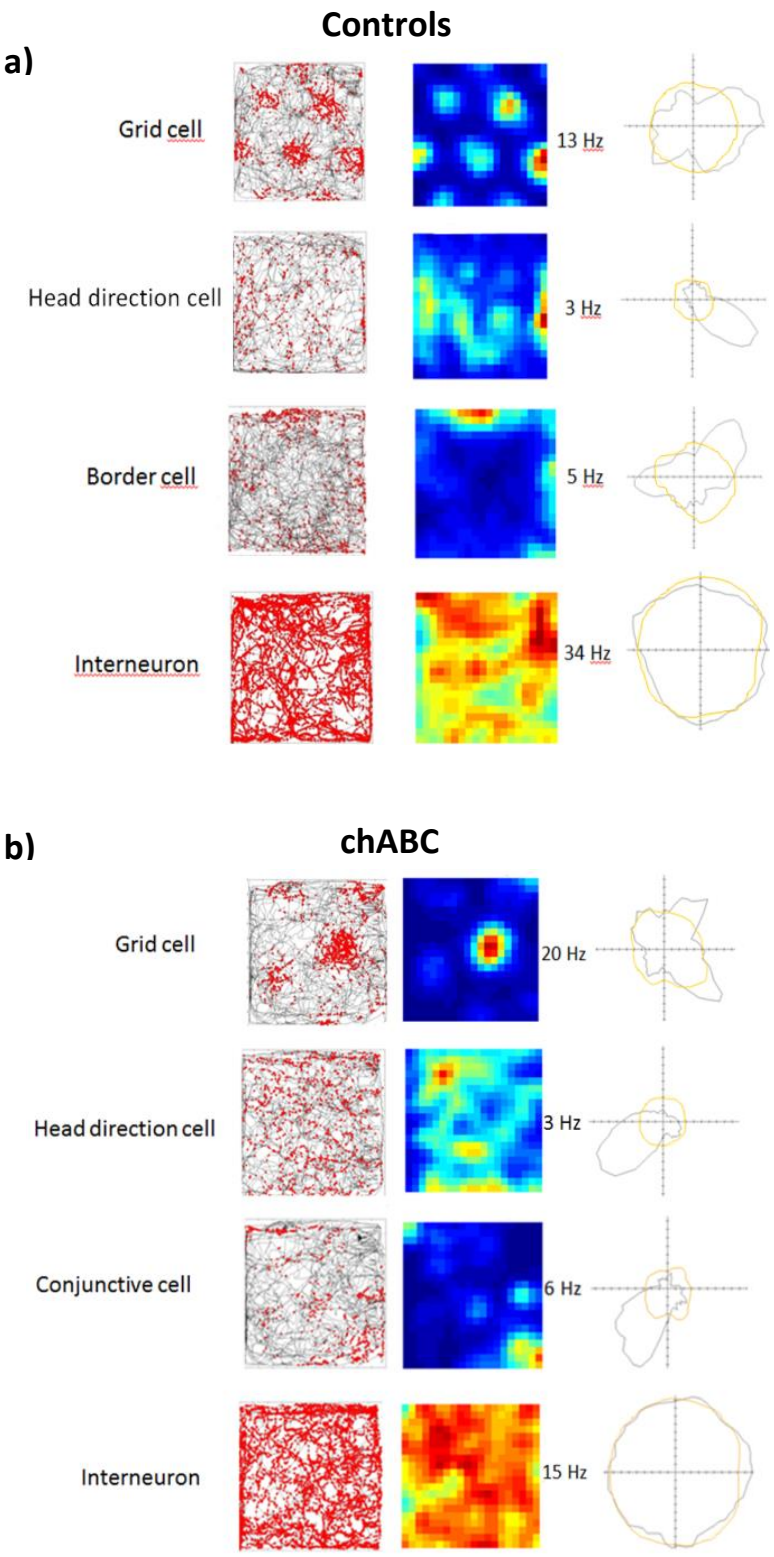

Figure 3.8.Different cell types recorded from medial entorhinal cortex (MEC) in a control animal and an animal injected with chondroitinase ABC (chABC). Trajectories of the rats are shown (black) with spikes superimposed (red), color coded rate maps with peak firing rate (Hz), and polar plots of preferred head direction (black shows the preferred head direction of the recorded cell; orange shows the mean head direction of the animal during neuronal activity through the recording session). Note the spiking activity of interneurons which covers the entire surface of the box. a) Control animals. b) chABC treated animal.

3.4 The effect of PNN degradation on interneuron activity

The PNNs are thought to support the high firing rates of PV+ fast-spiking inhibitory interneurons. Therefore, the differences in average interneuron firing rates between the chABC treated animal and controls were investigated.

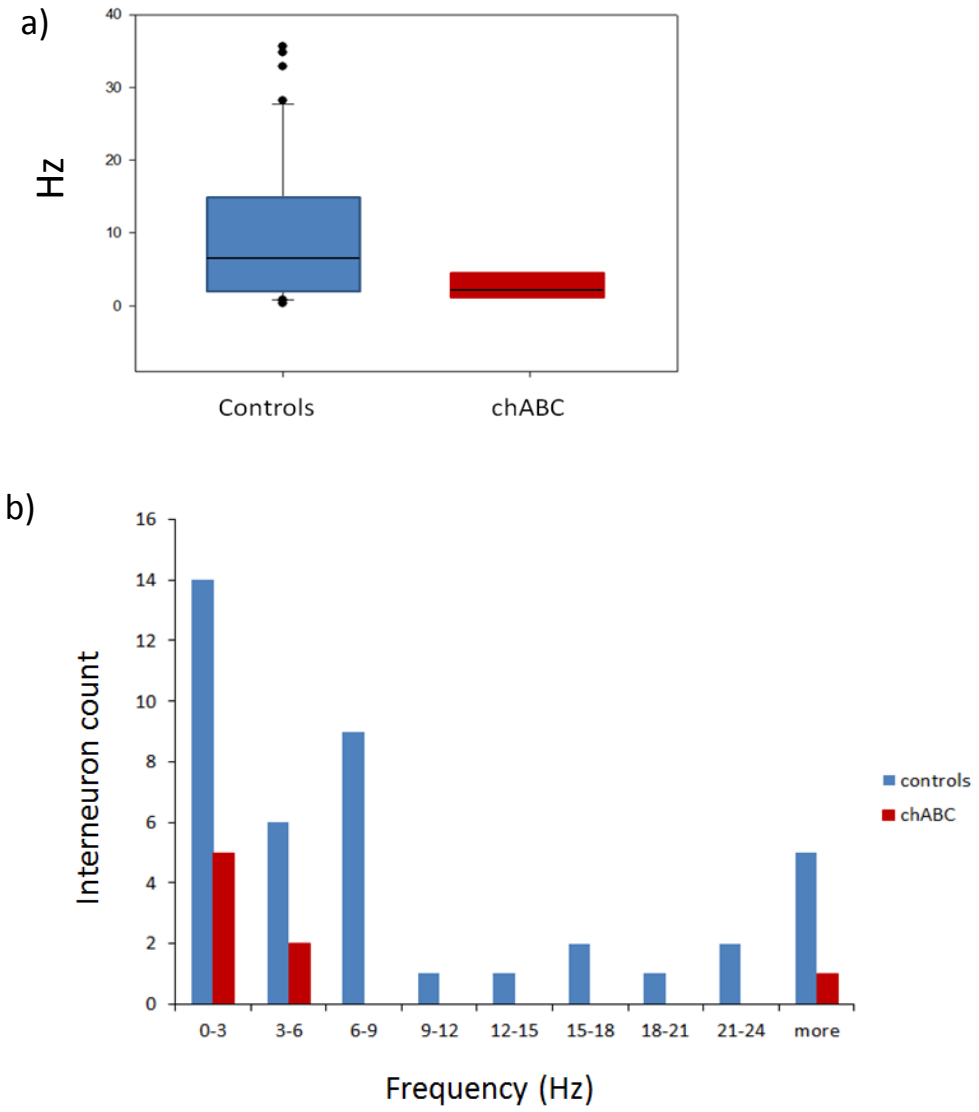

Figure 3.9. Interneuron mean firing rate in the chondroitinase treated animal and controls. a) Average firing rate of inhibitory interneurons recorded from the medial entorhinal cortex (MEC) in five control animals (cells n= 41, mean firing rate = 9.6 ± 1.59, median = 6.31) and one animal injected with chondroitinase ABC (chABC) (cells n = 8, mean = 6.8, SEM = ± 5.10, median = 2.32). Mann-Whitney rank sum test was used (P = 0.172). An equal variance test was applied and found a difference in variance of 2,858 and p = 0,487. b) Comparison of distribution of interneuron firing rates (Hz) in the chABC treated animal and five control animals.

Comparison of interneuron firing rates showed no statistical significant difference (P = 0.172, Mann-Whitney rank sum test), however interneurons from the chABC animal (n = 8, mean = 6.8, ± 5.10, median = 2.32) showed a tendency of lower firing rates compared to controls (n = 41, 9.6 ± 1.59, median = 6.31).

The distribution of interneuron firing rates showed that a large proportion of the interneurons from control animals had low firing rates, but still a number of neurons had firing rates above 10 Hz (n=12). Interneurons from the chABC treated animal showed that only one cell had a firing frequency above 6 Hz (figure 3.12b).

3.5 The effect of PNN degradation on normal principal cell function

Fast-spiking inhibitory neurons are thought to control the firing activity of principal neurons in MEC, and this fast-spiking activity may be supported by PNNs. While firing rates of inhibitory neurons were not significantly different in the two groups, there was a tendency for neurons from the chABC injected animal to have lower activity. Thus, PNN degradation may have an indirect effect on principal neuron activity. To assess this, the firing properties of grid cells were investigated in controls and in the chABC treated animal.

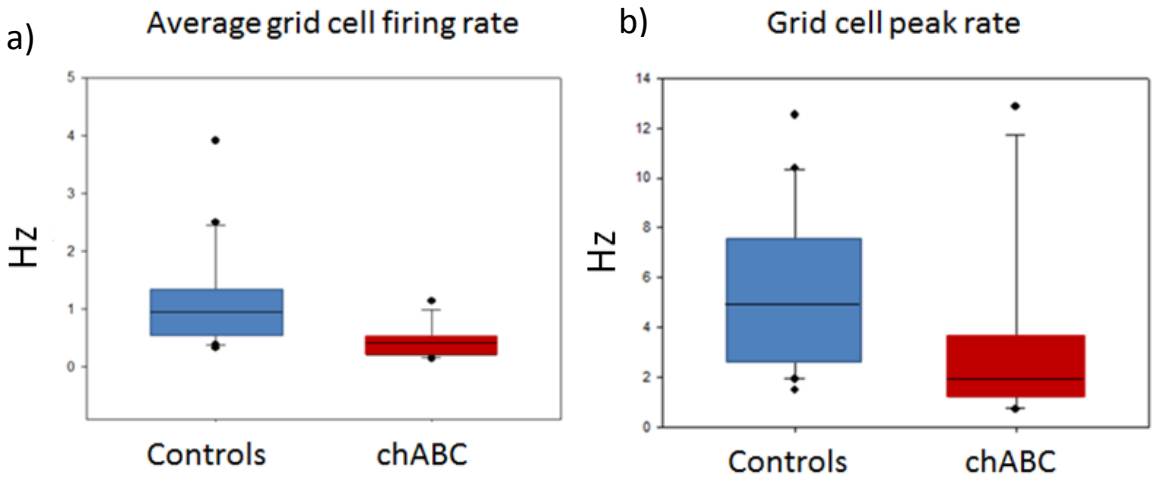

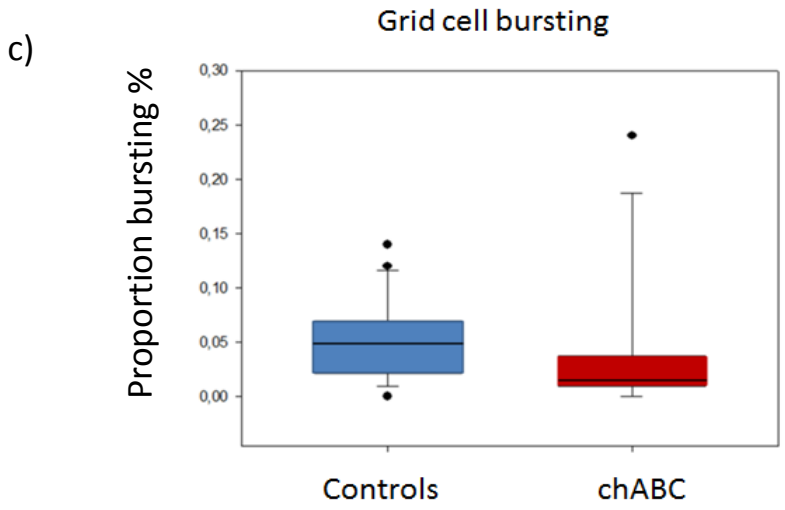

Figure 3.10. Firing properties of grid cells recorded from medial entorhinal cortex (MEC) in an animal injected with chondroitinase ABC (chABC) (n= 14)and five control animals (n=20). Average firing rate, peak rate and proportion of bursting was calculated. a) Average firing rate was lower in the chABC animal compared to controls, P<0.001. Controls, median = 0,910± 0.19; chABC, median = 0,395 ± 0.07. b) Peak rate was lower in the chABC animal compared to controls, P = 0.009. Controls, median = 4,85 ± 0.69; chABC, median = 1,9 ± 1.0. c) Proportion of bursting was lower in the chABC animal compared to controls, P = 0.037. Controls median = 0,05 ± 0.008; chABC median = 0,015 ± 0.018. Mann-Whitney rank sum test.

Grid cells from five control animals (cell n = 20) were compared to grid cells from one chABC treated animal (cell n = 14). Mean values from grid cells recorded on consecutive trials were calculated before including them in the analyses. The data was tested for normality by use of a Student's t-test, in which normality failed (P < 0,050). Grid cells from the chABC treated animal had a statistically significant reduced average firing rate (0.4± 0.07 Hz) compared to controls (0.9± 0.19 Hz) (P <0.001), and a statistically significant lower peak rate (1.9 ± 1.0 Hz) compared to controls (4,85 ± 0.69 Hz) (P = 0.009, Mann-Whitney rank sum test). Furthermore, the proportion of bursting activity was significantly lower in the chABC (0.015±0.018) animal compared to controls (0.05±0.008). (P = 0.037, Mann-Whitney rank sum test).

Firing properties of HD cells recorded from MEC in the two groups were also compared. This comparison is highly relevant as HD cells seem to be stronger driven by their inputs (from e.g. presubiculum) compared to the more internally drive grid cells (Bonnevie et al., 2013).

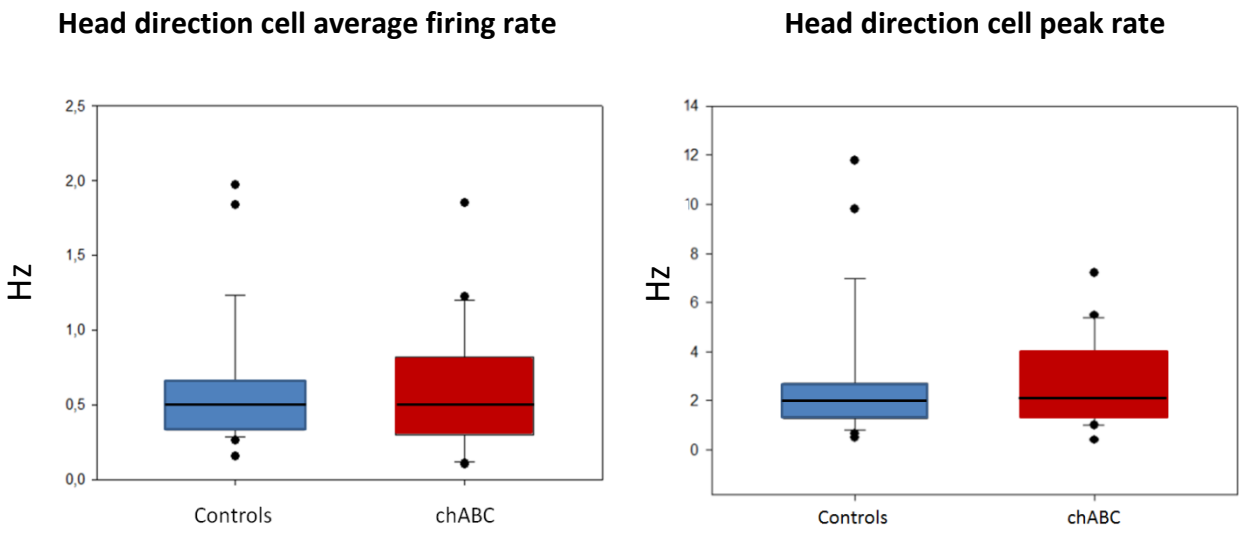

Figure 3.11. Firing rates of head direction (HD) cells in an animal injected with chondroitinase ABC (n= 22), compared to HD cells(n =26) from five control animals. Both HD cell average firing rate and peak rate are unchanged in the chABC treated animal a) HD cell average firing rate: no differences were observed for. Controls, median = 0,5 ± 0.08; chABC, median =0,505 ± 0.09, P = 0,942, Mann-Whitney rank sum test. b) HD cell peak rate; no differences were observed between chABC and controls for controls, median = 1,99± 0.52; chABC, median = 2,16± 0.37, P = 0,463 Mann-Whitney rank sum test.

In contrast to the reduced activity of grid cells in the chABC treated animal, no statistical significant differences were found in firing rate (P=0.942) or peak rate (P=0.463) for HD cells between the chABC treated animal (n=22, median = 0.5±0.09, 2.16±0.37) and controls (n=26, median=0.5±0.08, 1.99±0.52) (Mann-Whitney rank sum test).

3.6 Comparison of grid cells in a chABC treated animal and controls

The firing activity of grid cells creates a repetitive pattern of firing fields with regular spacing covering the surface explored by the animal. The PNNs have been shown to restrict plasticity in adult animals, and the enwrapping of neurons in the MEC by PNNs may contribute to the hard-wired grid cell network. Therefore, disruption of PNNs by chABC might affect the rigidity of the grid pattern. In order to investigate this, rate maps of grid cells recorded from MEC of the chABC treated animal and control animals were investigated.

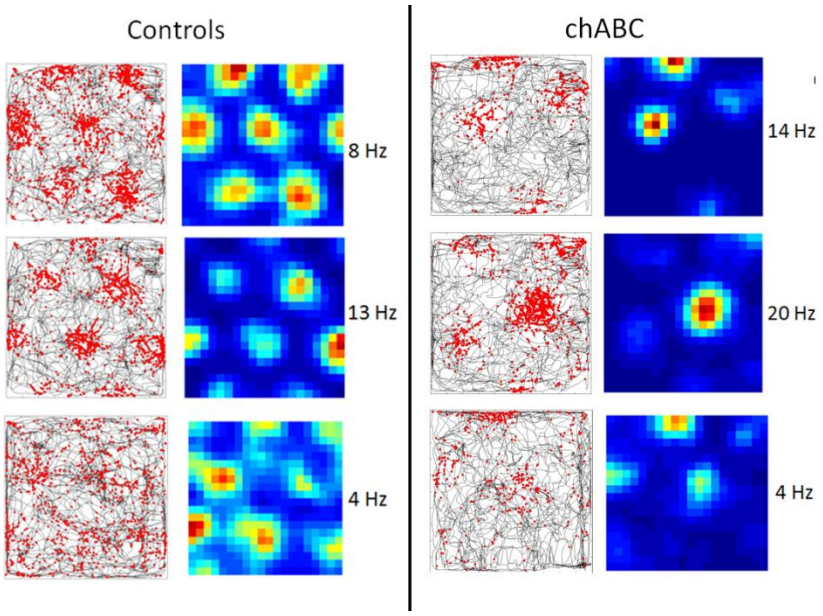

Figure 3.12. Three grid cells from two control animals (left column) and three grid cells from a chondroitinase ABC injected animal (right column) recorded from the medial entorhinal cortex (MEC). Trajectory of the rat (black) with action potentials from the grid cell (red) superimposed and color coded rate maps with peak rate (Hz) are shown. Note the regular grid pattern seen in controls and the less regular pattern in the chABC treated animal.

Irregular firing fields in grid cells have not previously been reported. From visual inspection of the rate maps, grid cell patterns in the chABC treated animal appear less regular than those of control grid cells. Further investigation of this finding was beyond the scope of this project and the regularity of grid patterns was not further quantified.

3.7 Grid cell stability

The firing pattern of grid cells normally show high stability over time and may persist over days if the animal is repeatedly exposed to the same environment (Hafting et al., 2005). In the current project, grid cells recorded from MEC in control animals showed a stable firing activity on repeated trials and over consecutive days in the familiar environment (figure3.13).

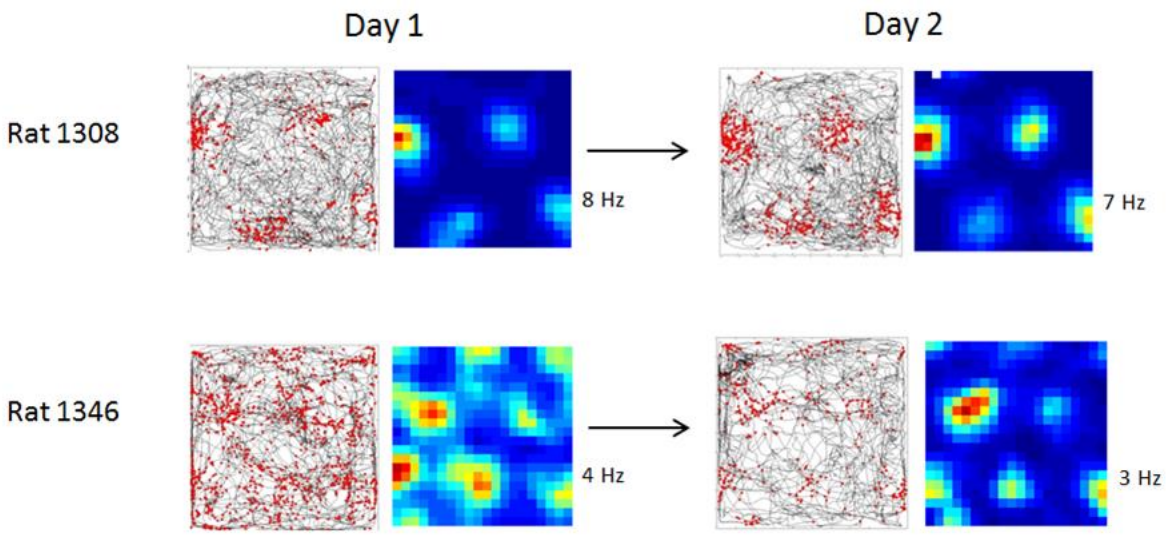

Figure 3.13. Two grid cells recorded from medial entorhinal cortex in two control animals. Both cells remain stable and fire at the same locations on two consecutive days in a familiar environment. The trajectory of the rat is shown in black with spiking activity superimposed in red. Corresponding rate maps show firing activity with red as peak activity and dark blue with no firing activity, and peak firing rate (Hz) is shown to the right.

3.8 The effect of PNN removal upon novelty exposure

In order to navigate in a new environment, the animal must quickly update and encode new spatial codes for self-localization. This process is likely to involve plasticity mechanisms. Upon novelty, grids cells tend to shift their firing pattern relative to a familiar one (Hafting et al, 2005; Barry et al., 2012). Digestion of PNNs by chABC may open up for plasticity and alter the grid cells networks' ability to encode new spatial memories. Therefore, the chABC treated animal was introduced to a novel environment in order to investigate the effect of PNN removal on novel spatial representations in MEC.

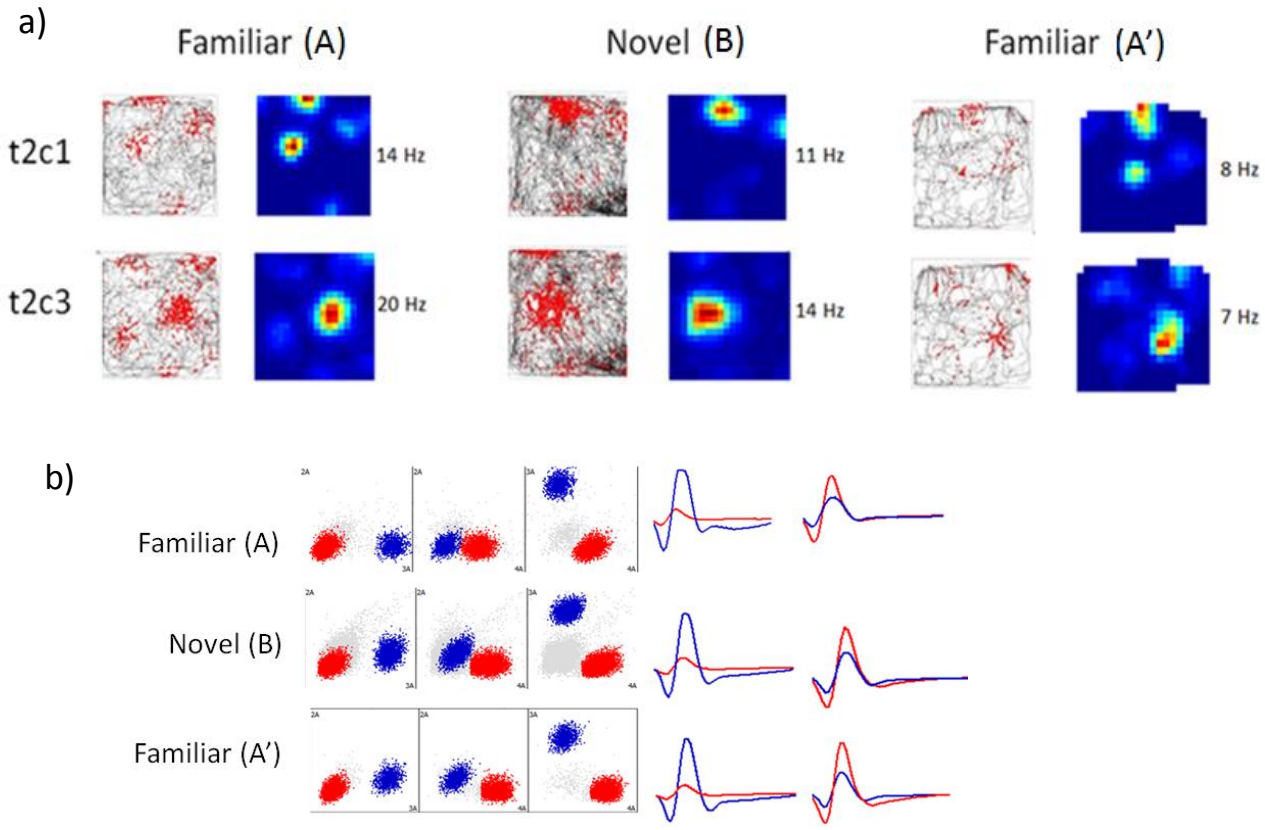

Figure 3.14. Two grid cells recorded on the same tetrode in a chondroitinase ABC treated animal during a novelty task. a) Trajectory (black) with cell spikes superimposed (red), corresponding color coded rate map and peak rate (Hz) of cell 1 and cell 3 on tetrode 2, recorded on subsequent trials in familiar arena (20 min), a novel arena (40 min) and familiar arena (20 min). b) Cluster cutting window from Tint for the same grid cells and corresponding waveforms in familiar1, novel and familiar2. Note the stability of clusters and cell waveforms on consecutive trials, while there is a change in the grid firing pattern in the novel arena.

The grids seemed to expand their fields in the novel arena and appeared irregular compared to the familiar arena. Grid expansion in novel environments has been reported previously (Barry et al, 2012). Additionally, cell number t2c1 appeared to have irregular grid spacing in the familiar arena (figure 3.14a). Such irregularity of grid fields has not been previously reported. While grid fields reorganized between the two environments, the two grid cells formed highly distinguishable clusters and could easily be followed and separated across all trials (figure 3.14b).

To further investigate the possible effect of PNN removal on plasticity when exposed to a novel environment, the formation (its stability) of grid fields in the novel arena was closer investigated.

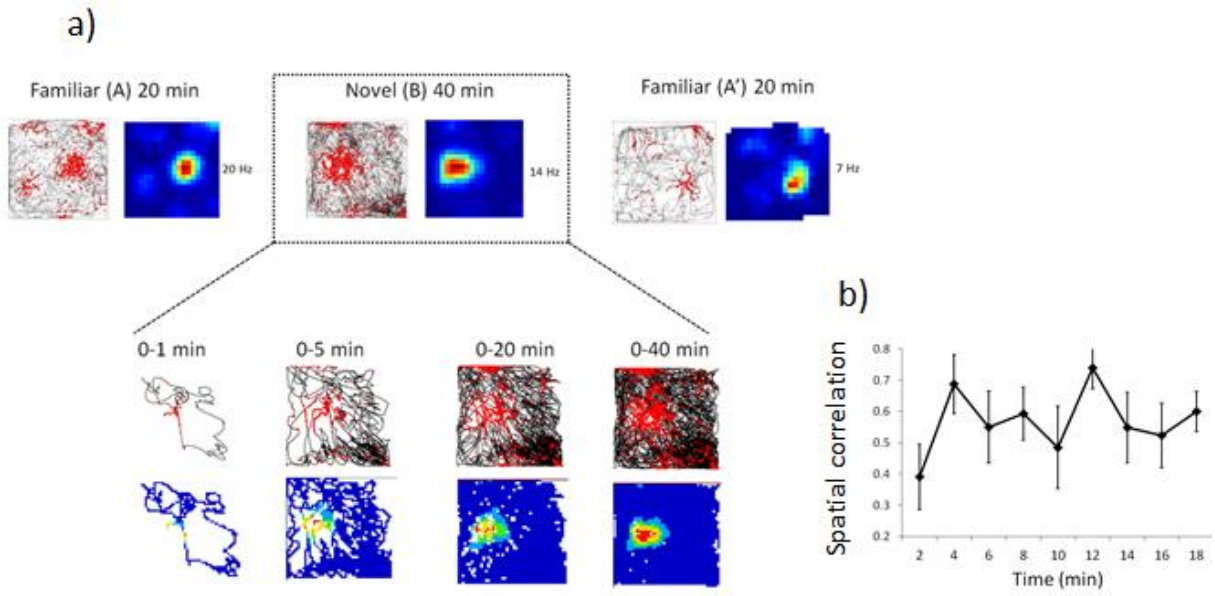

Figure 3.15. The formation of grid fields in a novel environment in an animal injected with chondroitinase ABC (chABC). a) Top panels show the trajectory of the rat with cell spikes superimposed in red, and corresponding rate maps of the same cell recorded in familiar (A), novel (B) and familiar (A'), respectively. Bottom panels show trajectories and rate maps as the grids establish in the novel environment after 1, 5, 20 and 40 mins, respectively. b) Mean spatial correlation two-by-two minutes in a novel arena for five grid cells in a chABC treated animal. The spatial correlation of preceding 2 min blocks of the trial and the final firing field (last 20 min) is compared. Cells n = 5, SEM = ±0.06 to ±0.13.

The formation of grid fields in the novel environment was rapid and established after a few minutes (figure 3.15). This was confirmed by calculating the spatial correlation of five grid cells for the first twenty minutes of the trial in the novel environment. The spatial correlation rapidly stabilized within the first five minutes (4 min=0.7±0.01; 6 min=0.550±0.115) and remained at a high level throughout the recording session (figure 3.15b). All mean values and SEM are found in table 6.1 in the Appendix.

3.9 The effect of PNN removal on grid stability

In order to further investigate the effect of PNN digestion on the stability of grid cell firing patterns, firing activity of the same cell was followed across three days as the novel environment became familiar to the animal. In the following, the familiar arena will be referred to as room A and the separate room (which serves as the novel arena on day 1) is referred to as room B.

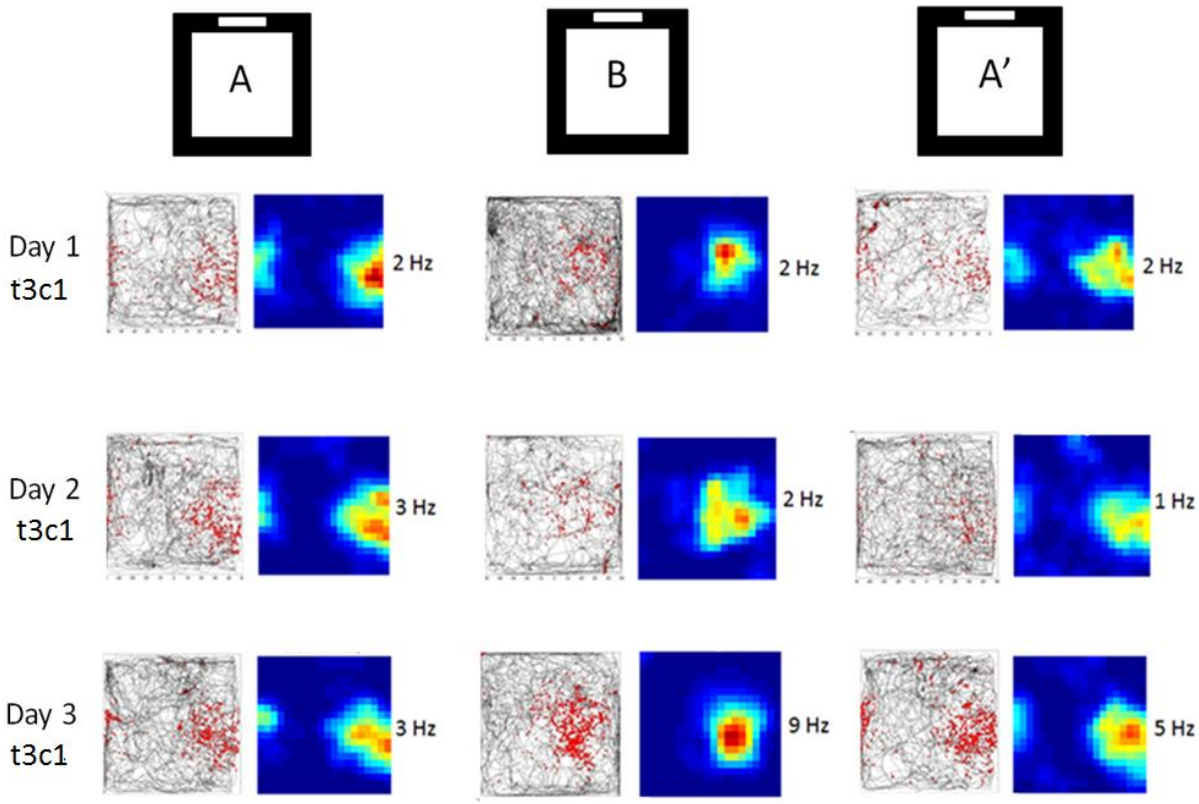

Figure 3.16. A grid cell (cell number t3c1) recorded from medial entorhinal cortex (MEC) in an animal injected with chondroitinase ABC (chABC) during trials in a familiar (A), novel (B) and familiar (A') arena, respectively, over 3 consecutive days. On day 1, a 20 min session in a familiar arena (A) was followed by a 60 min session in a novel arena (B). Thereafter, the rat was placed back in the familiar arena (A') for 20 mins. On day 2 and 3 the session in B was reduced to 20 min. The cell was recorded at a ventral location (DV 2900 µm) in MEC where the grid spacing is larger compared to more dorsal locations, the grid therefore expands the recording arena.

During the course of three days, the grid cell showed stable firing fields in both room A and room B, as seen from the trajectories and rate maps (figure 3.16). In order to confirm this, spatial correlation of the grid cell was calculated for day 2 and 3 using day 1 as reference. This was done for room A and room B, respectively.

The spatial correlation of the grid fields across three days ranged from 0.7-0.85 (room B) and 0.85-0.9 (room A). Thus, the spatial correlation was high in both rooms indicating that the grid fields quickly formed into stable spatial representations that were recognized across days (see figure 6.4 in the Appendix).

3.10 The effect of PNN removal on the local field potential

The local field potential (LFP) is the synchronized firing activity of neuronal ensembles, and is important for the maintenance of many cognitive functions including the encoding of spatial memories. In the MEC, a strong theta oscillation activity can be recorded in the 6-12 Hz band (Hafting et al., 2005). Due to the possible importance of PNNs for the activity and thus oscillatory synchrony of PV^+ cells, the digestion of PNNs in the EC may affect the LFP. Therefore, EEG was recorded in all trials to investigate if degradation of PNNs affected theta band activity.

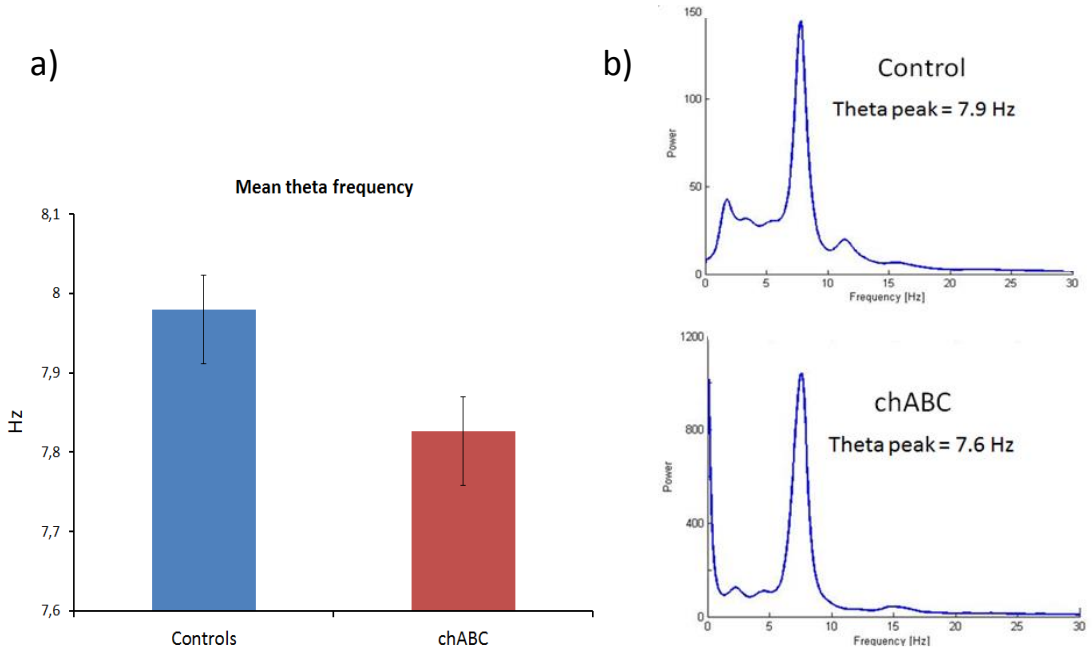

Figure 3.17. Theta band frequency in the local field potential (LFP) in four control animals and a chABC treated animal a) Mean theta frequency calculated for controls (session values n= 205, median = 7,9, ±0.043) and the chABC animal (session values = 97, median = 7,7 ± 0.068).P = <0,001, Mann-Whitney rank sum test. b) Power spectra from a control animal and chABC animal showing theta peak values. X-axis, theta frequency (Hz); Y-axis, power (the quantification of a frequency during one recording session).

Mean theta frequency was significantly lower in the chABC treated animal (mean = 7.83 ± 0.068, median 7.7) compared to controls (mean =7.98 ± 0.043, median 7.9) ($P < 0.001$, Mann-Whitney rank sum test), as seen in figure 3.17a.

For further investigation of theta frequency after PNN removal, the LFP data from the novelty tasks and remapping experiments were assessed. Upon an animals' first encounter with a novel environment, Jeewajee and collegues (2008) have showed that mean theta frequency is

reduced. In agreement with this, the control animals in my study showed a reduction of theta frequency of 0.2 Hz upon novelty exposure and a subsequent rise back to the "familiar" level when placed back in the familiar arena. In contrast, the chABC treated animal showed an increase of 0.2 Hz in the theta frequency band when the animal was placed in the novel arena (figures 3.18 and 3.19).

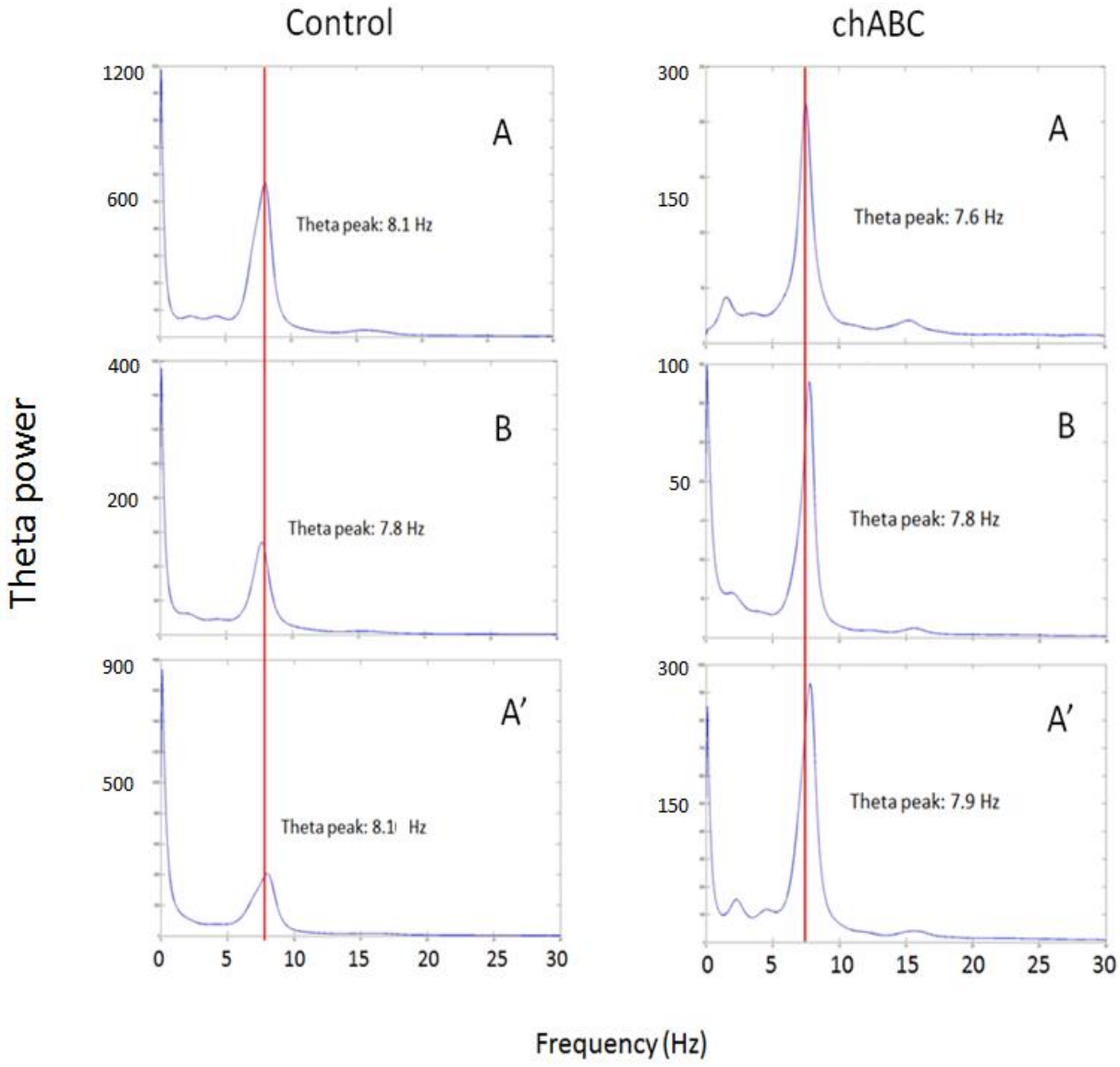

Figure 3.18. Theta power spectra in familiar (A), novel (B) and familiar (A) arenas (subsequent recordings on the same day) for the chondroitinase ABC (chABC) treated animal and controls. Top panels, familiar arena; middle panels, novel arena; bottom panels, familiar' arena. Note that for the control animal, the theta peak is lowered in the novel arena, whereas in the chABC animal, the theta peak increases.

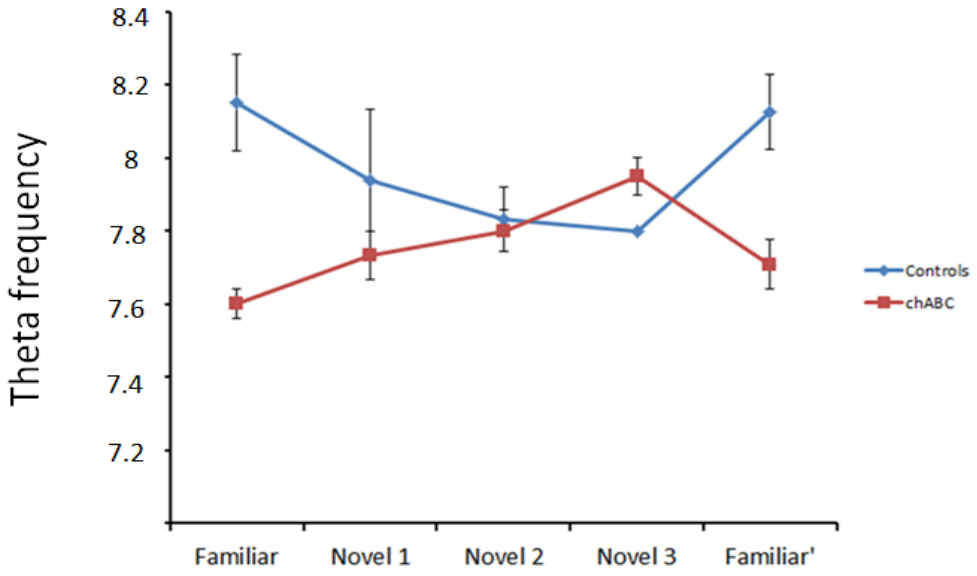

Figure 3.19. Mean theta frequency (Hz) in a chondroitinase ABC (chABC) treated animal (red) and controls (N=4) (blue) during a novelty task. Recording sessions lasted as follows: Familiar = 20 min; novel 60 min (Novel 1 = 20 min, novel 2= 20 min, novel 3 = 20 min, novel 1-3 was a continous recording session); familiar' = 20 min. For each time point, the groups were tested against each other using a Mann-Whitney rank sum test: Fam p = 0.007; novel1 p = 0.373; novel2 p = 0.768; novel3 p = 0.333; familiar' p = 0.015. Each control animal underwent one novelty task; the chABC animal underwent two novelty tasks.

In order to investigate the change in theta frequency compared to the "familiar" levels, the change in mean theta frequency were calculated between the familiar arena and the novel arena, and compared to the change between familiar and familiar' (table 3.1).

Table 3.1. Theta frequency change during a novelty task, where animals are moved from a familiar to a novel arena, and subsequently placed back in the familiar arena. When moving from the familiar to to novel arena, theta frequency decreased in controls and increased in the chABC animal. When placed back into the familiar arena, theta frequency increased to the "familiar" level in control animals, but was still elevated in the chABC animal relative to the familiar level. Mean values for novel arena: controls N = 4, sessions n = 4., mean = 7.86 ± 0.03; chABC N = 1, sessions n = 2;, mean = 7.82 ± 0.05. Mean values for familiar arena: controls = 8.15 ± 0.13, chABC = 7.6 ± 0.04. Mean values for familiar' arena: controls 8.125 ± 0.1; chABC 7.7 ± 0.07.

	Δ Hz Familiar – novel	Δ Hz Familiar – familiar'
Controls	-0.268	-0.025
chABC	0.217	0.11

In control animals (N=4), mean theta frequency was reduced from 8.15 ± 0.13 Hz in the familiar arena to 7.86 ± 0.03 Hz. In contrast, for the chABC animal frequency increased from 7.6 ± 0.04 Hz in the familiar arena to 7.82 ± 0.05 Hz in the novel arena.

The novelty task was repeated for two consecutive days, during which the "novel" arena became familiar to the animal. Recording of theta frequency was conducted in all sessions, and mean theta frequency change between familiar and novel arena was calculated. The values are presented in table 3.2 as Δ frequency in Hz.

Table 3.2. Theta frequency change between familiar and "novel" as the novel environment becomes familiar to the animal. Mean theta frequency values from three control animals (3 remapping experiments) and one chondroitinase ABC treated animal (two remapping experiments).controls novel day 2 mean = 7.7 ± 0.11,

	Δ Hz day 1	Δ Hz day 2	Δ Hz day 3
Controls	-0.268	-0.17	0.033
chABC	0.217	0.125	0.400

During the animal's familiarization with the novel arena, theta frequency in control animals showed a gradual reduction of the frequency change between environments over the course of three days (table 3.2). This indicates that the new environment eventually was experienced as familiar. In contrast, in the chABC animal the difference in theta frequency between the two environments did not decrease across days. In order to obtain a larger dataset from the chABC treated animal, two novelty experiments were conducted in this animal, where two different novel rooms were used. The two experiments were separated by five days. The same tendency appeared in both remapping experiments. This may indicate that the novel environment was not treated as familiar to the animal over the course of the experiments.

4. Discussion

This is the first study to remove PNNs for investigation of neuronal activity and spatial representations in the MEC. Furthermore it is one of very few studies (Lensjø, 2013; Christensen, 2014) to combine microinjections of chABC and chronic electrophysiological recordings at all. Numerous studies have been conducted for investigations of synaptic plasticity in terms of LTP/LTD induction in the EC (Alonso et al., 1990; Yun et al 2002; Cheong et al., 2001), however the role for PNNs in EC plasticity has not been investigated. The purpose of the study was to investigate the role of PNN for the grid cell network, the general activity of principal neurons and interneurons, and for the LFP oscillations in MEC.

4.1 Main findings

Histology showed dense PNN expression in layer II/III of MEC and a moderate expression in layer V/VI. Similar to other cortical areas, I showed that PNNs in MEC mainly enwrap PV+ neurons, but due to a small sample the overlap is yet to be quantified. The chABC treatment in MEC leads to a complete enzymatic digestion of PNNs after three days, and shows a regeneration of approximately 30% after 21 days.

Importantly, a significant reduction in grid cell firing rate and bursting was observed in the chABC animal compared to controls. At the same time, no significant differences were observed in interneuron or HD cell firing rate between the chABC treated animal and controls. Furthermore, the grid fields from the chBAC treated animal showed a surprising irregularity that has not yet been reported.

Upon novelty exposure, oscillations in the theta frequency band in the chABC treated animal increased. In control animals on the other hand, theta frequency decreased when exposed to a novel environment, which is in accordance to previous reports. Also, theta frequency in the chABC animal continued to show a difference when moving from room A to room B on three consecutive days, whereas the difference disappeared in the control animals during the same time course.

4.2 Methodological considerations

Chronic multi-electrode recordings in awake and behaving animals provides several advantages compared to acute single electrode recordings First, using a tetrode configuration instead of single electrodes, the signal from different cells is detected on four channels simultaneously. This makes the units easier to separate from each other (figure 2.4). Furthermore, multiple tetrodes enable simultaneous recordings from the activity of whole neuronal ensembles is recorded and the interplay between cells within ensembles can be investigated. In the current project, animals were chronically implanted with tetrodes permitting us to follow neurons over time. In addition, the Microdrive which anchor the tetrode can be adjusted during the experimental period enables the search for additional single units at different anatomical locations. Altogether, large data sets from each animal can be acquired with this technique. In studies of cognitive functions such as memory processing, experiments in awake and behaving animals are necessary to facilitate a more natural representation of animal behavior. However the drawback is that chronic electrophysiology recordings are technically challenging and time consuming.

Sorting of spikes into separate single unit is subject to some degree of bias, as spike sorting is performed manually and will therefore be affected by subjective decisions (Harris et al., 2000). As an attempt to reduce bias, all spike sorting was performed prior to statistical analyses. If clusters had a large degree of overlap or the autocorrelograms showed a lag time below 2 ms, the clusters were excluded from the analyses. It has previously been shown that reliable unit separation can be achieved by following these criteria (Harris et al., 2000). Units that did not adhere to these criteria were excluded, however it is worth noting that some units that show overlap can sometimes represent two cells instead of one. In these scenarios, all cells that could potentially be two units were separated based on their respective functional attributes, in an effort to minimize overlap errors.

With regards to the interneuron classification, a limitation was that some of the cells fulfilling the criteria of waveform parameters showed features belonging to principal cells (grid cells and HD cells). Thus, classification was complemented by manual inspection of spatial distribution of spikes. Also, polar plots for head direction provided an additional tool for cell classification. Some degree of subjectivity is unavoidable with manual inspection, and we

cannot be entirely certain that neurons were unnecessarily excluded from the interneuron pool. However, the present results are more reliably referring to the effect on interneurons.

In order to establish coordinates for the microinjections, surgery training was conducted on three animals. Surgery procedures for microinjections in MEC pose challenges due to the proximity of the transverse sinus, and the depth and specific angle of the MEC relative to the surface of the brain. As surgery lasts several hours, many potential pitfalls may occur. Even if quality of the electrodes, microinjections and implantation of electrodes are successful, post-surgical screening for cells, the implant, and stability of recordings need to be perfect in order to acquire data of interest. In my study, I obtained single unit recordings from grid cells together with LFP from one animal with successful PNN digestion in the MEC.

A large number of studies with intracortical microinjections have been conducted using a Hamilton syringe and a single large injection. Such injections may leave tissue damage to the cortex and pressure load on the tissue, which may impede electrophysiological recordings. As an attempt to avoid this, thin glass pipettes were chosen to conduct several small injections at multiple sites. The pipettes were pulled with a minimum taper length of 3.2 mm and outer diameter at the opening of no more than 30 µm. The "kimwipe" method for opening of the pipettes allows for a large opening while maintaining a relatively small outer diameter, as this method produces an angled break of the pipette opening. The histology revealed minimal tissue damage after microinjections of chABC. A previous study in our group by K. Lensjø (master thesis, 2013) showed that the amount of chABC injected (3.7 µL/hemisphere) during surgery was sufficient to completely digest PNNs in the rat visual cortex, and the PNNs reassemble over the course of 60 days. In the current project, the amount of chABC for microinjections in MEC was reduced to approximately 1.5 µL per hemisphere because this was found to be sufficient to reduce PNNs to a minimum in the area. Histology showed good coverage of the enzyme in the MEC (see figure 3.3). Reassembly of PNNs reached 30% after 21 days, hence all electrophysiological recordings were conducted within three weeks after surgery in the chABC treated animal.

Due to time limitations, no controls with "sham" injections were used in the project. To further validate the results obtained from the chABC injected animal, negative controls with sham injections of artificial cerebrospinal fluid (aCSF) and Fast Green should be performed in

combination with tetrode implantation. This would unveil whether differences in single unit and LFP activity were caused by chABC action or by the injection of fluid in general.

4.3 Discussion of main findings

4.3.1 Perineuronal nets and PV^+ cells in MEC

Labeling with WFA/DAB reaction showed dense expression of PNNs in MEC. The superficial layers II/III showed denser staining than deep layers V/VI (figure 3.1). The superficial layers of MEC project to the hippocampus through the perforant path and are suggested to feed the hippocampus with information about self-location. The deep layers of MEC receive projections coming back from the hippocampus (reviewed by Canto et al., 2008).). Thus, the distinct layers of the MEC serve different functions in relation to spatial information processing and it is plausible that the differences in density of PNN is due to the functional diversity of different neuronal circuits. Previous findings have shown that PNNs tightly enwrap cell somata and proximal dendrites of subsets of neurons and opens up around points of synaptic contacts (see section 1.7). The two-photon laser microscopy images of PNNs around neurons in the MEC (figure 3.2) show hole-like openings in the structure on cell somata and dendrites and supports the idea that these holes represent points of synaptic contacts. Further ultrastructure investigations of this type and perhaps electron microscopy are needed to fully understand how PNNs enwrap neurons and synapses.

Several previous findings have shown a high abundance of PV^+ cells in MEC layers II/III (Wouterlood et al., 1995; Beed et al., 2013). It has also been shown that PNN and PV+ overlap vary across different brain areas and across species. In the adult rat hippocampus, PV/PNN overlap was found to be 37% (Callahan et al., 2013). In the adult mouse cortex it was approximately 60-70% (Cabungcal et al., 2013), and in the Zebra finch the overlap was approximately 40% in adult song-related nuclei (Balmer et al., 2009). The results in my study show that PV+ and PNN overlap may be lower in the EC compared to other cortical areas such as the frontal cortex (figure 3.5). The tendency found in the present study indicates that PNN and PV^+ cells co-localization should in future studies be quantified for verification.

In previous studies it has been proposed that brain areas with low PNN expression might hold a higher degree of plasticity than areas with dense PNNs (Hylin et al., 2013; Callahan et al, 2013).. Callahan and co-workers (2013) proposed that low PNN/PV^+ expression may apply to high levels of adult plasticity observed in the hippocampus. They further proposed that neocortical areas with dense PNN expression and a high PNN/PV^+ overlap have less plasticity. The density of PNNs and its relation to levels of plasticity is further supported by the study of Donato and coworkers (2013) who demonstrated that a low PV^+ configuration induced synaptic plasticity, and enhanced memory consolidation and retrieval after PNN removal.

4.3.2 Degradation and regeneration of PNNs

In order to conduct chronic electrophysiology over a long time period, it was necessary to investigate the time course of PNN regeneration after chABC treatment in MEC. Compared to previous finding in our group (Lensjø 2013,Christensen 2014), regeneration of PNNs in MEC was somewhat slower in MEC (figure 3.5) compared to visual cortex and hippocampus (regeneration at day 21: MEC = 30%, visual cortex = 43%, HPC = 60%) Based on regeneration of the PNNs I decided to conduct electrophysiological recordings within three weeks after chABC treatment.

Enzymatic digestion by chABC targets the chondrotitin sulfate proteoglycans of the ECM and leaves behind a sulphated 6-monosaccharide on the CS chain (Kwok et al., 2011). The overall ECM composition of the adult CNS contains CSPGs, both within the PNNs and in more general ECM structures (Kwok et al., 2011). Thus, the enzymatic treatment affects not only PNNs, but disrupts the ECM in general in the injected area. The remaining “stub” on the CS chain has been shown to remain in brain tissue for months after chABC treatment (Brückner et al., 1998). Hence, it cannot be ruled out that other long-term effects of chABC treatment may have influenced the findings in the present study.

Studies have shown that PNNs protect neurons against oxidative stress and thus could have a protective effect in the early stages of neurological diseases such as Alzheimer’s disease and schizophrenia (Baig et al., 2005; Cabungcal et al., 2013; Shah and Lodge, 2013). The protective role of PNNs in the adult brain has been further supported by human studies showing a reduction of PNNs in prefrontal cortex and abnormal structure of PNNs in EC and amygdala in post mortem brains of schizophrenia patients (Mauney et al., 2013;

Pantazopoulos et al., 2010). It is possible that the protective role of PNNs is removed along with the structure upon chABC treatment, producing an unfavorable extracellular milieu for neuron activity. As a consequence e.g. increased oxidative stress from PNN digestion in the MEC may have accounted for some of the observed the effects in the current study.

While WFA appears to specifically label PNNs, it remains to be shown which epitope it recognizes. However, WFA labeling together with labeling of aggrecan, brevican and other key components of PNNs have shown extensive overlap during development, and WFA is considered the gold standard for labeling of PNNs (Costa et al., 2007; Giamanco et al., 2010).

A therapeutic role of chABC treatment has also been suggested, as it promotes axonal sprouting and functional recovery after spinal cord injury (Bradbury et al., 2002; Massey et al., 2006).

The exact mechanism for plasticity induction upon PNN disruption remains elusive, and several studies point to various explanations. One study has demonstrated the involvement of lateral diffusion of neurotransmitter receptors (Frischknecht et al., 2009). Lateral diffusion is an extracellular process in which receptors are constantly exchanged and replaced between synaptic and extrasynaptic reservoirs (Frischknecht and Gundelfinger, 2012). This is important for replacement of desensitized receptors. Digestion of CSPGs by chABC removes the "barrier" provided by the PNN, leaving the extrasynaptic area available for lateral receptor diffusion. This may cause an increase in the turnover of unused and used receptors, and lead to increased synaptic plasticity (Frischknecht et al., 2009).

4.3.3 The effect of PNN degradation on interneurons in MEC

The PNNs are thought to encompass a high buffering capacity for the extracellular ionic milieu of PV^+ cells, thus supporting their high metabolic turnover of ions. It is plausible that the degradation of PNNs by chABC renders the interneurons of the MEC less active. The present study showed a tendency of reduced interneuron firing rate in the chABC treated animal, however the interneuron sample from the injected animal was low (n=8) and the result was not statistically significant. A recent study by Lensjø (2013) showed that interneuron firing

rate in the visual cortex showed a tendency of strong reduction in chABC treated rats compared to controls. Together these results suggest that chABC treatment reduce the firing rate of interneurons, and should be further investigated.

4.3.4 The effect of PNN degradation on response properties of principal neurons

The firing activity of principal cells in MEC is under inhibitory control by interneurons. When PNNs are digested their spiking activity may be reduced, thus lowering the inhibitory input to principal cells. The observed reduction in grid cell average firing rate, peak rate and grid cell bursting in the chABC treated animal is therefore surprising. Nevertheless, these observations propose that PNN removal had affected neuronal activity in the MEC.

Simultanously recorded head direction cells showed unaltered firing rate in chABC compared to controls. A recent study by Bonnevie and coworkers (2013) showed that inactivation of the hippocampus abolished the grid cell firing pattern, but did not affect firing rate or directional preference of simultaneously recorded head direction cells. Furthermore, as the grid cells lost their grid patterns, they became directionally modulated. This study indicated that hippocampal output is needed for the grid fields but that head direction cells are strongly driven by their inputs. The indication in my study that firing patterns of inhibitory neurons and grid cells are affected in the chABC animal while the HD cells remain their activity patterns are in support of the findings of Bonnevie and coworkers (2013). Furthermore, the dissociated effects in HD cells and grid cells, depending on an intact intrinsic network, support that the effects I find in the chABC treated animal is due to the chABC treatment itself. It would be interesting to follow up these studies with electrophysiological recordings from the EC when PNNs are removed in hippocampus and the other way around.

4.3.5 Irregular grid fields after PNN degradation

PNNs restrict adult plasticity and are densely expressed around neurons in MEC, with most prominent staining in layers II/III (figure 3.1). Considering that these layers encompass a high proportion of grid cells, it is likely that the PNNs indirectly support their rigid firing pattern. Grid cells have regular hexagonal firing patterns universal for all environments experienced by

the animal and show high temporal stability. Consistent with previous findings, the grid cells recorded from control animals in the current study showed spatial regularity and temporal stability across days (figure 3.10).

Although grid cell firing frequency was significantly reduced in the chABC animal, the cells displayed firing patterns of multiple fields covering the recording arena. However, some grid cells from the chABC treated animal showed an irregular firing pattern in the familiar environment. Since such irregularity has not previously been reported, it is tempting to speculate that the patterns seen in the chABC treated animal is due to removal of PNNs (figure 3.9). However, regularity of the recorded grid fields was not quantified and the sample size too small to draw any conclusions.

4.3.6 Formation of the grid map after PNN degradation

Barry et al. (2012) showed that grid fields expand in scale and become more irregular in novel environments, but the grids will gradually obtain their original size and "gridness" as the novel environment becomes familiar. In their study they concluded that grid expansion and subsequent reduction might serve as a novelty signal and familiarity signal, respectively. In my study, grid cells recorded from the chABC treated animal appeared to expand their firing fields in the novel arena, consistent with the finding of Barry and co-workers.

In accordance with previous studies of grid cells (Hafting et al., 2005), the grid pattern of cells recorded from the chABC treated animal established rapidly in the novel environment (figure 3.14). This indicates that PNN digestion had not affected the ability for the animal to form new spatial representations of separate environments.

4.3.7 Effect of PNN degradation on LFPs

For unknown reasons, different animals tend to have different theta frequency during the same behavior and cognitive task. The differences in mean theta frequencies observed in controls also varied to some extent within the control group in my study (ranging from 6.1 Hz

to 11.4). Thus, the lower theta frequency observed in the chABC animal compared to controls may be due to normal variation between individual animals.

However, the response to exposure to the novel environment seems to be an effect of PNN removal. In control animals, theta frequency was reduced by 0.2 Hz in a novel environment (figure 3.21). This reduction is in accordance with previous studies (Jeewajee et al., 2008). In contrast, the chABC treated animal showed an increase in theta frequency in the novel environment. Although only one chABC treated animal underwent the novelty task in the current project, a reduction of the same scale was observed in two independent experiments, as two novelty tasks were performed in this animal. Furthermore, Jeewajee and co-workers showed that theta frequency in the novel arena became similar to that in the familiar arena as the novel arena became familiar to the animal over subsequent days. Whereas my findings in the control animals are in accordance to this, the chABC animal stands in contrast to these findings. Theta frequency in the chABC treated animal continued to be different between the two arenas for three consecutive days after introduction to the novel arena (table 3.2). This may indicate that the novel environment never became familiar to the animal during this time. This suggests that PNN removal may have affected the encoding of the novel environment. Perhaps an increased plasticity due to PNN removal made newly encoded memories less stable. This possibility needs to be investigated in additional animals.

Whether grid pattern formation is dependent on theta oscillations has been largely debated, as studies have demonstrated that grid cells in bats are not dependent of such network activity, because there is no apparent theta in bat entorhinal cortex (Yartsev et al., 2011).

My analyses were concentrated to the theta frequency band. However, gamma oscillations (40-100 Hz) after PNN removal should be investigated in the current data set. This was beyond the scope of the current study. Gamma oscillations are thought to be generated by the PV^+ cells (Freund, 2003) and are important for activity in the EC-hippocampal system (Colgin et al., 2009). A reduction in gamma frequency has been observed in schizophrenia, which is probably caused by reduced GABAergic release from PV+ cells. Furthermore, oscillatory disturbances caused by PV cell impairment disrupts the synchronization of activity in neuronal populations (McRae and Porter, 2012). Gamma oscillation investigation after

PNN removal should be of high interest in order to look for plasticity changes. How PNNs and PV+ cells contribute to gamma activity in the MEC remain unknown.

A recent study by Beed and co-workers (2013) found a decreasing inhibitory microcircuitry in the dorsoventral axis of the MEC which is suggested to correspond to a decrease in PV cell density. This may also correspond to the increasing grid size down this axis.

4.4 Future perspectives

A quantification of PV^+ and PNN co-localization would be interesting in order to investigate possible variations of PV^+/PNN overlap between brain areas and to look for differences in different layers within the same brain area. This may be performed by the use of WFA/DAB and WFA/parvalbumin for light microscopy, or by WFA and parvalbumin fluorescent staining. In addition, it would be interesting to combine WFA staining with different specific cell markers, in order to investigate which other types of neurons that are enwrapped by PNNs in MEC.

A valuable tool for verifying the PNN digestion by chABC is to stain the remaining chondrotitin sulphate residues after chABC treatment ("stubs"). Double staining with WFA at different time points after chABC application will reveal the morphology of freshly synthesized PNN components as the nets regenerate. The ultimate combination for such investigation of PNN morphology and co-localisation with different subsets of neurons, would be a triple fluorescent staining using WFA, parvalbumin and "stub" staining of PNNs, combined with two-photon laser or confocal microscopy. Additionally, further molecular assessments of PNN components, their turnover rates and transport from their sites of origin would be useful.

As for the results from the present study remain inconclusive due to sample size, future studies should make effort to increase the population size of both interneurons and principal cells from the chABC affected area. Further analyses on interneuron activity and further classification of fast-spiking basket cells should be conducted.

4.5 Conclusions

From the main findings in this study, I conclude that superficial layers of the MEC have a high abundance of PNN which wrap around somata and proximal dendrites of neurons, including PV^+ cells. Enzymatic digestion of PNNs leads to a reduction in grid cell activity. Furthermore, the LFP responses seem different upon novelty exposure after PNN digestion. A non-significant tendency of reduced firing rate of interneurons was observed and there was no alteration in head direction cell activity.

Together, these findings suggest that the high expression of PNNs in the MEC may contribute to the hard-wiring of the grid cell network, and to the synchrony of activity in local populations of neurons. Thus, the PNN is indicated as important for the encoding of spatial representations in the mammalian brain.

5.References

Baig, S., Wilcock, G.K., Love, S.(2005). Loss of perineuronal net N-acetylgalactosamine in Alzheimer's disease. *Acta Neuropathologica*. 110, 393-401.

Balmer, T.S., Carels, V.M., Frisch, J.L., Nick, T.A. (2009) . Modulation of perineuronal nets and parvalbumin with developmental song learning. *The Journal of Neuroscience* 29, 12878-12885.

Barry, C., Bush (2012). From A to Z: a potential role for grid cells in spatial navigation. *Neural Systems and Circuits* 2, 6.

Barry, C., Ginzberg. L.L., O'Keefe, J., Burgess, N.(2012) Grid cell firing patterns signal environmental novelty by expansion. *Proceedings of the National Academy of Sciences* 109, 17687-17692.

Bartos, M., Elgueta, C. (2012). Functional characteristics of parvalbumin- and cholecystokinin-expressing basket cells. *The Journal of Physiology* 590, 669-681.

Beed, P., Gundlfinger A., Schneiderbauer, S., Song, J., Böhm, C., Burgalossi, A., Brecht, M., Vida, I., Schmitz, D. (2013). Inhibitory gradient along the dorsoventral axis in the medial entorhinal cortex. *Neuron* 79, 1197-1207.

Bhatt, D.H., Zhang, S., Gan, W.B. (2009) Dendritic spine dynamics. *Annual Reviews in Physiology* 71, 261-282.

Boccara, C.N., Sargolini, F., Thoresen, V.H., Solstad,T., Witter, M.P., Moser, E.I., Moser, M-B. (2010). Grid cells in pre- and parasubiculum. *Nature Neuroscience* 13, 987–994.

Bonnevie, T., Dunn, B., Fyhn, M., Hafting, T., Derdikman, D., Kubie, J.L., Roudi, Y., Moser, E.I.,Moser, M-B. (2013). Grid cells require excitatory drive from the hippocampus. *Nature Neuroscience* 16, 309–317.

Bradbury, E.J., Moon, L.D.F., Popat, R.J., King, V.R., Bennett, G.S., Patel, P.N., Fawcett, J.W., McMahon, S.B. (2002). Chondroitinase ABC promotes functional recovery after spinal cord injury. *Nature* 416, 636-640.

Brun, V.H., Leutgeb, S., Wu, H-Q., Schwarcz, R., Witter, M.P., Moser, E.I., Moser, M-B. (2008). Impaired spatial representation in CA1 after lesion of direct input from entorhinal cortex. *Neuron* 57, 175-177.

Brun, V.H., Solstad, T., Kjelstrup, K.B., Fyhn, M., Witter, M.P., Moser, E.I., Moser, M-B. (2008). Progressive increase in grid scale from dorsal to ventral medial entorhinal cortex. *Hippocampus* 18, 1200–1212.

Brückner, G., Bringmann, A., Härtig, W., Köppe, G., Delpech, B., Brauer, K. (1998a). Acute and long-lasting changes in extracellular-matrix chondroitin-sulfate proteoglycans induced by injection of chondroitinase ABC in the adult rat brain. *Experimental Brain Research* 121, 300–310.

Buzsáki, G. (1989). Two-stage model of memory trace formation: a role for "noisy" brain states. *Neuroscience* 31, 551-570.

Buzsáki, G. (2002). Theta Oscillations in the Hippocampus. *Neuron* 33, 325–340.

Buzsáki, G ., Moser, E.I. (2013). Memory, navigation and theta rhythm in the hippocampal-entorhinal system. *Nature Neuroscience* 16, 130-138.

Callahan, L.S., Thibert, K.A., Wobken, J.D., Georgieff, M.K. (2013). Early-life iron deficiency anemia alters the development and long-term expression of parvalbumin and perineuronal nets in the rat hippocampus. *Developmental Neuroscience* 35, 427-436.

Canto, C.B., Wouterlood, F.G., Witter, M.P. (2008): What does the anatomical organization of the entorhinal cortex tell us? *Neural plasticity* 2008, doi:10.1155/2008/381243.

Christensen, A.C. (2014). The role of perineuronal nets for spatial representations in the hippocampus. Master thesis, Department of Biosciences, University of Oslo.

Costa C, Tortosa R, Domènech A, Vidal E, Pumarola M, Bassols A.(2007). Mapping of aggrecan, hyaluronic acid, heparin sulphate proteoglycans and aquaporin 4 in the central nervous system in the mouse. *The Journal of Chemical Neuroanatomy* 33, 111-123.

Couey, J.J., Witoelar, A., Zhang, S-J., Zheng, K., Ye, J., Dunn, B., Czajkowski, R., Moser, M-B., Moser, E.I., Roudi, Y., Witter, M.P. (2013) Recurrent inhibitory circuitry as a mechanism for grid formation. *Nature Neuroscience* 16, 318-324.

Deepa, S.S., Carulli, D., Galtrey, C., Rhodes, K., Fukuda, J., Mikami, T., Sughara, K., Fawcett, J. (2006). composition of perineuronal net extracellular matrix in rat brain: A different disaccharide composition for the net-associated proteoglycans. *The Journal of Biological Chemistry* 281, 17789-17800.

del Rio, J.A., de Lecea, L., Ferrer, I., Soriano, I. (1994). The development of parvalbumin-immunoreactivity in the neocortex of the mouse. *Developmental Brain Research* 81, 247-259.

Dhillon, A., Jones, R.S.G. (2000). Laminar differences in recurrent excitatory transmission in the rat entorhinal cortex in vitro. *Neuroscience* 99, 413-422.

Dityatev, A., Schachner, M. (2003). Extracellular matrix molecules and synaptic plasticity. *Nature Neuroscience* 4, 456-468.

Dityatev, A., Bruckner, G., Dityateva, G., Grosche, J., Kleene, R., Schachner, M. (2007). Activity-dependent formation and functions of chondroitin sulfate-rich extracellular matrix of perineuronal nets. *Developmental Neurobiology* 67, 570–588.

Dityatev, A. (2010). Remodeling of extracellular matrix and epileptogenesis. *Epilepsia* 5, 61–65.

Donato, F., Rompani, S.B., Caroni, P. (2013). Parvalbumin-expressing basket-cell network plasticity induced by experience regulates adult learning. *Nature* 504, 272–276.

Dolorfo, C.L., Amaral, D.G. (1998). Entorhinal cortex of the rat: organization of intrinsic connections. *The Journal of Comparative Neurology* 398, 49-82.

Domnisoru, C., Kinkhabwala, A.A., Tank, D.W. (2013). Membrane potential dynamics of grid cells. *Nature* 495, 199-204.

Fagiolini, M., Hensch, T.K. (2000). Inhibitory threshold for critical period activation in primary visual cortex. *Nature* 404, 183-186.

Freund, T. F. (2003). Interneuron Diversity series: Rhythm and mood in perisomatic inhibition. *Trends in Neuroscience* 26, 489–495.

Frischknecht, R., Gundelfinger, E.D. (2012). The Brain's Extracellular Matrix and Its Role in Synaptic Plasticity. *Synaptic Plasticity Advances in Experimental Medicine and Biology* 970, 153-171.

Frischknecht, R., Heine, M., Perrais, D., Seidenbecher, C.I., Choquet, D., Gundelfinger, E.D.(2009). Brain extracellular matrix affects AMPA receptor lateral mobility and short-term synaptic plasticity. *Nature Neuroscience* 12, 897 – 904.

Fyhn, M., Molden, S., Hollup, S.A., Moser, M-B., Moser, E.I. (2002). Hippocampal Neurons respond to first-time dislocation of a target object. *Neuron* 35, 555-566.

Fyhn, M., Molden, S., Witter M.P., Moser, E.I., Moser, M-B. (2004). Spatial Representation in the entorhinal cortex. *Science* 305, 1258-1264.

Fyhn, M., Hafting, T., Treves, A., Moser, M-B., Moser, E.I. (2007). Hippocampal remapping and grid realignment in entorhinal cortex. *Nature* 466, 190-194.

Giocomo, L.M., Stensola, T., Bonnevie, T., Van Cauter, T., Moser, M-B., Moser, E.I. (2014). Topography of head direction cells in medial entorhinal cortex. *Current Biology* 24, 252–262.

Giamanco, K.A., Morawski, M., Matthews, R.T. (2010).Perineuronal net formation and structure in aggrecan knockout mice. *Neuroscience* 10, 1314-1327.

Gogolla, N., Caroni, P., Luthi, A. and Herry, C. (2009). Perineuronal nets protect fear memories from erasure. *Science* 325, 1258-1261.

Huntley, G.W. (2012) . Synaptic circuit remodelling by matrix metalloproteinases in health and disease. *Nature Reviews Neuroscience* 13, 743-57.

Hafting, T., Fyhn, M., Molden, S., Moser, M-B., Moser, E.I. (2005). Microstructure of a spatial map in the entorhinal cortex. *Nature* 436, 801-806.

Hafting, T., Fyhn, M., Bonnevie, T., Moser, M-B., Moser, E.I. (2008). Hippocampus-independent phase precession in entorhinal grid cells. *Nature* 453, 1248-1253.

Härtig, W., Brauer, K., Brückner, G. (1992). Wisteria floribunda agglutinin-labelled nets surround parvalbumin-containing neurons. *Neuroreport.* 3, 869-72.

Harris, K.D., Henze, D.A., Csicsvari, J., Hirase, H., Buzsáki, G. (2000). Accuracy of tetrode spike separation as determined by simultaneous intracellular and extracellular measurements. *The Journal of Neurophysiology* 84, 404-414.

Hensch, T.K. (2005). Critical period plasticity in local cortical circuits. *Nature Reviews Neuroscience* 6, 877-888.

Hensch, T., K., Fagiolini, M., Mataga, N., Stryker, M.P., Baekkeskov, S., Kash, S.F. (1998). Local GABA circuit control of experience-dependent plasticity in developing visual cortex. *Science* 282, 1504-1508.

Hylin, M.J., Orsi, S.A., Moore, A.N. (2013). Disruption of the perineuronal net in the hippocampus or medial prefrontal cortex impairs fear conditioning. *Learning and Memory* 20, 267-273.

Insausti, R., Herrero, M.T., Witter, M.P. (1997). Entorhinal cortex of the rat: Cytoarchitectonic subdivisions and the origin and distribution of cortical efferents. *Hippocampus* 7, 146-83.

Iurilli, G., Olcese, U., Medini, P. (2013). Preserved excitatory-inhibitory balance of sortical synaptic inputs following deprived eye stimulation after a saturating period of monocular deprivation in rats. *PLoS ONE* 8, e82044.

Jeewajee' A., Lever, C., Burton, S., O'Keefe, J., Burgess, N. (2008). Environmental novelty is signaled by reduction of the hippocampal theta frequency. *Hippocampus* 18, 340-348.

Kandel, E.R., Schwartz, J.H., Jessell, T.M. (2000). *Principles of Neural science*. New York, McGraw-Hill XLI, fourth edition.

Khan, U.A., Liu, L., Provenzano, F.A., Berman, D.E., Profaci, C.P., Sloan, R., Mayeux, R., Duff, K.E., Small, S.A. (2013). Molecular drivers and cortical spread of lateral entorhinal cortex dysfunction in preclinical Alzheimer's disease. *Nature Neuroscience* 17, 304–311.

Kochlamazashvili, G., Henneberger C, Bukalo O, Dvoretskova E, Senkov O, Lievens PM, Westenbroek R, Engel AK, Catterall WA, Rusakov DA, Schachner M,Dityatev A.(2010). The extracellular matrix molecule hyaluronic acid regulates hippocampal synaptic plasticity by modulating postsynaptic L-type Ca(2+) channels. *Neuron* 67, 116-28.

Kwok, J.C., Dick, G., Wang, D., Fawcett, J. (2011). Extracellular matrix and perineuronal nets in CNS repair. *Developmental Neurobiology* 71, 1073-1089.

Leutgeb, S., Leutgeb, J.K., Treves, A., Moser, M-B., Moser, E.I. (2004) Distinct Ensemble Codes in Hippocampal Areas CA3 and CA1. *Science* 27, 1295-1298.

Levelt, C.N., Hübener, M. (2012). Critical-period plasticity in the visual cortex. *Annual Reviews of Neuroscience* 35, 309-330.

Maguire, E.A., Frackowiak, R.S.J., Frith, C.D. (1997). Recalling routes around London: Activation of the right hippocampus in taxi drivers. *The Journal of Neuroscience* 17, 7103-7110.

Malenka, R.C., Bear, M.F. (2004). LTP and LTD: An Embarrassment of Riches. *Neuron* 44, Pages 5-21.

Maren, S., Fanselow, M.S. (1997) Electrolytic lesions of the fimbria/fornix, dorsal hippocampus, or entorhinal cortex produce anterograde deficits in contextual fear conditioning in rats. *Neurobiology of Learning and Memory* 67, 142–149.

Martin, S.J., Grimwood, P.D., Morris, R. G. M. (2000). Synaptic plasticity and memory: An evaluation of the hypothesis. *Annual Reviews of Neuroscience,* 23, 649-711.

Massey, J.M., Hubscher, C.H., Wagoner, M.R., Decker,J.A., Amps, J., Silver, J., Onifer, S.M. (2006). Chondroitinase ABC digestion of the perineuronal net promotes functional collateral sprouting in the cuneate nucleus after cervical spinal cord Injury. *The Journal of Neuroscience,* 26, 4406-4414.

Mauney, S.A., Athanas, K.M., Pantazopoulos, H., Shaskan, N., Passeri, E., Berretta, S., Woo, T.U.W. (2013). Developmental pattern of perineuronal nets in the human prefrontal cortex and their deficit in schizophrenia. *Biological Psychiatry* 74, 427–435.

McNaughton, B.L., Battaglia, F.P., Jensen, O., Moser, E.I., Moser, M-B. (2006). Path integration and the neural basis of the 'cognitive map'. *Nature Reviews Neuroscience* 7, 663-678.

McRae, P.A, Porter, B.E. (2012). The perineuronal net component of the extracellular matrix in plasticity and epilepsy. *Neurochemistry International* 61, 963–972.

Melzer, S., Michael, M., Caputi, A., Eliava, M., Fuchs, E.C., Whittington, M.A., Monyer, H. (2012). Long-range-projecting GABAergic neurons modulate inhibition in hippocampus and entorhinal cortex. *Science* 335, 1506-1510.

Morris, R.G., Garrud, P., Rawlins, J.N., O'Keefe , J. (1982) Place navigation impaired in rats with hippocampal lesions. *Nature* 297, 681-683.

Morris, N.P., Henderson, Z. (2000). Perineuronal nets ensheath fast spiking, parvalbumin-immunoreactive neurons in the medial septum/diagonal band complex. *European Journal of Neuroscience* 12, 828-38.

Moser, E.I., Witter, M.P., Moser, M-B. (2010) Entorhinal cortex. In: Handbook of Brain Microcircuits. Shepherd GM, Grillner, S Eds. Oxford University Press, Oxford, UK, 175-192.

Moser, E.I., Moser, M-B., Roudi, Y. (2014). Network mechanisms of grid cells. *Philosophical Transactions of the Royal Society* 369, 20120511.

Oesterle, S.I.C.A. (2011). The Pipette Cookbook. Rev G.

O'Keefe, J. (1976). Place units in the hippocampus of the freely moving rat. *Experimental Neurology* 51, 78-109.

Pantazopoulos, H., Woo, T-U.W., Lim, M.P., Lange, N., Beretta, S. .(2010). Extracellular matrix-glial abnormalities in the amygdala and entorhinal cortex of subjects diagnosed with schizophrenia. *Archives of General Psychiatry* 67, 155-166.

Pizzorusso, T., Medini, P., Berardi, N., Chierzi, S., Fawcett, J.W., Maffei, L. (2002). Reactivation of ocular dominance plasticity in the adult visual cortex. *Science* 298, 1248-1251.

Pizzorusso, T., Medini, P., Landi, S., Baldini, S., Berardi, N., Maffei, L. (2006). Structural and functional recovery from early monocular deprivation in adult rats. *Proceedings of the National Academy of Sciences* 103, 8517-8522.

Romberg, C., Yang, S., Melani, R., Andrews, M.R., Horner, A., E., Spillantini, M.G., Bussey, T., J., Fawcett, J.W., Pizzorusso, T., Saksida, L.M. (2013). Depletion of perineuronal nets enhances recognition memory and long-term depression in the perirhinal Cortex. *The Journal of Neuroscience 33,* 7057–7065.

Sargolini, F., Fyhn, M., Hafting, T., Witter, M.P., Moser, M-B., Moser, E.I. (2006) Conjunctive representation of position, direction and velocity in entorhinal cortex. *Science* 312, 758-762.

Scoville, W.B., Milner, B.(1957).Loss of recent memory after bilateral hippocampal lesions. *Journal of Neurol Neurosurgery Psychiatry 1.* 11-21.

Shah, A.,Lodge, D.J. (2013) . A loss of hippocampal perineuronal nets produces deficits in dopamine system function: relevance to the positive symptoms of schizophrenia. *Translational Psychiatry* 3, e215.

Soleman, S., Filippov, M.A., Dityatev, A., Fawcett, J.W. (2013). Targeting the neural extracellular matrix in neurological disorders. *Neuroscience* 253, 194–213.

Solstad, T., Moser, E.I., Einevoll, G.T. (2006). From grid cells to place cells: A mathematical model. *Hippocampus* 16, 1026-1031.

Solstad, T., Boccara, C.N,, Kropff, E., Moser, M-B., Moser, E.I. (2008) Representation of geometric borders in the entorhinal cortex. *Science* 322, 1865-1868.

Steffenach, H.A., Witter, M., Moser, M.B., Moser, E.I. (2005). Spatial memory in the rat requires the dorsolateral band of the entorhinal cortex. *Neuron* 45, 303-313.

Sik, A., Penttonen, M., Ylinen, A., Buzsaki, G. (1995). Hippocampal CA1 Interneurons: An in vivo Intracellular Labeling Study. *The Journal of Neuroscience* 75, 6651-6665.

Simic, G., Bexheti, S., Kelovic, Z., Kos, M., Grbic, K., Hof, P.R., Kostovic, I. (2005). Hemispheric asymmetry, modular variability and age-related changes in the human entorhinal cortex. *Neuroscience* 130, 911-925.

Schmidt-Hieber, C., Häusser, M. (2013). Cellular mechanisms of spatial navigation in the medial entorhinal cortex. *Nature Neuroscience* 16, 325-331.

Schwarcz, R., Witter, M.P. (2002). Memory impairment in temporal lobe epilepsy: the role of entorhinal lesions. *Epilepsy Research* 50, 161-77.

Squire, L.R., Stark, C.E., Clark, R.E.(2004). The medial temporal lobe. *Annual Reviews in Neuroscience.* 2, 279-306.

Stranahan, A.M., Mattson, M.P. (2010). Selective vulnerability of neurons in layer II of the entorhinal cortex during aging and Alzheimer's disease. *Neural Plasticity* 2010, 108190

Tahvildari, B., Alonso, A. (2005). Morphological and electrophysiological properties of lateral entorhinal cortexLayers II and III principal neurons. *The Journal of Comparative Neurology* 491, 123–140.

Tsien, R.Y. (2013). Very long-term memories may be stored in the pattern of holes in the perineuronal net. *Proceedings of the National Academy of Sciences* 110, 12456-12461.

van Hove, I., Lemmens, K., Van de Velde, S., Verslegers, M., Moons, L.(2012). Matrix metalloproteinase-3 in the central nervous system: A look on the bright side. *The journal of neurochemistry* 123, 203-216.

van Strien, N. M., Cappaert, N. L. M., Witter, M. P.(2009). The anatomy of memory: an interactive overview of the parahippocampal–hippocampal network, *Nature Reviews Neuroscience* 10, 272-282.

Whitlock, J.R., Heynen, A.J., Shuler, M.G., Bear, M.F. (2006). Learning Induces long-term potentiation in the hippocampus. *Science* 313, 1093-1097.

Wouterlood, F.G., Härtig, W., Brockner, G., Witter, M.P. (1995) Parvalbumin-immunoreactive neurons in the entorhinal cortex of the rat: localization, morphology, connectivity and ultrastructure. *Journal of Neurocytology* 24, 135-153.

Xu, T., Yu, X., Perlik, A.J., Tobin, W.F., Zweig, J.A., Tennant, K., Jones, T., Zuo, Y. (2009). Rapid formation and selective stabilization of synapses for enduring motor memories. *Nature* 462, 915-919.

Yamada, J., Jinno, S. (2013). Spatio-temporal differences in perineuronal net expression in the mouse hippocampus, with reference to parvalbumin. *Neuroscience* 253, 368–379.

Yang, G., Pan, F., Gan, W-B. (2009). Stably maintained dendritic spines are associated with lifelong memories. *Nature* 462, 920-924.

Yang, S., Lee, D.S., . Chung, C.H., Cheong, M.Y., Leeb, C-J., Jung, M.W . (2004). Long-term synaptic plasticity in deep layer-originated associational projections to superficial layers of rat entorhinal cortex. *Neuroscience* 127, 805–812.

Yartsev, M.M., Witter, M.P., Ulanovsky, N. (2011). Grid cells without theta oscillations in the entorhinal cortex of bats. *Nature* 479, 103–107.

Yun, S.H., Mook-Jung, I., Jung, M.W.(2002). Variation in effective stimulus patterns for induction of long-term potentiation across different layers of rat entorhinal cortex. *Journal of Neuroscience* 22, RC214.

Zimmermann, D.R., Dours- Zimmermann, M.T. (2008). Extracellular matrix of the central nervous system: from neglect to challenge. *Histochemistry and Cell Biology* 130, 635–653.

6. Appendix

6.1 List of abbreviations

aCSF	artificial cerebrospinal fluid
AP	anterior-posterior
CA	*Cornu ammonis*
CC	corpus callosum
chABC	chondroitinase ABC
CNS	central nervous system
CP	critical period
CSPG	chondroitin sulphate proteoglycan
CS GAG	chondrotitin sulfate glycosaminoglycan
DAB	diaminobenzidine
DG	dentate gyrus
DV	dorso-ventral
EC	entorhinal cortex
ECM	extracellular matrix
EEG	electroencephalogram
GABA	gamma-aminobutyric acid
GAG	glycosaminoglycan
HA	hyaluronic acid
HAS	hyaluronan synthase
HD	head direction
HPC	hippocampus
IP	intraperitoneal

LDP	long term depression
LEC	lateral entorhinal cortex
LFP	local field potential
LTP	long term potentiation
MEC	medial entorhinal cortex
ML	mediolateral
MMP	metalloproteinase
NMDA	N-methyl-D-aspartat
OB	olfactory bulb
PNN	perineuronal net
PP	perforant path
PV	parvalbumin
SC	subcutanous
WFA	*Wisteria floribunda* agglutinin

6.2 Solutions for immunohistochemistry and histochemistry

10X PBS

80g of NaCL

2.0g of KCl

14.4g of Na_2HPO_4

2.4g of KH_2PO_4

Dissolve in 800 ml ddH_2O adjust pH to 7.4 and adjust volume to 1L.

Dilute 1:10 with ddH_2O for 1X solution.

TS-PBS

3% Normal Goat Serum

0.3% Triton X-100

Dissolve in 1X PBS

T-PBS

0.3% Triton X-100 in 1X PBS

Tris HCL 500 ml:

500ml dH_2O

3,03g Tris -(hydroxymethyl) aminomethane.

Mix on magnetic stirrer for 2 min. Adjust pH with HCL to ca pH 7.6.

TNS

6g Trizma-HCl

1L dH_2O adjust pH to 7.4 with 1M NaOH

TBS –TX: 100 ml

100ml ddH_20

3,03 g Tris

4,48 NaCl

2.5 ml Triton X-100

Mix on magnetic stirrer for 2 min. Adjust pH with HCL to ca pH 8.0.

96% ethanol with acetic acid

500 mL absolute ethanol

2.5 mL acetic acid

Cresyl violet staining solution

0.5g cresyl violet acetate

1.25 nL glacial acetic acid

500 mL ddH_20

Heat to 60°C and filter before use.

4% paraformaldehyde (PFA)

40g PFA

1L 1X PBS

Heat to 50-60°C, leave with stirring until everything is dissolved (3-4 hours).

Filter before use.

6.3 Immunohistochemistry and histochemistry protocols

6.3.1 Staining of PNNs for light microscopy

Primary antibody: biotinylated *Wisteria floribunda* lectin (Sigma L-1516).

Secondary antibody: anti-rabbit IgG (also reactive against biotin) (ABC kit, Vector PK-6101).

1. Rinse sections with 1xPBS, 3x5 minutes.
2. Block sections with TS-PBS for 1 hour at room temperature.
3. Dilute WFA-biotin in TS-PBS 1:200, add WFA-biotin to sections. Keep sections at 4°C overnight. Prepare the DAB pellet: 15mL Tris-HCl to 1 pellet (10mg), in 50ml Nunc™ tube. Light shield and keep on roller/shaker for approx. 2 hours. Remains from this solution can be stored at 4°C and activated later by adding H_2O_2.
4. Prepare ABC staining solution: 90µL Reagent A, 10 mL PBS, 90µL Reagent B. Incubate at room temperature for 30 minutes.
5. Rinse sections with T-PBS, 3x5 minutes at room temperature.
6. Quenching endogenous peroxidase: 3%H_2O_2 in ddH_2O. Incubate for 5 minutes, rinse with T-PBS, 2x5 minutes.
7. Add ABC solution to sections; incubate 1 hour at room temperature.
8. Rinse sections with TNS, 3x5 minutes.
9. Add 12µL H_2O_2 to DAB solution, filter it and add the DAB/H_2O_2 solution to the sections under fume hood. Incubate until desired color is observed (5-15 min).
10. Rinse minimum 3 times with TNS. Mount sections on slides using a fine brush and TNS/PBS. Dry sections.
11. Dehydrate sections with 95% EtOH, then 100% etOH and finally xylene. Mount sections with DRX/entellan.

6.3.2 Staining of PNNs and PV for fluorescence microscopy:

Primary antibodies: Biotinylated *Wisteria floribunda* lectin (Sigma L-1516) and rabbit anti-parvalbumin (Swant PV 25).

Secondary antibodies: Streptavidin Alexa Fluor® 488 conjugate (Invitrogen S-11223) and Texas Red-X goat anti-rabbit IgG (Invitrogen T-6391).

1. Rinse sections with 1xPBS, 3x5 minutes.
2. Block sections with TS-PBS for 90 min at room temperature.
3. Dilute WFA-biotin (1:200) and rabbit anti-parvalbumin (1:2000) in TS-PBS, add primary antibodies to sections. Keep sections at 4°C overnight.
4. Rinse sections with TBS-TX, 3x10 minutes.
5. Incubate with secondary antibody streptavidin, Alexa Flour 488 conjugate (1:1000), in TBS-TX, 1 hour in room temperature.
6. Rinse sections with TBS-TX, 3x10 minutes.
7. Incubate with secondary antibody Texas Red-X goat anti-rabbit (1:1000) in TBS-TX, 4 hours in room temperature.
8. Rinse sections 3x10 minutes with TBS-TX.
9. Rinse sections 2x5 minutes with Tris/HCl.
10. Mount sections on slides using a fine brush, dry sections for approx. 20 minutes.
11. Rinse sections with ddH_2O and mount with FluorSave Reagent.

6.3.3 Staining for Nissl bodies using Cresyl violet

Manually shake the specimen holder.

1. ddH_2O for 1 minute.
2. Cresyl violet solution 3-10 minutes (depends on tissue and how fresh the solution is, the sections should obtain a dark blue color).
3. ddH_2O for 1 minute.
4. 70% ethanol for 2 minutes.
5. 80% ethanol for 2 minutes.
6. 90% ethanol for 2 minutes.
7. 96% with acetic acid for 30 seconds to 2 min, depending on color fading.
8. >100% ethanol for 2 minutes.
9. Xylene for 2-10 minutes.
10. Mount sections with cover slip and Entellan - leave in fume hood overnight.

Alcohol solutions are made with absolute ethanol, diluted in ddH_2O.

6.4 Supplementary figures

Tetrode tracks

Control animals

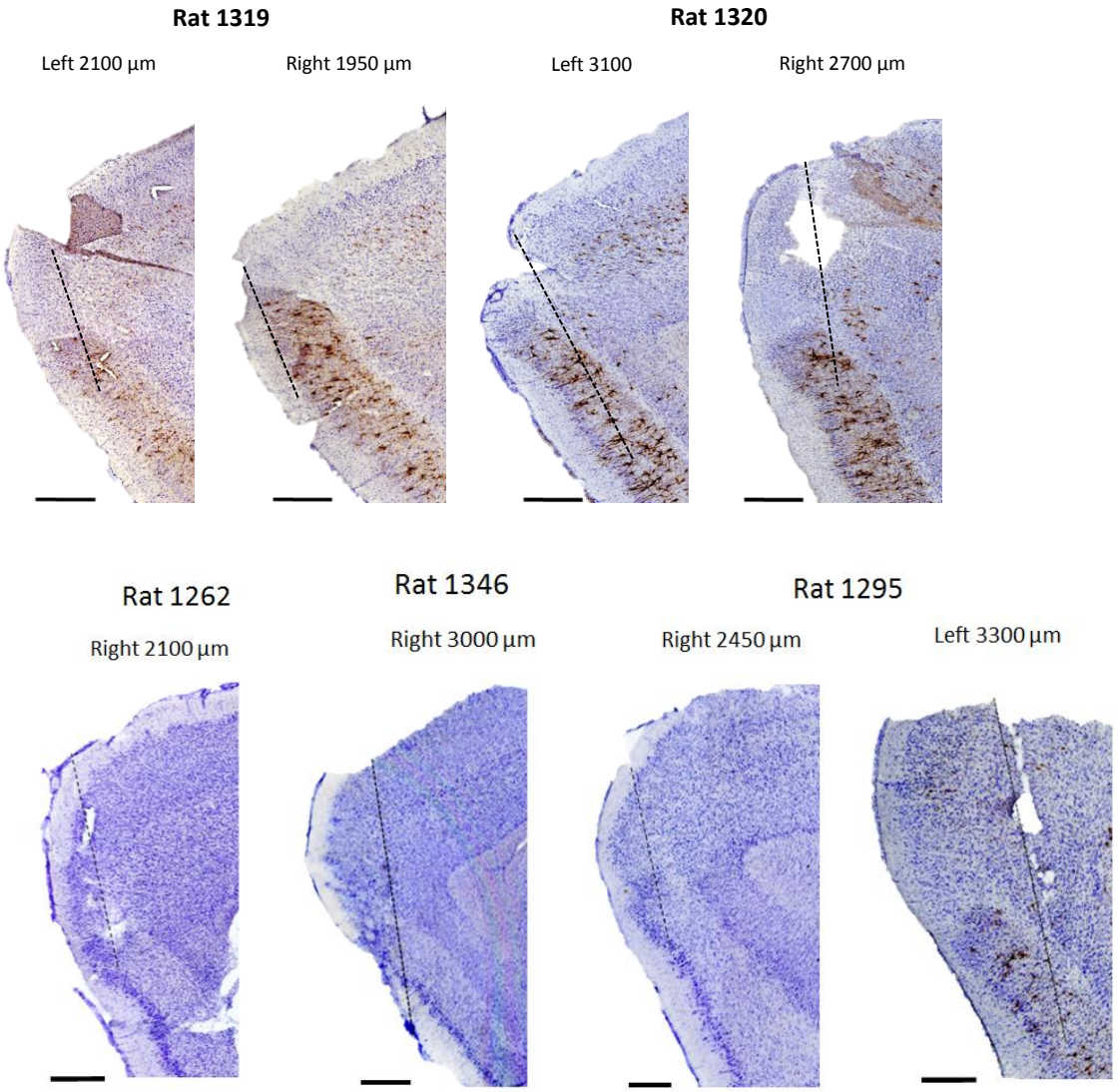

Figure 6.1 Sagittal sections showing tetrode tracks in MEC in control animals. Tracks can be seen next to the dotted line. Sections from control animals stained with *Wisteria floribunda* (WFA) and Cresyl violet (upper panel). Three sections from control animals stained with Cresyl violet and one section stained with WFA and Cresyl violet (bottom panel).

Animal injected with chindroitinase ABC

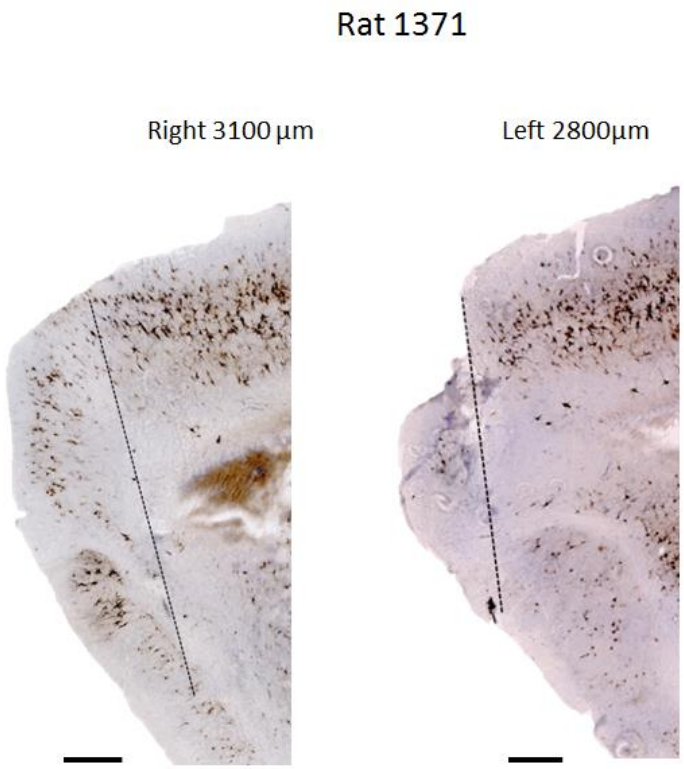

Figure 6.2. Saggital sections from the chondroitinase treated animal stained with *Wisteria floribunda* for perineuronal nets (PNNs) and Cresyl violet for visualization of tetrode tracks. Tracks can be seen next to the dotted line. Note the weak staining of PNNs in MEC due to chABC digestion. The animal was sacrificed at day 21.

Grey scale measurements for regeneration of PNNs

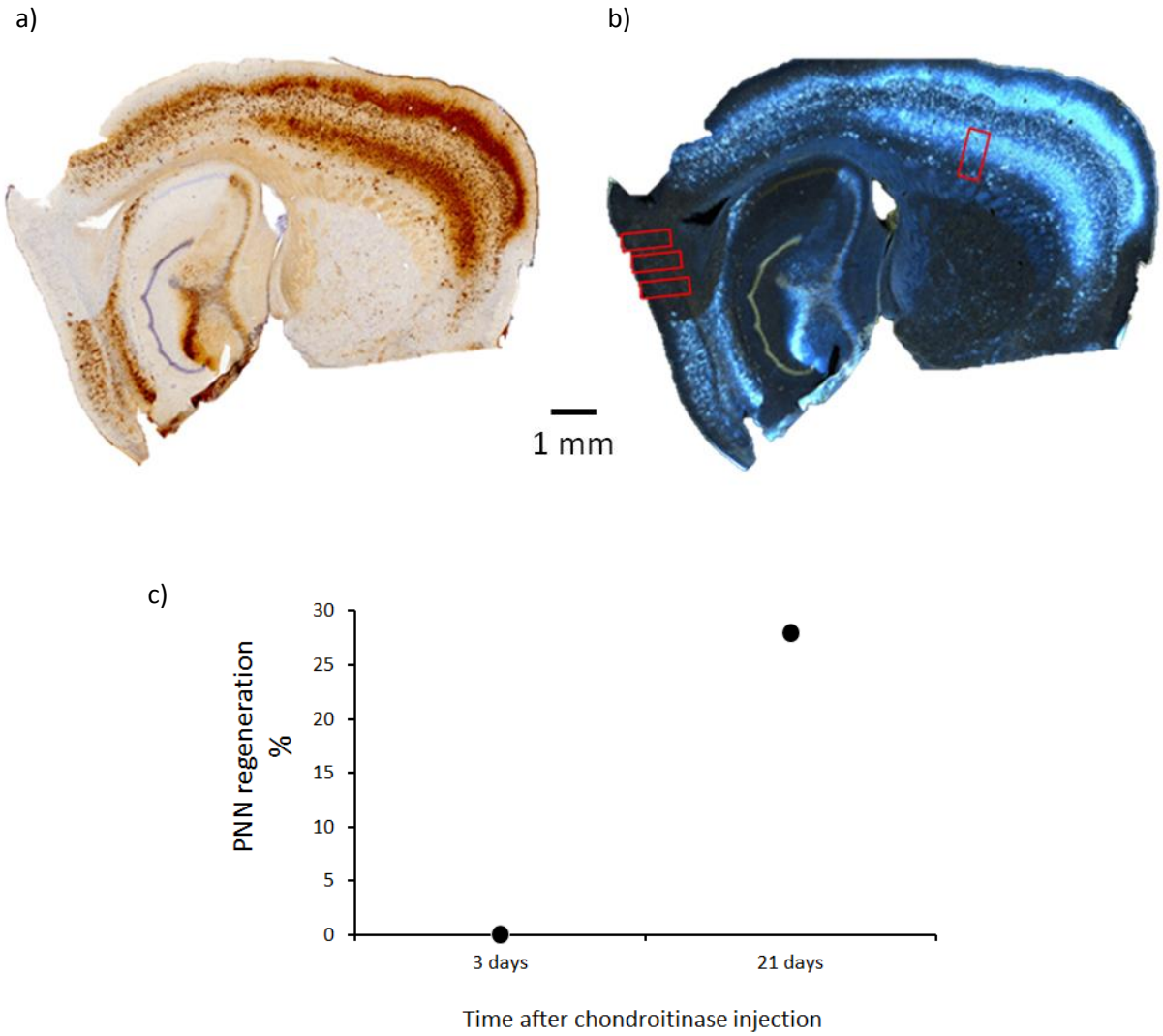

Figure 6.3 Regeneration of perineuronal nets (PNNs) in medial entorhinal cortex (MEC) after chondroitinase ABC (chABC) treatment. a) Sagittal section stained with *Wisteria floribunda* agglutinin showing PNN digestion by chABC three days after injection. b) Image converted to grey scale in ImageJ. The intensity of PNN staining was measured from a control area in the frontal cortex and compared to three locations within the injected area of MEC (red squares). Ratios between injected area and control area was calculated and the 3 day control was set as 0% regeneration of PNNs. c) The PNN regeneration (%) after 3 days and after 21 days.

Table 6.1. Values for spatial correlation of five grid cells in a chondroitinase ABC treated animal during grid formation in a novel arena. The values represent the spatial correlation of grids in two minute blocks compared to the spatial correlation of the fields for the last 20 min of the trial.

	Time(min)								
Cell #	0-2	2-4	4-6	6-8	8-10	10-12	12-14	14-16	16-18
1	0.198	0.633	0.276	0.325	0.525	0.463	0.188	0.714	0.382
2	0.682	0.722	0.608	0.384	0.705	0.847	0.503	0.555	0.574
3	0.508	0.282	0.194	0.63	0.409	0.637	0.323	0.057	0.517
4	-0.016	0.959	0.958	0.831	-0.082	0.867	0.881	0.514	0.671
5	0.578	0.841	0.715	0.794	0.864	0.885	0.848	0.778	0.854
Mean	0.390	0.687	0.550	0.592	0.484	0.734	0.549	0.524	0.600
SEM	0.106	0.094	0.115	0.084	0.132	0.067	0.113	0.103	0.064

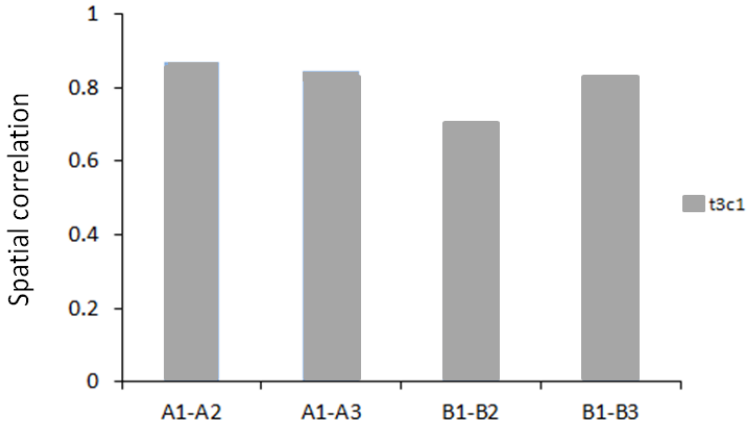

Figure 6.4. Spatial correlation of the same grid cell between day 1 and day 2 (A1-A2), and day 1 and day 3 (A1-A3) in the familiar arena, and between days in arena B (B1-B2 AND B1-B3, respectively). The spatial correlation is generally high, however somewhat lower in room B between day 1 and day 2.

Table 6.2. Standard error mean (SEM) values for theta frequency in chABC animal and controls during a novelty task (figure 3.21).

	Familiar	Novel1	Novel2	Novel3	Familiar'
Controls	0.13	0.20	0.09	0	0.10
chABC	0.04	0.07	0.06	0.05	0.07